UC Riverside

UC Riverside Electronic Theses and Dissertations

Title

Thermal Transformation of Vitamin E Acetate During E-Cigarette Vaping: Dynamic Chemistry and Toxicity

Permalink

Author

Canchola, Alexa Nicole

Publication Date

2024

Peer reviewed|Thesis/dissertation

UNIVERSITY OF CALIFORNIA
RIVERSIDE

Thermal Transformation of Vitamin E Acetate During E-Cigarette Vaping: Dynamic
Chemistry and Toxicity

A Dissertation submitted in partial satisfaction of the
requirements for the degree of

Doctor of Philosophy

in

Environmental Toxicology

By

Alexa Nicole Canchola

March 2024

Dissertation Committee:
      Dr. Ying-Hsuan Lin, Chairperson
      Dr. Roya Bahreini
      Dr. Yinsheng Wang
      Dr. Prue Talbot

The Dissertation of Alexa Nicole Canchola is approved:

_____

_____

_____
                                              Committee Chairperson

University of California, Riverside

Acknowledgements

This dissertation would not have been possible without the support and guidance of my amazing family, friends, and advisors. Firstly, I would like to express my deep gratitude and appreciation for my Ph.D. advisor, Dr. Ying-Hsuan Lin, who welcomed me into her lab and provided me with constant trust, advice, and room to explore all of the ideas bouncing around in my head. Dr. Lin, I will always be grateful for all the time that you spent working alongside me to troubleshoot experiment or instrument troubles, even late into the night. You not only helped me immensely to grow into an independent Ph.D. researcher, but continue to model the type of mentor that I wish to be as I move forward in my career.

I would also like to thank the many faculty members on my committees over the past several years for their time, advice, encouragement and support. Thank you to Dr. Roya Bahreini, Dr. Prue Talbot, Dr. Yinsheng Wang, Dr. Wenwan Zhong, and Dr. David Crocker. Thank you as well to all the ETOX and ENSC faculty and staff for their inspiration and assistance throughout my Ph.D. program. I would also like to acknowledge the funding support for my education, research and professional development, including the Dissertation Year Program Award (2024), the Yvonne Danielson Endowed Graduate Award for Academic and Research Excellence (2023), the National Institute of Environmental Sciences (NIEHS) T32 Training grant (2021-2023) and the UCR Graduate Student Association (GSA) Travel awards.

To the members of the Lin Lab, past and present, who I have had the privilege to work with: Dr. Jin Y. Chen, Dr. C.M. Sabbir Ahmed, Dr. Huanhuan Jiang, Dr. Junli Wang, Dr. Linhui Tian, Kunpeng Chen, Michael Lum, Md Rubaiat Nural Alam, Wonsik Woo, and Lillian Tran, thank you. Thank you for all your time, patience, encouragement, and ideas in lab. Thank you for the movie nights, card games, Dungeons and Dragons sessions, pumpkin carvings, Renaissance Faires, and potlucks. You all made this lab a supportive and fun environment and I will always be grateful.

Another massive thank you is due to all my amazing mentees – Maya KC-Jordan, Jing Ye, Janet Albarrán, Annette Mercado Sanchez, Ruth Meletz, Rise Ara Khandakar (Holy), and Siri Langmo. Thank you for your time and hard work in the lab, no matter how long we were able to work together; I hope that I could help you as much as you helped me. A special thank you to Ruth and Siri; these two were absolutely instrumental to the projects presented in this dissertation and I'm so thankful for their hard work, time, curiosity, and patience. Ruth and Siri, acting as your graduate mentor was an honor and privilege that I am beyond grateful to have had the opportunity to do.

Next, a massive thank you to all of my friends who have supported me through the years. To Dr. Alex Malinick and Future Dr. Desiree Malinick, I cannot express just how grateful I am to you both for your friendship, encouragement, advice, and support over the past 9 years that I've known you. From dumb undergrads to dumb Ph.Ds. and beyond, I could not have gotten to this point without you.

Finally, I want to thank my amazing family to whom this dissertation is dedicated. I am beyond grateful for my parents, Alex and Liz Canchola, who have given me nothing but their unconditional support and love throughout my Ph.D. journey and have always believed in me no matter what path I take in life. Dad, thank you for inspiring me and instilling a strong sense of determination and perseverance in me from a young age. I think you might be more excited about me getting a Ph.D. than even I am! Mom, thank you for always being willing to listen to my rants about failed experiments, even when the words I was saying meant nothing to you. I think at this point, you've learned enough about GC/MS to get an honorary degree! And last but certainly not least, thank you to my sisters, Alyssa and Ashlyn, who have continued to be a source of inspiration, love, and encouragement. I hope you're as proud of me as I am the both of you.

Dedicated to

my parents, Alex and Liz, and my sisters, Ashlyn and Alyssa for their constant support and encouragement.

Also dedicated to my late grandmothers, Maria Canchola and Franciska Tanacsos. Guess what nagymama? Your Kewpie doll is a doctor now.

ABSTRACT OF THE DISSERTATION

Thermal Transformation of Vitamin E Acetate During E-Cigarette Vaping: Dynamic
Chemistry and Toxicity

by

Alexa Nicole Canchola

Doctor of Philosophy, Graduate Program in Environmental Toxicology
University of California, Riverside, March 2024
Dr. Ying-Hsuan Lin, Chairperson

The use of e-cigarettes for the inhalation of nicotine and cannabis products has become popular in the United States across many demographics. Their rise in popularity is largely attributed to their ease of access, customization options, and perception as safer alternatives to traditional methods. However, despite their perceived safety, inhalation of vaping emissions has great potential to cause adverse health outcomes in users, as evidenced by events such as the outbreak of e-cigarette- or vaping-associated lung injuries (EVALI) in the U.S. in 2019. While many e-liquid ingredients are considered safe for dermal or oral exposure, the vaping process has been found to result in the thermal degradation of e-liquid ingredients. As a result, the emitted aerosols are complex mixtures of chemicals formed during vaping that may have different chemical and toxicological properties than their parent compounds. However, characterization of these compounds remains challenging due to the wide range of customizable options – such as temperature, use patterns, device construction, and more – that may influence the resulting chemical composition of e-cigarette emissions.

This dissertation aims to address the knowledge gaps in the relationship between user- and device-driven parameters on the thermal degradation behavior of e-liquids and the chemical and toxicological properties of e-cigarette aerosol emissions, using VEA as a model e-liquid. First, this work identifies novel VEA vaping products and their potential mixture effects on toxicity upon exposure to human lung cells using a combination of chemical and cellular-based analyses. Second, the change in VEA vaping emission product distribution as a function of variable voltage/temperature settings was characterized using non-target gas chromatography/mass spectrometry (GC/MS) analysis. Finally, a tube furnace reactor system was used to investigate the role of oxygen (O_2) and transition metals in the thermal degradation behavior and emission product distribution of VEA. Results from this dissertation contribute to an improved understanding of the thermal degradation behavior and chemistry of e-liquids, and how varying user- and device-driven parameters can alter the chemical and toxicological properties of vaping emissions. Detailed compositional and mechanistic information on e-cigarette emissions will be helpful for future hazard identification and the public health risks associated with e-cigarettes.

Table of Contents

Chapter 4

List of Tables

Chapter 1: Introduction

1.1 Background Significance

First introduced to the United States market in 2007, electronic cigarettes (e-cigarettes) or vaping devices are nicotine or cannabis delivery systems that provide heat to a formulation of nicotine or cannabis along with various solvents and flavoring agents to generate aerosols that can be inhaled by a user. While e-cigarettes were first introduced as nicotine-delivery systems that closely resembled cigarettes without the typical burning or tar, the current generations of e-cigarettes have expanded to include a wide variety of flavors and delivery methods. (1) For example, tetrahydrocannabinol (THC)- and cannabidiol (CBD)-containing vape products have recently gained popularity among e-cigarette users with the implementation of the 2018 Agriculture Improvement Act, which legalized the sale of hemp-derived CBD products and products with less than 0.3% Δ^9-THC in the U.S., (2,3) paving the way for a variety of THC and CBD-containing e-liquids. As of 2023, the global e-cigarette and vape market was valued at $22 billion and is only expected to grow over the next few years. (4)

Since their introduction, e-cigarettes in all forms have gained widespread popularity across many demographics in the U.S., particularly among younger generations. According to the 2021 National Health Interview Survey (NHIS) conducted by the Centers for Disease Control (CDC), 4.5% of adults aged 18 and older had used e-cigarette or other vaping products in 2021, with the highest reported usage being adults 18-24 (11% of users). (5) Among adolescents, a reported 14.1% of high school students

and 3.3% of middle school students were current users of e-cigarettes; 84.9% of the current users reported that they primarily used flavored e-cigarette products, (6) despite efforts to regulate and even ban the sale of flavored products in the U.S. This continued interest in e-cigarette and other vaping products has been attributed to a variety of factors, including the perceived health benefits and/or safety of vaping products compared to traditional combustible tobacco and cannabis products, easy accessibility and discretion, the high degree of customizability of e-liquid composition and device construction, the general reduced annual cost compared to traditional tobacco and cannabis products, and social pressure from peers and advertising. (7,8) E-cigarettes remain mostly unregulated in the U.S. despite some efforts by the Food and Drug Administration (FDA) to reduce access to e-cigarettes for minors. (9) However, despite their alleged safety among users, recent events and research have highlighted the potential of e-cigarette aerosols to negatively impact the lungs of users.

The most notable event was the 2019–2020 outbreak of e-cigarette or vaping product use-associated lung injuries (EVALI) that resulted in over 2,800 hospitalizations and 60 deaths across the United States. (10) Patients with EVALI demonstrated a wide array of respiratory, gastrointestinal, and constitutional symptoms, including coughing, shortness of breath, chest pain, nausea, vomiting, abdominal pain, and fever. Initial tests found no signs of infection among patients, nor any common history of pre-existing respiratory conditions that could explain the onset of pulmonary disease. (10-12) However, a further survey of hospitalized patients found that 80% had used THC-containing vaping products within 3 months preceding the onset of any symptoms; 75%

of those who reported THC-use also reported that they had used THC-containing vaping products daily. (11,13)

Vitamin E acetate (VEA) was subsequently identified as a potential causative agent, after several studies found a high prevalence of VEA in both the bronchioalveolar lavage (BAL) of hospitalized patients[11] and in vaping cartridges used by EVALI patients. (14-16) VEA – which is a clear, odorless oil with a viscosity similar to THC – was believed to have been used as a thickening or cutting agent in primarily non-commercial THC-vaping products (i.e., products acquired from sources such as friends, family, or illicit in-person or online dealers). (10) In some cases, cartridges were found to contain > 95% VEA. (14) Despite the clear link between VEA and EVALI cases, the molecular mechanism of VEA-induced injury remained unclear, as VEA and other vitamin E ester derivatives are largely considered safe for human ingestion and dermal absorption. Inadequate intake of vitamin E has even been linked to a variety of metabolic diseases as vitamin E may provide cellular membranes with protection against reactive oxygen species. (17-18) Inhalation of VEA and VEA vaping aerosols, however, was largely unstudied.

In the aftermath of the EVALI outbreak, several mechanisms of actions have been suggested for VEA toxicity including mechanical injury to the lungs and biosurfactant-like activity. (19) Of particular interest to researchers were studies that found that VEA and other e-liquids (the solvent-based liquids added to a vaping cartridge to be converted to an aerosol during vaping) undergo both aerosolization and thermal degradation during the vaping process. (20-23) E-liquids – commercial and homemade – typically consist of

an active ingredient such as nicotine or CBD, flavoring ingredients, diluents such as propylene glycol (PG) and vegetable glycerin (VG) in varying ratios, and preservatives. The structures of commonly identified e-liquid diluents (solvents and thickening agents) and active ingredients are shown in **Scheme 1.1**. The application of heat by the e-cigarette heating coil encourages both breakdown of e-liquid compounds and interaction between degradation products within the e-cigarette emissions, resulting in the formation of complex mixtures of aerosols that may have drastically different physiochemical and toxicological properties than the parent e-liquid components. In essence, e-cigarette aerosols are a mixture of gases and solid and liquid particles that may be generated during vaping, posing serious questions regarding the health effects of e-liquids like VEA that are considered to be "safe." Thermal degradation of VEA during vaping, in particular, was found to produce a wide variety of compounds, the most notable being duroquinone (DQ) (20) and ketene, (21, 24) which are both known to cause oxidative damage to the lungs upon exposure in humans and mice. (25,26) These findings quickly made it clear that in order to understand the potential health impacts of vaping, characterization of compounds formed during vaping is crucial. However, while many common thermal degradation products such as formaldehyde and other carbonyls have been identified and quantified in the previous studies, the overall chemical composition and reported levels of aerosol components vary significantly across the literature.

a) Common Diluents
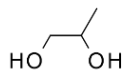
Propylene Glycol (PG)
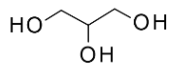
Vegetable Glycerin (VG)
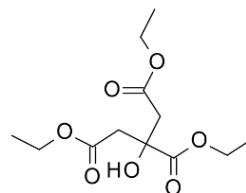
Triethyl Citrate (TEC)
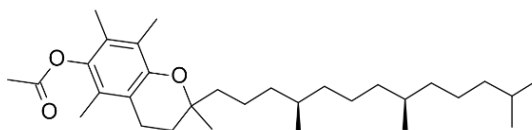
Vitamin E acetate (VEA)
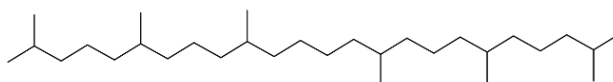
Squalane
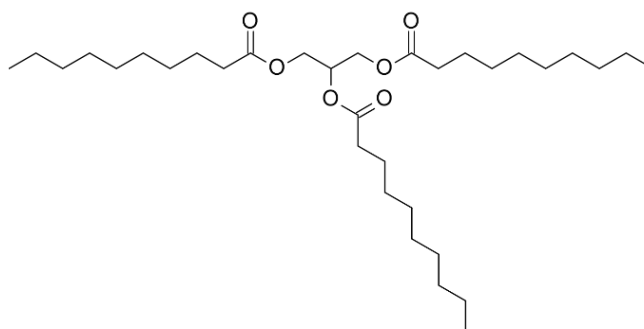
Medium Chain Triglyceride (MCT) oil

b) Common Active Ingredients
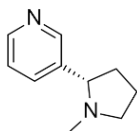
L-Nicotine
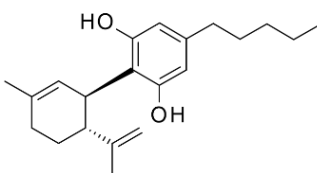
Cannabidiol (CBD)
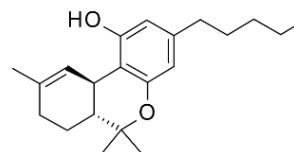
Tetrahydrocannabinol (THC)

Scheme 1.1. Chemical structures of common (a) e-liquid diluents including solvents and thickening agents, and (b) active ingredients.

This variability may be due to the high degree of customizability within e-cigarette vaping environments, device construction, and user behavior that may alter the physiochemical profile of emitted aerosols. The basic construction of an e-cigarette device includes a mouthpiece, an e-liquid storage component in the form of a cartridge or soaked wick, a heating element/atomizer, a microprocessor, and a battery, (27,28) with differing degrees of complexity and design features depending on the generation of e-cigarette (**Figure 1.1**). First-generation "Cig-a-Likes" were typically pre-filled, single-use devices with fixed, low-voltage batteries; second- and third-generation devices are larger, refillable, and may have variable voltages/temperatures the device can be operated at. (28) Even within the same generation, the construction of the device – including the elemental composition of the heating elements, air-flow tubes, wicks, soldered battery connector plates, other connection and scaffolding components – can differ drastically between brands. (28-30) Even within the same brand and e-cigarette model, manufacturing variability has been identified in device aspects such as coil resistance, airflow required to produce an aerosol, pressure drop, and cartridge lifetime. (31-33) As a result, e-cigarettes of a similar size, shape, and physical construction may expose users to drastically different levels of transition or heavy metals as the metals leech into the e-liquid and/or are transferred to the aerosols during vaping. (34, 35) Furthermore, these elements may interact with e-liquids to influence pyrolysis behavior and the resulting chemical composition of emitted aerosols. Research by Saliba et al. (2018) and Jensen et al. (2017) found evidence that the composition of heating coils may influence the temperature needed for e-liquids such as PG and VG to thermally degrade, suggesting a

potential surface catalysis to allow for low-temperature vaping. (36, 37) The type and construction of the heating coil may also impact the release of degradation products such as reactive oxygen species (ROS) and carbonyl compounds, (38) which could have negative health impacts on users. While some research has begun to investigate the role of device construction in the production of potentially toxic byproducts, the extent to which these device-driven parameters may affect e-cigarette aerosol composition and the reaction mechanisms involved have not been fully characterized in the literature.

First Generation ("Cig-a-Likes")	Second Generation ("Vape Pens")	Third Generation ("Tank or Vape Mods")	Fourth Generation ("Pod Mods")	Other devices
• Disposable • Pre-filled cartridge • Fixed voltage	• Refillable cartridge • Adjustable voltage • Replaceable battery or rechargeable	• Refillable cartridge • Adjustable voltage • Large size • Open mod system	• Replaceable or refillable pod cartridges • Temperature & flow sensing • Rechargeable battery	• Disposable, prefilled e-cigarettes • E-Cigars, E-Hookah • Dab/Wax pens

Figure 1.1. Evolution and variety of e-cigarette devices and features.

User-driven parameters – including puffing topography (e.g., number of puffs per session, time interval between puffs, etc.), battery voltage setting/operating temperature, and more – may also change based on user history and preferences. Studies such as Robinson et al. (2015) and Behar et al. (2015) that have attempted to characterize common use patterns have found significant variability between individuals, even when

using the same generation or brand of e-cigarette. (39,40) Frequency of use and puff duration are the most commonly reported factors that show major variability within a user population. (39, 41-43) There has been great interest in understanding a typical user's behavior in order to best estimate aerosol exposure. Puffing topography has a strong influence on total aerosol mass and particle size, (44, 45) which can impact both the estimated dosage of aerosolized e-liquids as well as the ability of particles to penetrate deeper into the respiratory tract. (46-48) For example, Mikheev et al. (2020) found that as airflow rate increase, particle size of vaped VEA aerosol emissions decreased; high flow rates resulted in the formation of particles as small as 50 nm, which have a greater ability to reach the alveolar sacs if entered into the respiratory tract. (44) Flow rate, puff duration, and coil temperature have all been found to be positively correlated with puff volumes/total aerosol mass, but negatively correlated with particle size. (49-51) In regard to the thermal degradation of e-liquids, several studies have found that factors such as flow rate and coil temperature impact the emission of potentially toxic degradation products including organic products, ROS, metals. (45, 52) An increase in coil temperature, which began to be customizable with the introduction of second-generation e-cigarettes, significantly enhances the production of known hazardous carbonyl-containing species such as formaldehyde, acetaldehyde, and acrolein. (45) These findings indicate that depending on the behavior and preferences of a particular user, the risk of exposure and the dosage that an individual is exposed to may vary widely among a population. As a result, a full characterization of how these factors impact the formation of potentially toxic degradation products, and the reaction mechanisms

involved in generating them, is of critical importance when trying to estimate exposure risk.

1.2 Current knowledge gaps

Because e-cigarettes have only existed in the U.S. markets for less than 20 years, the health effects resulting from inhalation exposure to e-cigarette aerosols are largely unknown. At the time of this dissertation, much of the current literature surrounding e-cigarette health effects focused heavily on the influence of intact parent e-liquid compounds (i.e., solvent compounds such as VEA, PG, or VG, or active ingredients such as nicotine or THC). Thermal degradation of these parent compounds during vaping poses a serious risk to user health that is underestimated in the current literature. Estimating these health impacts and the risk of exposure to potentially toxic degradation products, however, is only made difficult by the vast range of device- and user-driven parameters that may alter the physiochemical properties of the e-cigarette emissions, which may, in turn, alter the toxicity profile of the aerosols. Moreover, while there has been some interest in understanding how these parameters may affect the production yields of potentially toxic carbonyl compounds, the vaping process has been suggested to produce compounds from a wide range of chemical classes, each with their own toxicological properties. These chemicals, which may include compounds such as alkenes and short- and long-chain alcohols, may have significant impacts on user health, but have been underrepresented in the e-cigarette literature. Not only could these additional compounds have their own toxicity, but they may also interact with other compounds in the e-liquid or emitted aerosols to form secondary products. Finally, there is sparse

information regarding how these individual parameters may interact to alter thermal degradation. The described parameters and user customizations are likely to influence aerosol generation and resulting health impacts, but the exact effects and mechanisms involved have yet to be fully characterized in the literature.

Due to the significant popularity of e-cigarettes in the U.S., and the ever-evolving nature of the e-cigarette market and design, assessing how differences in e-cigarette construction and use patterns influence user health is imperative. A better understanding of these factors and their influence is crucial to helping estimate the exposure risk to users and bystanders.

1.3 Objectives of the Dissertation

This dissertation aims to address the lack of understanding regarding how device and user-driven factors may influence e-liquid thermal degradation behavior and chemical composition of resulting aerosols. Detailed chemical characterization and investigation into the e-cigarette aerosol constituents is crucial for scientific understanding of the public health risk to e-cigarette users and bystanders who may be passively exposed to e-cigarette aerosols. This information will provide greater insight into identifying the hazards of e-cigarette aerosols as well as elucidating molecular mechanisms of toxicity upon exposure.

In this dissertation, VEA was as used a model e-liquid to characterize thermal degradation behavior and toxicity under various operating conditions, such as temperature settings and device metal composition. Particle-phase VEA thermal

degradation products were chemically characterized using a variety of analytical techniques, including gas chromatography mass spectrometry (GC/MS). Using these techniques, novel degradation products were identified and quantified that assist in our understanding of the public health risk of e-cigarettes.

In Chapter 2, VEA vaping emissions were collected and analyzed using a combination of chemical and cellular-based techniques to explore particle-phase chemical composition, size distribution, and the ability of aerosol emissions to induce oxidative stress in human bronchial epithelial cells (BEAS-2B). Results from this study provide further evidence that vaping emissions are highly complex mixtures of various classes of compounds and particle sizes that may influence exposure risk and health effects. Furthermore, this study was among the first to highlight that individual constituents cannot alone explain toxicity upon exposure to e-cigarette aerosols; instead, there may be interactions – additive or antagonistic – between compounds within the mixture to induce toxicity through multiple pathways.

In Chapter 3, the impact of variable voltage or temperature settings on the chemical composition of VEA vaping emissions was assessed. Non-targeted analysis of particle-phase constituents of e-cigarette emissions was performed using GC/MS to investigate the hypothesis that elevated heating coil temperatures during vaping enhances thermal degradation of VEA. Not only does this study support the hypothesis that chemical composition and thus exposure risk are dependent on operating temperature and other external parameters, but it also provides evidence of the role of device or environmental factors in e-liquid degradation mechanisms.

Chapter 4 expands upon the findings from Chapter 3 to investigate the effects of device and environmentally-driven parameters on VEA vaping emission thermal degradation behavior and chemical composition. In this study, VEA thermal behavior was observed under oxidizing and inert atmospheres, in the presence or absence of metal alloys commonly found in e-cigarette devices. Using a combination of thermogravimetric analysis (TGA) and GC/MS analysis, these results demonstrated a clear relationship between the presence of oxygen, the type of metal used to construct the e-cigarette device, and the vaping emission product distribution. The results from this study highlight additional thermal degradation mechanisms that may occur during vaping alongside the predominantly studied pyrolysis pathways, as well as the potential for low-temperature vaping to produce harmful degradation products.

Finally, Chapter 5 summarizes the conclusions derived from this dissertation. The implications of this work and suggested future directions are also discussed.

1.4 References

1.   Morean, M. E.; Butler, E. R.; Bold, K. W.; Kong, G.; Camenga, D. R.; Cavallo, D. A.; Simon, P.; O'Malley, S. S.; Krishnan-Sarin, S., Preferring more e-cigarette flavors is associated with e-cigarette use frequency among adolescents but not adults. *PLOS ONE* **2018,** *13* (1), e0189015.

2.   Leas, E. C.; Moy, N.; McMenamin, S. B.; Shi, Y.; Benmarhnia, T.; Stone, M. D.; Trinidad, D. R.; White, M. Availability and Promotion of Cannabidiol (CBD) Products in Online Vape Shops *Int. J. Environ. Res. Public Health*, **2021,** *18*(13), 6719.

3.   Love, C. A.; Schichlein, K. D.; Clapp, P. W.; Jaspers, I., Cannabinoid Vaping Products Present Novel Challenges for Assessment of Respiratory Health Effects. Oxford University Press: **2022**; Vol. 188, pp 1-3.

4.   Company, T. B. R. Vaporizers Global Market Report 2023. https://www.thebusinessresearchcompany.com/report/vaporizers-global-market-report (accessed 01/16/2024).

5.   Kramarow, E. A.; Elgaddal, N., Current Electronic Cigarette Use Among Adults Aged 18 and Over: United States, 2021. NCHS Databrief no. 475, *Hyattsville, MD: National Center for Health Statistic*s. **2023**.

6.   Birdsey, J.; Cornelius, M.; Jamal, A.; Park-Lee, E.; Cooper, M. R.; Wang, J.; Sawdey, M. D.; Cullen, K. A., Tobacco Product Use Among US Middle and High School Students—National Youth Tobacco Survey, 2023. *MMWR. Morb. Mortal. Wkly* **2023,** *72* (44), 1173-1182.

7.   Sapru, S.; Vardhan, M.; Li, Q.; Guo, Y.; Li, X.; Saxena, D., E-cigarettes use in the United States: reasons for use, perceptions, and effects on health. *BMC public health* **2020,** *20* (1), 1-10.

8.   Romijnders, K. A. G. J.; Van Osch, L.; De Vries, H.; Talhout, R., Perceptions and reasons regarding e-cigarette use among users and non-users: a narrative literature review. *Int. J. Environ. Res. Public Health* **2018,** *15* (6), 1190.

9.   Food, U. S.; Adminstration, D., FDA finalizes enforcement policy on unauthorized flavored cartridge-based e-cigarettes that appeal to children, including fruit and mint. *Silver Spring, MD:* **2020**.

10.   CDC Outbreak of Lung Injury Associated with the Use of E-Cigarette, or Vaping, Products. https://www.cdc.gov/tobacco/basic_information/e-cigarettes/severe-lung-disease.html#map-cases (accessed 7/29/2021).

11.   Blount, B. C.; Karwowski, M. P.; Shields, P. G.; Morel-Espinosa, M.; Valentin-Blasini, L.; Gardner, M.; Braselton, M.; Brosius, C. R.; Caron, K. T.; Chambers, D.; Corstvet, J.; Cowan, E.; De Jesús, V. R.; Espinosa, P.; Fernandez, C.; Holder, C.; Kuklenyik, Z.; Kusovschi, J. D.; Newman, C.; Reis, G. B.; Rees, J.; Reese, C.; Silva,

L.; Seyler, T.; Song, M.-A.; Sosnoff, C.; Spitzer, C. R.; Tevis, D.; Wang, L.; Watson, C.; Wewers, M. D.; Xia, B.; Heitkemper, D. T.; Ghinai, I.; Layden, J.; Briss, P.; King, B. A.; Delaney, L. J.; Jones, C. M.; Baldwin, G. T.; Patel, A.; Meaney-Delman, D.; Rose, D.; Krishnasamy, V.; Barr, J. R.; Thomas, J.; Pirkle, J. L., Vitamin E Acetate in Bronchoalveolar-Lavage Fluid Associated with EVALI. *N. Engl. J. Med.* **2019,** *382*(8), 697-705.

12.   Reagan-Steiner, S.; Gary, J.; Matkovic, E.; Ritter, J. M.; Shieh, W.-J.; Martines, R. B.; Werner, A. K.; Lynfield, R.; Holzbauer, S.; Bullock, H., Pathological findings in suspected cases of e-cigarette, or vaping, product use-associated lung injury (EVALI): a case series. *Lancet Respir. Med.* **2020,** *8* (12), 1219-1232.

13.   Lozier, M. J.; Wallace, B.; Anderson, K.; Ellington, S.; Jones, C. M.; Rose, D.; Baldwin, G.; King, B. A.; Briss, P.; Mikosz, C. A., Update: demographic, product, and substance-use characteristics of hospitalized patients in a nationwide outbreak of e-cigarette, or vaping, product use–associated lung injuries—United States, December 2019. *MMWR Morb. Mortal. Wkly* **2019,** *68* (49), 1142.

14.   Duffy, B.; Li, L.; Lu, S.; Durocher, L.; Dittmar, M.; Delaney-Baldwin, E.; Panawennage, D.; LeMaster, D.; Navarette, K.; Spink, D., Analysis of Cannabinoid-Containing Fluids in Illicit Vaping Cartridges Recovered from Pulmonary Injury Patients: Identification of Vitamin E Acetate as a Major Diluent. *Toxics* **2020,** *8* (1), 8.

15.   Lu, S. J.; Li, L.; Duffy, B. C.; Dittmar, M. A.; Durocher, L. A.; Panawennage, D.; Delaney-Baldwin, E. R.; Spink, D. C., Investigation of vaping fluids recovered from New York State e-cigarette or vaping product use-associated lung injury patients. *Front. Chem.* **2021,** *9*, 919.

16.   Taylor, J.; Wiens, T.; Peterson, J.; Saravia, S.; Lunda, M.; Hanson, K.; Wogen, M.; D'Heilly, P.; Margetta, J.; Bye, M., Characteristics of e-cigarette, or vaping, products used by patients with associated lung injury and products seized by law enforcement—Minnesota, 2018 and 2019. *MMWR Morb. Mortal. Wkly* **2019,** *68* (47), 1096.

17.   Berton, T. R.; Conti, C. J.; Mitchell, D. L.; Aldaz, C. M.; Lubet, R. A.; Fischer, S. M., The effect of vitamin E acetate on ultraviolet-induced mouse skin carcinogenesis. *Mol. Carcinog.* **1998,** *23* (3), 175-184.

18.   Burton, G. W., Vitamin E: molecular and biological function. *Proc. Nutr. Soc.* **1994,** *53* (2), 251-262.

19.   DiPasquale, M.; Gbadamosi, O.; Nguyen, M. H. L.; Castillo, S. R.; Rickeard, B. W.; Kelley, E. G.; Nagao, M.; Marquardt, D., A Mechanical Mechanism for Vitamin E Acetate in E-cigarette/Vaping-Associated Lung Injury. *Chem. Res. Toxicol.* **2020**.

20.   Jiang, H.; Ahmed, C. M. S.; Martin, T. J.; Canchola, A.; Oswald, I. W. H.; Garcia, J. A.; Chen, J. Y.; Koby, K. A.; Buchanan, A. J.; Zhao, Z.; Zhang, H.; Chen, K.; Lin, Y.-H., Chemical and Toxicological Characterization of Vaping Emission

Products from Commonly Used Vape Juice Diluents. *Chem. Res. Toxicol.* **2020,** *33* (8), 2157-2163.

21.	Wu, D.; O'Shea, D. F., Potential for release of pulmonary toxic ketene from vaping pyrolysis of vitamin E acetate. *PNAS* **2020,** *117* (12), 6349-6355.

22.	El-Hage, R.; El-Hellani, A.; Salman, R.; Talih, S.; Shihadeh, A.; Saliba, N. A., Vaped humectants in e-cigarettes are a source of phenols. *Chem. Res. Toxicol.* **2020,** *33* (9), 2374-2380.

23.	Chen, J. Y.; Canchola, A.; Lin, Y.-H., Carbonyl Composition and Electrophilicity in Vaping Emissions of Flavored and Unflavored E-Liquids. *Toxics* **2021,** *9* (12).

24.	Narimani, M.; da Silva, G., Does 'Dry Hit'vaping of vitamin E acetate contribute to EVALI? Simulating toxic ketene formation during e-cigarette use. *PLOS ONE* **2020,** *15* (9), e0238140.

25.	Audi, S. H.; Bongard, R. D.; Krenz, G. S.; Rickaby, D. A.; Haworth, S. T.; Eisenhauer, J.; Roerig, D. L.; Merker, M. P., Effect of chronic hyperoxic exposure on duroquinone reduction in adult rat lungs. *Am. J. Physiol. Lung Cell Mol. Physiol.* **2005,** *289* (5), L788-L797.

26.	Audi, S. H.; Bongard, R. D.; Dawson C. A.; Siegel, D.; Roerig, D. L.; Merker, M. P.; Duroquinone reduction during passage through the pulmonary circulation. *Am. J. Physiol. Lung Cell Mol. Physiol.* **2003,** *285* (5), L1116-31.

27.	Omaiye, E. E.; Williams, M.; Bozhilov, K. N.; Talbot, P., Design features and elemental/metal analysis of the atomizers in pod-style electronic cigarettes. *PLOS ONE* **2021,** *16* (3), e0248127.

28.	Williams, M.; Talbot, P., Design features in multiple generations of electronic cigarette atomizers. *Int. J. Environ. Res. Public Health* **2019,** *16* (16), 2904.

29.	Williams, M.; Li, J.; Talbot, P., Effects of Model, Method of Collection, and Topography on Chemical Elements and Metals in the Aerosol of Tank-Style Electronic Cigarettes. *Sci. Rep.* **2019,** *9* (1), 13969.

30.	Williams, M.; Bozhilov, K. N.; Talbot, P., Analysis of the elements and metals in multiple generations of electronic cigarette atomizers. *Environ. Res.* **2019,** *175*, 156-166.

31.	Saleh, Q. M.; Hensel, E. C.; Robinson, R. J., Method for quantifying variation in the resistance of electronic cigarette coils. *Int. J. Environ. Res. Public Health* **2020,** *17* (21), 7779.

32.	Saleh, Q. M.; Hensel, E. C.; Eddingsaas, N. C.; Robinson, R. J., Effects of manufacturing variation in electronic cigarette coil resistance and initial pod mass on coil lifetime and aerosol generation. *Int. J. Environ. Res. Public Health* **2021,** *18* (8), 4380.

33.   Williams, M.; Talbot, P., Variability among electronic cigarettes in the pressure drop, airflow rate, and aerosol production. *Nicotine Tob. Res.* **2011,** *13* (12), 1276-1283.

34.   Aherrera, A.; Olmedo, P.; Grau-Perez, M.; Tanda, S.; Goessler, W.; Jarmul, S.; Chen, R.; Cohen, J. E.; Rule, A. M.; Navas-Acien, A., The association of e-cigarette use with exposure to nickel and chromium: A preliminary study of non-invasive biomarkers. *Environ. Res.* **2017,** *159*, 313-320.

35.   McDaniel, C.; Mallampati, S. R.; Wise, A., Metals in Cannabis Vaporizer Aerosols: Sources, Possible Mechanisms, and Exposure Profiles. *Chem. Res. Toxicol.* **2021,** *34* (11), 2331-2342.

36.   Saliba, N. A.; El Hellani, A.; Honein, E.; Salman, R.; Talih, S.; Zeaiter, J.; Shihadeh, A., Surface chemistry of electronic cigarette electrical heating coils: Effects of metal type on propylene glycol thermal decomposition. *J. Anal. Appl. Pyrolysis* **2018,** *134*, 520-525.

37.   Jensen, R. P.; Strongin, R. M.; Peyton, D. H., Solvent chemistry in the electronic cigarette reaction vessel. *Sci. Rep.* **2017,** *7* (1), 1-11.

38.   Cirillo, S.; Urena, J. F.; Lambert, J. D.; Vivarelli, F.; Canistro, D.; Paolini, M.; Cardenia, V.; Rodriguez-Estrada, M. T.; Richie, J. P.; Elias, R. J., Impact of electronic cigarette heating coil resistance on the production of reactive carbonyls, reactive oxygen species and induction of cytotoxicity in human lung cancer cells in vitro. *Regul. Toxicol. Pharmacol.* **2019,** *109*, 104500.

39.   Behar, R. Z.; Hua, M.; Talbot, P., Puffing Topography and Nicotine Intake of Electronic Cigarette Users. *PLOS ONE* **2015,** *10* (2), e0117222.

40.   Robinson, R. J.; Hensel, E. C.; Morabito, P. N.; Roundtree, K. A., Electronic cigarette topography in the natural environment. *PLOS ONE* **2015,** *10* (6), e0129296.

41.   Vansickel, A. R.; Edmiston, J. S.; Liang, Q.; Duhon, C.; Connell, C.; Bennett, D.; Sarkar, M., Characterization of puff topography of a prototype electronic cigarette in adult exclusive cigarette smokers and adult exclusive electronic cigarette users. *Regul. Toxicol. Pharmacol.* **2018,** *98*, 250-256.

42.   Voos, N.; Smith, D.; Kaiser, L.; Mahoney, M. C.; Bradizza, C. M.; Kozlowski, L. T.; Benowitz, N. L.; O'Connor, R. J.; Goniewicz, M. L., Effect of e-cigarette flavors on nicotine delivery and puffing topography: results from a randomized clinical trial of daily smokers. *Psychopharmacology* **2020,** *237*, 491-502.

43.   Zhao, T.; Shu, S.; Guo, Q.; Zhu, Y., Effects of design parameters and puff topography on heating coil temperature and mainstream aerosols in electronic cigarettes. *Atmos. Environ.* **2016,** *134*, 61-69.

44.   Mikheev, V. B.; Klupinski, T. P.; Ivanov, A.; Lucas, E. A.; Strozier, E. D.; Fix, C., Particle size distribution and chemical composition of aerosolized vitamin E acetate. *Aerosol Sci. Technol.* **2020,** *54* (9), 993-998.

45.   Li, Y.; Burns, A. E.; Tran, L. N.; Abellar, K. A.; Poindexter, M.; Li, X.; Madl, A. K.; Pinkerton, K. E.; Nguyen, T. B., Impact of e-Liquid Composition, Coil Temperature, and Puff Topography on the Aerosol Chemistry of Electronic Cigarettes. *Chem. Res. Toxicol.* **2021,** *34* (6), 1640-1654.

46.   Carvalho, T. C.; Peters, J. I.; Williams Iii, R. O., Influence of particle size on regional lung deposition–what evidence is there? *Int. J. Pharm.* **2011,** *406* (1-2), 1-10.

47.   Lippmann, M.; Yeates, D. B.; Albert, R. E., Deposition, retention, and clearance of inhaled particles. *Br. J. Ind. Med.* **1980,** *37* (4), 337.

48.   Su, W.-C.; Lin, Y.-H.; Wong, S.-W.; Chen, J. Y.; Lee, J.; Buu, A., Estimation of the dose of electronic cigarette chemicals deposited in human airways through passive vaping. *J. Expo. Sci. Environ. Epidemiol.* **2021**, *31* (6), 1008-1016

49.   Lechasseur, A.; Altmejd, S.; Turgeon, N.; Buonanno, G.; Morawska, L.; Brunet, D.; Duchaine, C.; Morissette, M. C., Variations in coil temperature/power and e-liquid constituents change size and lung deposition of particles emitted by an electronic cigarette. *Physiol. Rep.* **2019,** *7* (10), e14093.

50.   Robinson, R. J.; Eddingsaas, N. C.; DiFrancesco, A. G.; Jayasekera, S.; Hensel Jr, E. C., A framework to investigate the impact of topography and product characteristics on electronic cigarette emissions. *PLOS ONE* **2018,** *13* (11), e0206341.

51.   Kane, D. B.; Li, W., Particle size measurement of electronic cigarette aerosol with a cascade impactor. *Aerosol Sci. Technol.* **2021,** *55* (2), 205-214.

52.   Zhao, D.; Navas-Acien, A.; Ilievski, V.; Slavkovich, V.; Olmedo, P.; Adria-Mora, B.; Domingo-Relloso, A.; Aherrera, A.; Kleiman, N. J.; Rule, A. M.; Hilpert, M., Metal concentrations in electronic cigarette aerosol: Effect of open-system and closed-system devices and power settings. *Environ. Res.* **2019,** *174*, 125-134.

Chapter 2: Formation of Redox-Active Duroquinone from Vaping of Vitamin E Acetate Contributes to Oxidative Lung Injury

2.0 Abstract

In late 2019, the outbreak of e-cigarette or vaping-associated lung injuries (EVALIs) in the United States demonstrated to the public the potential health risks of vaping. While studies since the outbreak have identified vitamin E acetate (VEA), a diluent of tetrahydrocannabinol (THC) in vape cartridges, as a potential contributor to lung injuries, the molecular mechanisms through which VEA may cause damage are still unclear. Recent studies have found that the thermal degradation of e-liquids during vaping can result in the formation of products that are more toxic than the parent compounds. In this study, we assessed the role of duroquinone (DQ) in VEA vaping emissions that may act as a mechanism through which VEA vaping causes lung damage. VEA vaping emissions were collected and analyzed for their potential to generate reactive oxygen species (ROS) and induce oxidative stress-associated gene expression in human bronchial epithelial cells (BEAS-2B). Significant ROS generation by VEA vaping emissions was observed in both acellular and cellular systems. Furthermore, exposure to vaping emissions resulted in significant upregulation of *NQO1* and *HMOX-1* genes in BEAS-2B cells, indicating a strong potential for vaped VEA to cause oxidative damage and acute lung injury; the effects are more profound than exposure to equivalent concentrations of DQ alone. Our findings suggest that there may be synergistic interactions between thermal decomposition products of VEA, highlighting the multifaceted nature of vaping toxicity.

2.1 Introduction

Vaping, or inhalation of aerosolized e-cigarette liquids, has become increasingly popular over the last decade, particularly among adolescents and those trying to quit tobacco cigarettes. (1) The popularity of vaping has largely been attributed to the customization options available (through both the e-cigarette design and liquid flavors) as well as their perception as a safer alternative compared to traditional cigarettes. (2) However, the outbreak of the vaping-related illness, known as EVALI (e-cigarette, or vaping, product use-associated lung injury), in users of e-cigarettes and vaping products highlights the potential contribution of vaping to public health risks.

The wave of vaping-related injuries began in August of 2019, and by February of 2020, the Centers for Disease Control and Prevention (CDC) had reported over 2,800 hospitalizations of patients who displayed symptoms of coughing, dyspnea (shortness of breath), and chest pain characteristic of acute respiratory distress syndrome. (3) Majority of affected patients appeared to be young (under 35), with no history of pre-existing respiratory conditions that may have caused the damage. (4,5) Majority of patients did, however, report the use of e-cigarette or vape products within 3 months preceding the onset of any symptoms. (5) Over 80% of surveyed patients reported that they had used tetrahydrocannabinol (THC)-containing vaping products and 35% used THC exclusively. (4, 5) Evidence suggests that vitamin E acetate (VEA), found in high frequency in illicit cannabinoid-containing vaping cartridges and in the bronchoalveolar lavage of EVALI patients, is strongly linked to the outbreak. (6, 7) However, the exact causative agents and underlying molecular mechanisms remain unclear.

VEA is a synthetic derivative of vitamin E used in the black market or homemade vaping cartridges as a viscosity enhancer to dilute or "cut" THC. In some instances, the ratio of VEA to THC in cartridges linked to EVALI cases was found to be greater than 95%. (7) Alone, vitamin E and its derivatives are considered safe for consumption and are often used in skin-care products for protection against UV-induced damage. (8) However, recent studies have demonstrated that VEA and other e-liquids undergo drastic changes in chemical composition during the vaping process, forming products such as formaldehyde, acrolein, acetaldehyde, and more depending on the oil heated. (9−11) Vaping of VEA, in particular, was found to result in the formation of the reactive quinone species, duroquinone (DQ). (7, 10, 11)

Quinones like DQ are highly redox-active molecules that can undergo redox cycling — a process in which the quinone is reduced by a cellular reductase (such as NADPH quinone reductase) or reducing agent to a semiquinone radical. (12, 13) This radical can then react with molecular oxygen to produce superoxide and re-form the quinone, resulting in the generation of reactive oxygen species (ROS), including superoxide, hydrogen peroxide, and hydroxyl radicals. (14) The redox cycling can continue indefinitely until oxygen or a reducing agent concentration has been depleted, which ultimately leads to oxidative stress and damage to crucial molecules including lipids, proteins, and DNA. (14) In addition to ROS-mediated damage, quinones can act as electrophiles capable of direct damage via Michael addition to macromolecules such as DNA and proteins. (14, 15) Many studies have indicated that inhalation of various

quinone species can lead to detrimental effects on human lung health, especially to airway epithelium. (15−17)

To date, few studies have investigated the potential role of the thermal degradation products of VEA in acute lung injuries. For this reason, the objective of this study was to assess the potential of DQ produced during VEA vaping to induce oxidative damage in human airway epithelial cells as a possible contributing factor. VEA vaping emissions were analyzed using gas chromatography/mass spectrometry (GC/MS) methods and applied to human airway epithelial cells (BEAS-2B) to assess oxidative potential and toxicological responses upon exposure. Additionally, we investigated the size distribution of vaping aerosols and chemical constituents at different size fractions to characterize the potential risk of aerosol lung deposition.

2.2 Materials and Methods

2.2.1 Materials

dl-α tocopherol acetate (VEA, >97%), dl-α tocopherol (vitamin E, >97%), tetramethyl-1,4-benzoquinone (DQ, >98%), durohydroquinone (DHQ, >95%), tert-butyl hydroperoxide (TBHP, 70% in water), and sodium hydroxide (NaOH, 1.0 M in water) were purchased from Tokyo Chemical Industry (TCI America, Inc.). 1,3,5-Trichlorobenzene (TCB, 98%) was purchased from Alfa Aesar. Acetonitrile (ACN, 99.95%) was purchased from Fisher Chemical. Triton X-100 (10% w/v) was purchased from Roche. Cell-grade dimethyl sulfoxide (DMSO) was purchased from MP Biomedicals. 2′,7′-Dichlorodihydrofluorescein diacetate ($DCFH_2DA$) was purchased

from Cayman Chemical Company. Phosphate buffered saline (PBS, 1X) was purchased from Corning. Fluoro-Max Green Fluorescent Microspheres (0.27 μm) were purchased from Thermo Scientific.

2.2.2 Sample Collection

The procedure for collecting VEA vaping aerosols was adapted from previous studies (10, 11, 18) to maintain reproducibility with other e-cigarette research. The vape pen (CCell M3b) was operated at 3.6 V. The average peak temperature of the heating element was measured to be 218.6 ± 3.6 °C using a 1 mm grounded k-type thermocouple wire (MN Measurement Instruments) following the protocol previously described in Chen et al. (19) (**Figure S2.1**). The full protocol for the measurement of the heating element temperature is described in the Supporting Information (SI).

A fresh cartridge (CCell TH2; 0.5 mL, 2.2 Ω) was used for each collection. Prior to each collection, the cartridge was filled with VEA standard oil, weighed, and preconditioned by taking three to five puffs until the oil was properly warmed. Vaping emissions were collected using a cold trap apparatus on dry ice to condense emission products. One 4 s puff was taken at intervals of 30 s using a 0.4 L min–1 air flow rate, which was controlled by a 0.46 L min–1 critical orifice connected a diaphragm pump (Gast Manufacturing Inc.) (**Figure S2.2**). After 20 puffs, the vape pen was rested for 10–20 min to prevent overheating of the battery and cartridge. Collections were repeated a total of four times for quantification and statistical analysis.

Condensed vaping emissions were dissolved in ACN for chemical analysis or in cell culture media for cell exposure. To increase the solubility of VEA vaping emissions in aqueous media, DMSO was added to each collection so that the final concentration was 0.1% v/v DMSO.

2.2.3 GC/MS Analysis

GC/MS (Agilent 6890N GC and 5975C inert MSD equipped with an electron ionization (EI) ion source) analysis was performed to identify and quantify decomposition products from VEA vaping. The detailed procedures for the operation of GC/MS have been reported previously. (20) For nonpolar compounds such as untransformed VEA, 2 μL of samples were directly injected into an Agilent J&W DB-5MS column (30 m × 0.25 mm i.d., 0.25 μm film) for separation. The GC was set to 60 °C for 1 min, ramped to 150 °C at a rate of 3 °C min^{-1}, held at 150 °C for 2 min, ramped to 310 °C at a rate of 20 °C min^{-1}, and held at 310 °C for 5 min. A solvent delay of 6 min was used. For polar degradation products such as DQ, 2 μL of the sample was directly injected into an Rtx-VMS fused silica column (30 m × 0.25 mm i.d., 1.4 μm film). The GC was set to 35 °C for 1 min, ramped to 240 °C at a rate of 10 °C min^{-1}, and held 4 min. A solvent delay of 6 min was also used. Compounds were identified using the NIST 2008 mass spectral database; emission products were confirmed and quantified using corresponding authentic or surrogate standards dissolved in ACN.

2.2.4 Cell Culture

Human bronchial epithelial cells (BEAS-2B) were purchased from the American Type Culture Collection (ATCC). Cells were cultured in either Gibco LHC-9 medium (1X) (Invitrogen) or supplemented Bronchial Epithelial Growth Medium (BEGM; Lonza). Cells were incubated at 37 °C and 5% CO_2 until confluent (75–80%) and transferred to 96- or 24-well plates for exposure experiments.

2.2.5 Cytotoxicity Analysis

BEAS-2B cells were grown in 96-well plates at initial seeding densities of 6×10^3 cells per well and allowed 24 h for attachment. Wells were then treated with 2-fold dilutions of VEA vaping emissions, unvaped VEA, or DQ standard for 24 h. The highest concentration of VEA vaping emissions and unvaped VEA used to expose cells was 125 mg mL^{-1}, though the actual concentration available to cells may have been lower due to solubility issues. The highest concentration of DQ used was 25 μg mL^{-1} as this was the corresponding concentration of DQ produced in VEA vaping emissions at the time of cell exposure. Untreated cells were included as negative controls, while cells treated with 0.1% v/v Triton X-100 were used as positive controls to simulate 100% cell death. DMSO was added to each treatment so that the final concentration was 0.1% v/v. To account for cytotoxicity induced by DMSO, 0.1% v/v DMSO in media was used as a vehicle control. Finally, 100 puffs of vaped deionized (DI) water was used as a vaping device control. To measure cytotoxicity after exposure, the lactate dehydrogenase (LDH) cytotoxicity assay was used as a measure of cell membrane integrity. The assay was

performed following the manufacturer's protocol (Roche), and absorbance was measured on a TECAN SpectraFluor Plus microplate reader at 490 nm, with a reference wavelength at 620 nm. Light absorbance by the mixture of LDH assay reagent and treatments themselves was also considered and subtracted before analysis.

2.2.6 Detection of ROS

2.2.6.1 Acellular 2',7'-Dichlorodihydrofluorescein (DCFH2) Assay

To measure exogenous ROS production, the $DCFH_2$ fluorescent assay was used. Two hundred microliters of a 5 mM $DCFH_2DA$ solution in DMSO was chemically hydrolyzed with 4.8 mL of 0.01 M NaOH for 30 min in the dark. After 30 min, 10 mL of 1X PBS was added to neutralize the reaction and reduce the risk of auto-oxidation; [21] the solution was then placed on ice in the dark until use to prevent photo-oxidation. One hundred microliters of either dilutions of DQ, unvaped VEA, or VEA vaping emissions in DMSO were added to the wells of a black, clear-bottom 96-well plate (Corning), followed by 100 μL of chemically hydrolyzed $DCFH_2$. To account for background fluorescence or photo- or auto-oxidation of $DCFH_2$, $DCFH_2$ in DMSO only (no treatment added) was also assessed. To account for the role of metals in ROS generation, 100 puffs of vaped DI water were used as a vaping device control. Finally, 120 μm TBHP was used as a positive control to induce ROS production. Fluorescence intensity was measured every 5 min for 75 min (excitation: 485 nm, emission: 535 nm) using a GloMax Multi+ Plate Reader (Promega) with Instinct Software.

2.2.6.2 Cellular DCFH₂DA Assay

The DCFH₂DA assay was also performed in the cellular system to measure intracellular ROS in BEAS-2B cells. Cells were seeded in 96-well plates at densities of 6×10^3 cells per well for 24 h at 37 °C prior to exposure. After 24 h, the media was removed, and each well was washed with 50 μL of PBS. After washing, cells were exposed to 100 μL of a 15 μM solution of DCFH₂DA in cell culture media and incubated at 37 °C for 45 min. The dye solution was subsequently removed, and 100 μL of treatment or control groups were added upon exposure. All treatments in media contained 0.1% v/v of DMSO. Background fluorescence of cell-free DCFH₂DA in media with 0.1% v/v DMSO was also measured. The fluorescence intensity was measured following the same protocol as described in Section 2.6.1.

2.2.7 Biomarker Analysis

2.2.7.1 Cell Exposure, RNA Extraction, and Purification

To assess the alteration of oxidative stress-associated gene expression, BEAS-2B cells were seeded in 24-well plates at densities of 6×10^4 cells per well and allowed 24 h for attachment. Cells were then exposed to 65 mg mL⁻¹ of VEA vaping emissions, 65 mg mL⁻¹ of unvaped VEA, 12.5 μg mL⁻¹ of DQ standard, 100 puffs of vaped DI water, or 50 μM TBHP for 6 h to assess the expression of heme oxygenase I (*HMOX-1*) and 24 h to assess expression of NAD(P)H quinone dehydrogenase 1 (*NQO1*) (**Figure S2.3**). Untreated cells were included as negative controls. After exposure, cells were lysed with 300 μL of cold TRI reagent (Zymo Research) for total RNA isolation. The RNA was

extracted using the Direct-zol RNA MiniPrep kit (Zymo Research). A Nanodrop ND-2000C spectrophotometer (Thermo Fisher Scientific) was used to determine the RNA quality (A260/280 ratios) and concentrations. A260/280 ratios for all RNA samples chosen for gene expression analysis were above 1.8. Purified RNA samples were stored at −80 °C until further processing.

2.2.7.2 qPCR

Expression levels of NQO1 and HMOX-1 genes were measured using the one-step QuantiFast SYBR Green RT-PCR kit (Qiagen). The QuantiTect Primer Assays (Qiagen) of NQO1 (GeneGlobe ID: QT00050281) and HMOX-1 (GeneGlobe ID: QT00092645) were used in this study. The results were normalized to a housekeeping gene β-actin (ACTB) (Qiagen, GeneGlobe ID: QT00095431) and expressed as $\log_2$ fold changes over the unexposed controls. A CFX96 Touch Real Time PCR detection system (Bio-Rad) was used. Thermal cycling conditions for RT-PCR were set as follows: 10 min at 50 °C for reverse transcription, 5 min at 95 °C for initial denaturation, and 40 cycles of amplification (10 s at 95 °C and 30 s at 60 °C).

2.2.8 Aerosol Analysis

A Scanning Electron Mobility Spectrometer (SEMS; Brechtel Manufacturing Inc.) was used to determine the volume and size distribution of VEA vaping aerosols emitted directly from the vape pen. The aerosol collection efficiency of the cold trap method was determined by measuring the volume and number concentrations at the

inflow and outflow of a first cold trap and the outflow of a second cold trap (**Figure S2.4**).

A micro-orifice uniform deposit impactor (MOUDI, Mo. 110; MSP Corporation) was used to determine the distribution of identified compounds in different sizes of aerosols. To collect size-fractionated aerosol samples, the vape pen was connected to a 4 L jar; emissions were vaped into the jar using the previously described protocol. A diaphragm pump was used to pull emissions through the MOUDI at a flow rate of 30 L min^{-1}. The pump was allowed to run for 1 h after completion of aerosol generation to ensure that all particles were deposited on MOUDI stages lined with aluminum foil. Collected size-fractionated vaping aerosols on foil stages were extracted with 5 mL of ACN and sonicated for 30 min. Samples were dried with a gentle N_2 gas stream to 100 μL, with 10 μL of 1,3,5-TCB solution (2 μg $μL^{-1}$) added to the samples as an internal standard, and subsequently analyzed using GC/MS following the method described in Section 2.2.3. The experimental setup is shown in the SI (**Figure S2.5A**).

To verify the cut sizes of MOUDI stages, 0.27 μm of green fluorescent microspheres (Thermo Fisher Scientific) that correspond to the mode of vaping aerosol size distribution were nebulized and pulled through the MOUDI to deposit on foil-lined stages. **Figure S2.5B** shows the microspheres deposited at the expected cut size, confirming the stages expected to see the majority of VEA vaping emissions.

2.2.9 Statistical Analysis

GraphPad Prism 9 was used to analyze differences in $DCFH_2DA/DCFH_2$ activities and gene expression levels after treatment. Two-way analysis of variance (ANOVA) with Tukey HSD post-hoc analysis was used to determine the statistical significance of treatments compared to the untreated control. A *p*-value <0.05 was considered statistically significant.

2.3 Results

2.3.1 GC/MS Analysis of VEA Emissions
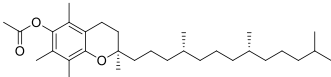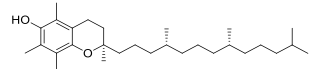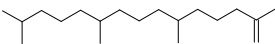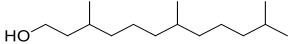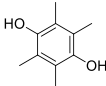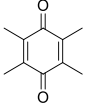
Previous studies have found that several factors can impact the formation and collection efficiency of various compounds in vaping emissions, including the model of e-cigarette tested, puffing topography (e.g., puff duration, puffing interval, and air flow rate), and collection method. (18, 22, 23) GC/MS analysis of VEA vaping emissions at 3.6 V revealed a wide range of decomposition products (**Figures S2.6** and **S2.7**). While a large portion of the spectra remains unidentified, we were able to attribute approximately 21% of the total mass of VEA consumed by the vape pen to major emission products of duroquinone, durohydroquinone (DHQ), vitamin E, and VEA. We have also tentatively identified 3,7,11-trimethyl-1-dodecanol as a decomposition product based on a consistent NIST MS spectral library reverse match score of 900 or greater, and 1-pristene based on comparison of experimental mass spectra with spectra previously reported in the literature by Mikheev et al., (24) which describes fragment ions of *m/z* 111, 126, and 181 that are consistent with our results. Due to the lack of available authentic standards, 1-

dodecanol was used as a surrogate to quantify 3,7,11-trimethyl-1-dodecanol and 1-pristane was used to quantify 1-pristene. **Table 2.1** summarizes the production yields of each identified compound per milligram of VEA consumed by the vape pen. Information regarding predicted molecular weight, boiling point, and vapor pressures of compounds was obtained from ChemSpider (25) based on the estimates from Environmental Protection Agency (EPA)'s EPI Suite program. The determined yields were used to calculate the concentrations of DQ standard expected to be found in corresponding vaped VEA collections for use in cell exposures. To account for variations between vaping aerosol collections, production yields of DQ were quantified prior to each cell exposure experiment to determine the corresponding DQ concentrations in each vaped VEA treatment.

The detection of these products is consistent with prior findings, (10, 11, 24) though the mass yield of DQ shown here is 3 times lower than that of previously reported. (11) This difference may be attributed to an increased flow rate compared to our previous study, which may decrease the residence time of parent oil in the cartridge and ultimately decrease the amount of VEA that is transformed by the heated coil. In addition, other studies have identified decomposition products that could not be found in our spectra, such as ketene or durohydroquinone monoacetate (DHQMA). (10, 24) Absence of these compounds in our spectra may be attributed to differences in the collection method and vape pen operation. The cold trap collection method used in this study was optimized for the collection of compounds such as DQ and VEA, whose boiling points are well above the temperature of dry ice and are easily captured for

analysis. For compounds with high vapor pressure, such as ketene, the use of dry ice to condense emissions may not capture gas-phase products as efficiently as liquid nitrogen used in prior studies. (10) Ketene, which has an approximate boiling point of −56 °C, (25) was not expected to be observed in our collection. In addition, observation of carbonyl-containing compounds from GC/MS often requires derivatization methods that were not used in this study. (10, 26) As such, it is highly likely that ketene and other higher volatility compounds are produced during the vaping process but cannot be observed in our results.

Table 2.1. Summary of VEA vaping emission production yields. Five major emission products were quantified using authentic or surrogate standards.

Name	Formula	M.W.[a]	B.P.[b]	Estimated vapor pressure[c]	Structure	EIC (*m/z*)[d]	Production Yield[e]
Vitamin E acetate (VEA)	$C_{31}H_{52}O_3$	472.7	485	4.03×10^{-8}		472	$(1.68 \pm 0.09) \times 10^{-1}$
Vitamin E	$C_{29}H_{50}O_2$	430.7	486	1.35×10^{-8}		205	$(2.21 \pm 0.01) \times 10^{-2}$
1-Pristene	$C_{19}H_{38}$	266.5	290	5.8×10^{-3}		126	$(1.07 \pm 0.07) \times 10^{-2}$
3,7,11-Trimethyl-1-dodecanol	$C_{15}H_{32}O$	228.4	279	2.11×10^{-4}		111	$(3.44 \pm 0.20) \times 10^{-4}$
Durohydroquinone (DHQ)	$C_{10}H_{14}O_2$	166.2	312	1.77×10^{-6}		166	$(2.20 \pm 0.13) \times 10^{-4}$
Duroquinone (DQ)	$C_{10}H_{12}O_2$	164.2	230	1.26×10^{-3}		121	$(7.70 \pm 0.28) \times 10^{-5}$

[a] M.W.: molecular weight (g mol^{-1})
[b] B.P.: boiling point (°C) at 1 atm
[c] Estimated vapor pressure: mmHg at 25 °C
[d] Extracted ion chromatogram (EIC); ion selected for quantification
[e] mg-Product recovered mg-VEA comsumed^{-1}

Furthermore, the current study analyzed vaping emissions produced at an average peak temperature of 218 °C (3.6 V), which is a lower temperature than what has previously been reported in the literature at similar applied voltages for VEA vaping. (27, 28) Differences in measured coil temperature may be attributed to the design of the device used. In Lynch et al. (27) and Wu et al., (10) where coil temperatures reach up to 600 °C, coils with 0.25–1.8 Ω resistance were used, compared to the 2.2 Ω resistance coil at 3.6 V used in our study. This difference in coil resistance may impact the resulting power output and the temperatures the heating element was able to reach, even when operated at the same voltage setting. The cartridge in this study was chosen as it is a product intended for use in THC vaping and was a brand found to be used by patients who developed EVALI symptoms. (7, 29) It is highly possible that the temperature used in VEA vaping may impact the identity and quantity of certain decomposition products. (30)

Finally, previous reports of VEA thermal degradation have found VEA to be thermally stable up to temperatures ≥ 250 °C; (31) in addition, the temperature used here (218 °C) is, to our knowledge, the lowest reported temperature at which DQ production has been observed. The differences in these findings may be attributed to a catalytic effect between VEA oil and the metal constituents of the cartridge that the oil must come into contact with during vaping. One study by Saliba et al. (32) recently investigated the pyrolysis of propylene glycol (PG) and found that the presence of a metal heating coil during pyrolysis greatly impacted the temperature at which PG began to decompose into carbonyl-containing compounds. In the presence of stainless steel, Kanthal, or aged

nichrome, the temperature at which peak methylglyoxal production was observed was decreased by nearly 300 °C compared to pure pyrolysis in the absence of metal. Thus, is it highly possible that VEA may be interacting with metals in the device in a similar way, resulting in a catalytic effect to degrade VEA at lower temperatures. However, further study into the impact of temperature and vaping device construction of VEA degradation should be explored.

2.3.2 Cytotoxicity Analysis

BEAS-2B cells were exposed to 2-fold serial dilutions of unvaped VEA, VEA vaping emissions, and DQ standard for 24 h before cytotoxicity was assessed. The results of the LDH assay support our prior findings of differential toxicity after the vaping process. (11) There is a considerable shift in cytotoxicity between cells exposed to unvaped VEA and those exposed to VEA vaping emissions (**Figure 2.1**); a clear dose-dependent response can likewise be observed when cells are exposed to DQ alone. Neither the vehicle nor device controls demonstrated significant cytotoxicity. At corresponding DQ concentrations, DQ can account for nearly 50% of the observed cytotoxicity in VEA vaping emission-exposed cells. Concentrations not found to be overly toxic (≤30%) within the 24 h exposure period were chosen for further gene expression analysis. (33)
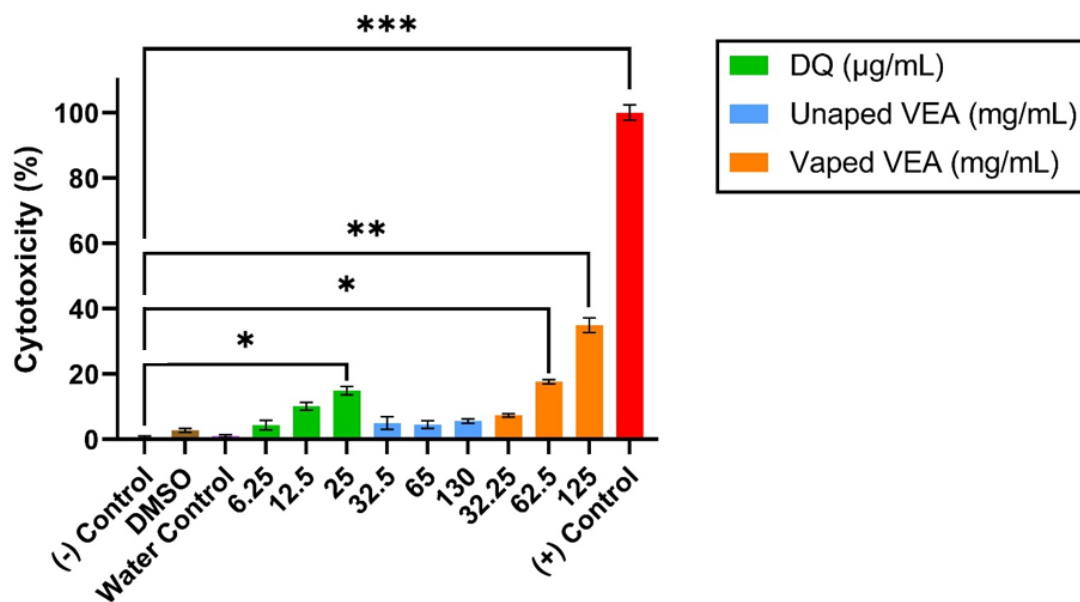
Figure 2.1. Cytotoxicity measured by the LDH assay for BEAS-2B cells exposed to (A) unvaped VEA and VEA vaping emissions and (B) DQ standard at corresponding concentrations based on determined production yields. The results are expressed as the mean of three technical replicates (n=3) ± the standard error of the mean (SEM). * Indicates $p < 0.05$; ** indicates $p < 0.01$; *** indicates $p < 0.001$.

2.3.3 ROS Production

DCFH$_2$DA is a fluorescent assay used to measure general oxidative potential in both cellular and acellular systems. In its nonfluorescent form, DCFH$_2$DA can easily enter through lipid membranes. (21, 34) Once transported into the cytosol, it may be deacetylated by intracellular esterases, converting it to DCFH$_2$, a nonfluorescent form that cannot cross cellular membranes as readily and can be oxidized by reactive species to form the fluorescent product 2′,7′-dichlorofluorescein (DCF). (21, 34−36) The deacetylation process can also be done in acellular systems by chemically hydrolyzing DCFH$_2$DA into DCFH$_2$ using NaOH; (35, 37, 38) this form can then be oxidized by a compound of interest and/or generated H$_2$O$_2$ (**Figure S2.8**).

Quinones such as DQ are highly electrophilic and have the potential to generate large amounts of ROS through redox cycling; generated ROS can then damage cellular membranes and other macromolecules critical to regular function. However, assessment of only this exogenous oxidative potential does not account for ROS generated by the cell itself during metabolic processes or immune responses to a xenobiotic. (39, 40) Endogenous ROS can contribute greatly to intracellular redox homeostasis, further inducing oxidative stress. (41, 42) Assessment of both the oxidative potential and the total cellular ROS produced upon exposure to a toxicant can help to better elucidate the mechanism of toxicity and the risk of oxidative damage to cells.

The DCFH$_2$DA/DCFH$_2$ assay was studied in both acellular and cellular systems over 75 min after either addition of the DCFH$_2$ or exposure of treatments and controls to BEAS-2B. The time course results of both assays can be found in the SI (**Figure S2.9**). **Figure 2.2** summarizes the exogenous oxidative potential of treatments in the acellular system (**Figure 2.2A**) and the intracellular ROS measured in BEAS-2B exposed to treatments (**Figure 2.2B**); results are expressed as the fold change in fluorescence intensity compared to the negative control. After 75 min, neither unvaped VEA nor the device control induces significant ROS generation in either system. In the acellular system, DQ and VEA vaping emissions both demonstrate the ability to generate ROS significantly compared to the solvent alone; note that equivalent concentrations of DQ standard alone show greater ROS production than VEA vaping emissions. In addition, all concentrations of DQ standard reacted more quickly with DCFH$_2$ than VEA vaping emissions (**Figure S2.9B, C**). In the cellular system, however, only the highest

concentration of VEA vaping emissions resulted in significant ROS generation (p = 0.0329).

In the acellular system, DQ was expected to demonstrate high $DCFH_2$ oxidation both through the generation of ROS during redox cycling, as well as through direct oxidation by DQ or adduct formation of DQ and $DCFH_2$ via Michael addition. While DQ is an electrophilic compound and has already been observed in vaping emissions, VEA emissions constitute a mixture of electrophiles, metals, and antioxidants (such as vitamin E) that may compete with the $DCFH_2$ probe to be oxidized. These nontarget interactions may suppress the overall response observed by VEA vaping emissions compared to DQ alone in the acellular system. In the cellular system, there exists an even larger array of scavengers — biomolecules, lipids, and other antioxidants — that may compete with the probe to be oxidized by generated ROS. Antioxidant molecules may also interact with the probe itself and cause attenuation of the probe before it is able to be oxidized by ROS, (43) resulting in a reduced signal compared to the acellular system. For DQ-treated cells, it is likely that the concentration of DQ is not great enough to overcome competition by scavengers, resulting in decreased ROS production or the ability to stimulate endogenous ROS production. In contrast, the highest concentration of VEA vaping emissions, being a mixture of degradation products, may have contained a greater amount of electrophilic species to compete with scavengers to oxidize DCFH2 and/or contained compounds able to induce endogenous ROS production by the cells. (41) Nevertheless, these findings support that VEA vaping emissions and DQ are both capable of generating ROS that may induce oxidative damage in exposed cells.
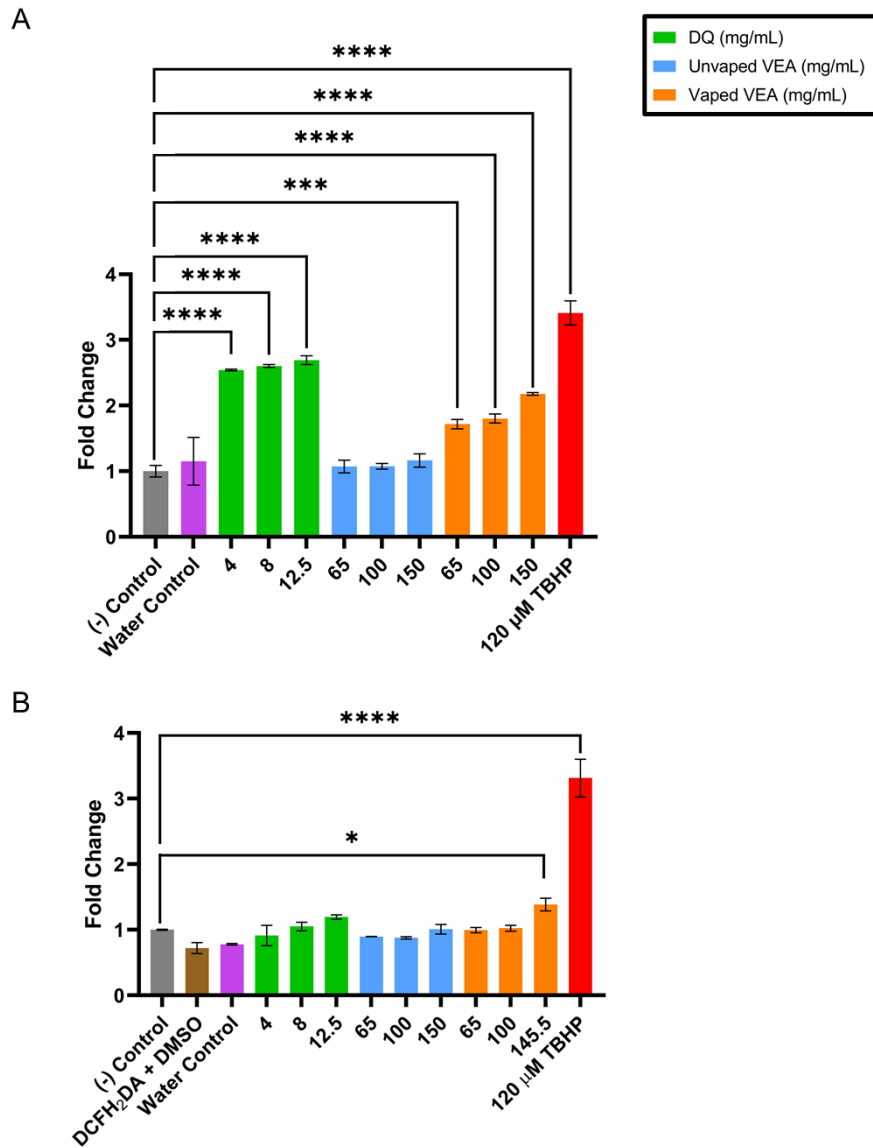
Figure 2.2. ROS generated at 75 minutes by unvaped VEA, VEA vaping emissions, DQ standard, and DMSO, water and TBHP positive controls in (A) acellular and (B) cellular systems. Results were normalized to their cytotoxicity and are expressed as fold change in fluorescence intensity over the untreated control in the acellular or cellular system. Each treatment is expressed as the mean ± SEM (n=3) for both acellular and cellular assays. Two-way ANOVA was used to determine statistical significance compared to the negative control. * Indicates $p < 0.05$; *** indicates $p < 0.001$; **** indicates $p < 0.0001$.

2.3.4 Gene Expression Analysis

The relative levels of gene expression for the exposure and control groups, expressed as the $\log_2$ fold changes, were calculated using the comparative cycle threshold ($2^{-\Delta\Delta CT}$) method. (44) *NQO1* was chosen as a biomarker of quinone toxicity as the enzyme is known to compete with quinone reduction pathways that may initiate quinone redox cycling; (45) DQ has been used in several studies as a model quinone substrate to induce *NQO1* expression in various cell types. (46−48) *HMOX-1*, in contrast, is a stress-induced enzyme and is a commonly used biomarker of downstream oxidative damage. (49) Our results show that exposure to DQ and VEA vaping emissions results in significant upregulation of *HMOX-1* and *NQO1* compared to the untreated control (**Figure 2.3**). *HMOX-1* and *NQO1* expression by vaping emissions was found to be significantly greater than expression seen in DQ-exposed cells ($p < 0.0001$ for *HMOX-1* expression and $p = 0.0391$ for *NQO1* expression). Neither unvaped VEA, the DMSO vehicle control, nor the water device control resulted in significant gene expression change of either biomarker.
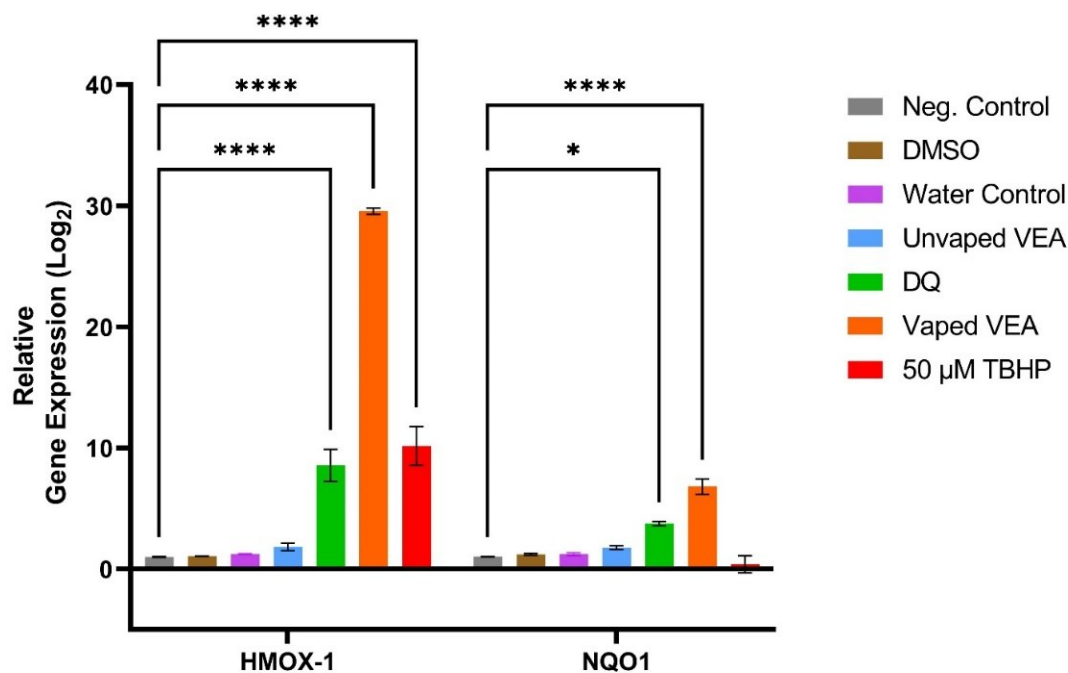
Figure 2.3. Relative expression in BEAS-2B cells of *HMOX-1* and *NQO1* genes after 6- and 24-hour exposure, respectively, to 65 mg/mL of VEA vaping emissions, 65 mg/mL of unvaped VEA oil, 12.5 µg/mL of DQ standard, and 100 puffs of vaped DI water collected in cell culture media. 50 µM TBHP was used as a positive control for *HMOX-1* expression. Results are expressed as the mean fold change ($\log_2$) over unexposed controls and normalized to a housekeeping gene (ACTB) ± SEM of 3 samples per treatment (n=3). Two-way ANOVA was used to determine statistical significance compared to the negative control. * Indicates *p<0.05*; **** indicates *p<0.0001*.

NQO1 and *HMOX-1* upregulation by DQ and VEA vaping emissions provides evidence that quinones are present in vaping emissions at concentrations that pose a risk to the alteration of cellular homeostasis, and that both DQ alone and VEA vaping emissions have the potential to induce oxidative damage through the production of ROS or reactions with biomolecules to disrupt redox signaling pathways. (50, 51) The ability of VEA vaping emissions to both induce greater *NQO1* and *HMOX-1* expression than DQ standard alone highly suggests that VEA vaping emissions may contain a mixture of

electrophiles and ROS inducers that are capable of inducing oxidative damage. The significant difference in *NQO1* expression between DQ and vaping emissions may imply the presence of more quinones and quinone-containing species than DQ alone. In addition, studies have found that oxidation of vitamin E by free radicals or ROS results in the generation of vitamin E quinone, which can be reduced by *NQO1* to hydroquinone and again act as an antioxidant. (52) Thus, the increased upregulation of both *NQO1* and *HMOX-1* may also be attributed to interactions between VEA decomposition products in the total mixture. These results overall support that quinone toxicity is one contributing mechanism through which the VEA vaping-induced lung oxidative damage occurs, but the presence of other degradation compounds and metals from the device may either enhance DQ toxicity or provide additional mechanisms of toxicity.

2.3.5 Aerosol Analysis

The majority of particles emitted directly from the vape pen existed between 200 and 400 nm in diameter, though a small fraction of particles can be observed between 60 and 100 nm (**Figure 2.4A, B**). This observed size distribution agrees with recent studies of aerosolized VEA at approximately the flow rate used. (11, 24) The total aerosol collection efficiency of our collection method was estimated to be $\geq$ 99.9% by both volume and number (**Figure 2.4B, C**) after tandem cold trap collection.
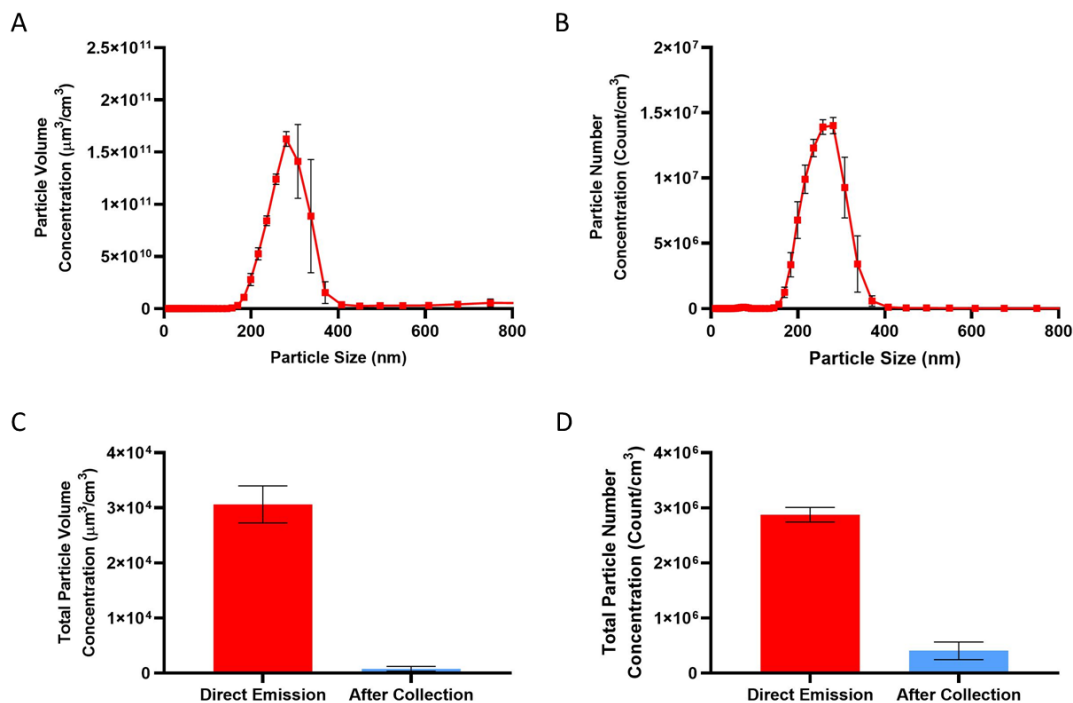
Figure 2.4. Size distribution of VEA vaping aerosols characterized by (A) volume and (B) number concentrations. Collection efficiency was determined by comparing the (C) total particle volume concentration and (D) total particle number concentration sampled immediately after emission from the vape pen and after tandem cold trap collection. Particle collection efficiency was estimated to be $\geq 99.9\%$ by both volume and by number. One puff was taken for each SEMS sampling cycle (3 min). Results are expressed as the average of 3 cycles (n=3) after background subtraction.

The size of emitted particles will greatly impact lung deposition, with smaller particles (≤ 100 nm) capable of penetrating into the lower conducting airways and the alveolar region of the lungs. (53, 54) Based on these results, VEA vaping emissions overall have the potential to penetrate into the lower respiratory system of vape users. To determine the sizes at which DQ and other identified compounds are enriched that have direct implications for the associated risk of lung deposition, we analyzed size-fractionated aerosol composition in vaping emissions. **Table 2.2** depicts the mass fractions of the major decomposition products found from chemical analysis. The stages

containing the largest total mass of particles deposited were those with cut sizes ranging between 180 and 1000 nm. We observed that VEA could be found at all sizes, while the first major decomposition product, vitamin E, favored particle sizes above 180 nm but was not detectable above 1000 nm. 3,7,11-Trimethyl-1-dodecanol showed the greatest fraction in the larger-sized particles (560 nm and above) but was found at detectable levels in particles smaller than 100 nm. DHQ was detectable at diameters greater than 180 nm but only showed substantial deposition above 560 nm. This contrasts with DQ, which could only be found at sizes below 560 nm. The greatest mass fraction of DQ was observed in particles 56–100 nm in diameter. 1-Pristene was not detectable at any particle size. The inability to detect 1-pristene is likely attributable to fast oxidation of the double bond by ozone from room air, which was present at background levels between 30 and 40 ppbv. (55, 56) This background concentration of ozone was not expected to substantially influence the detection of the other target compounds.

Table 2.2. Summary of size-fractioned VEA vaping aerosols. Results are expressed as the mass fraction of total mass collected on each MOUDI stage.

Compound name	Mass Fraction						
	$d \le 56$ (nm)	$56 \le d \le 100$ (nm)	$100 \le d \le 180$ (nm)	$180 \le d \le 320$ (nm)	$320 \le d \le 560$ (nm)	$560 \le d \le 1000$ (nm)	$1000 \le d \le 1800$ (nm)
Vitamin E acetate	9.98×10^{-1}	9.51×10^{-1}	9.99×10^{-1}	9.62×10^{-1}	9.60×10^{-1}	9.45×10^{-1}	9.93×10^{-1}
Vitamin E	b.d.l.[a]	b.d.l.	b.d.l.	3.68×10^{-2}	3.76×10^{-2}	5.02×10^{-2}	b.d.l.
1-Pristene	b.d.l.	b.d.l.	b.d.l.	b.d.l.	b.d.l.	b.d.l.	b.d.l.
3,7,11-Trimethyl-1-docecanol	b.d.l.	1.54×10^{-2}	3.23×10^{-4}	3.15×10^{-4}	1.34×10^{-3}	4.20×10^{-3}	4.86×10^{-3}
Durohydroquinone	b.d.l.	b.d.l.	b.d.l.	4.55×10^{-5}	1.50×10^{-5}	2.51×10^{-4}	1.83×10^{-3}
Duroquinone	1.78×10^{-3}	3.38×10^{-2}	5.30×10^{-4}	1.31×10^{-3}	6.62×10^{-4}	b.d.l.	b.d.l.
Total Mass (mg)[b]	0.852	0.143	2.82	11.2	18.8	19.5	0.415

[a] b.d.l.: below detection limit
[b] Total mass of detected compounds on each MOUDI stage

44

Ultimately, VEA 3,7,11-trimethyl-1-docecanol and DQ were observed to exist as particles with diameters less than 100 nm and therefore are likely the main products able to penetrate the alveolar region of the lungs. The decomposition products show clear potential for differential lung deposition in those who vaped VEA. One recent study found that the chemical composition of e-cigarette aerosols is size dependent and heavily dependent on boiling point and vapor pressure of the aerosol constituents. (57) As shown in **Table 2.1**, the vapor pressures of emitted products vary greatly, which in turn may impact their gas-particle partitioning behavior once released into the environment. This compositional difference in particle size may impact the risk of exposure and negative health effects to people in proximity to active vapers (i.e., passive vaping). With the exception of 1-pristene, transformation of aerosols, or aging, after vaping was not expected to substantially influence the results due to the short residence time in the jar and hydrophobic nature of the target compounds. It is possible that some more hygroscopic constituents may absorb water vapor from room air if leftover time. (58) This process could drastically impact the size of particles, resulting in larger particles that are more likely to deposit in different regions of the airways when inhaled by bystanders. However, to fully understand the dynamic nature of these particles in the environment and the exposure risk via passive vaping, further study is required.

2.3.6 Potential Limitations

Some further limitations to this study should be noted. First, VEA was studied individually in an isolated system to examine the formation and contribution of DQ to oxidative lung injuries, while cartridges linked to EVALI cases were often blended with

varying ratios of VEA and THC. A prior study reported that in both liquid and aerosol phases, THC and VEA can form hydrogen bonded complexes. (59) In addition, a study by Muthumalage et al. (60) recently found that the exposure of BEAS-2B cells and mice to CBD/counterfeit cartridges resulted in greater ROS generation and inflammatory responses than VEA alone. The role of the interactions between these complexes in VEA-induced lung toxicity has not been investigated at this time. Furthermore, toxicological responses following exposure were studied using an immortalized, monoculture cell line, which does not allow for investigation into the systemic effects in vivo. While the parent VEA molecule was not found to induce cytotoxicity in our study, recent reports have demonstrated that VEA and other e-liquids may interact with a pulmonary surfactant at the air–liquid interface, resulting in mechanical injury to the lungs that may contribute to EVALI-symptom onset. (61, 62) Finally, decomposition product formation was investigated at one voltage/temperature setting and puffing topography. However, vaping behavior may vary drastically between users, which has been found to alter the composition, (18, 63) and size and volume distributions (22, 24) of aerosols. The vaping topography used in this study was adapted from previous literature on nicotine vaping, but less is known about the parameters used in THC vaping. (64) As a result, those who vaped VEA could have been exposed to differing concentrations of DQ or aerosol compositions than observed in this study.

2.4 Conclusions

This study investigated the potential contribution of the thermal decomposition product DQ in VEA vaping emissions to induce oxidative stress in exposed lung cells. Our results show that DQ and VEA vaping emissions show significant potential to generate ROS, potentially causing oxidative damage to biomolecules. Moreover, VEA vaping emissions were found to be linked to the upregulation of *NQO1* (a quinone-metabolizing enzyme) and *HMOX-1* (an oxidative stress biomarker) genes, providing evidence of vaping-induced oxidative stress and quinone toxicity as one potential mechanism. Finally, our results support that the decomposition products of VEA may deposit at different lung depths. DQ, in particular, was found to exist at sizes below 100 nm, suggesting its potential to penetrate into the alveolar region of the lungs. Notably, the differential responses between DQ- and VEA vaping emission-exposed cells highlight the need to further investigate the decomposition products of VEA during vaping. The increased responses induced by VEA vaping emissions suggest that while quinone toxicity has a high potential to damage cells, it is likely that the vaping emissions contain a mixture of electrophilic compounds (e.g., aldehydes or ketones), ROS inducers, and metal catalysts that may enhance VEA's oxidative potential. In essence, while our results provide evidence that quinone toxicity may be one of the molecular mechanisms through which VEA vaping causes oxidative lung injuries, it may be one of several mechanisms. It is likely that EVALI symptoms may be the result of synergistic interactions between DQ and other vaping emission products from VEA and THC. (60) To fully understand the molecular mechanisms through which VEA vaping causes lung injury, future studies

are required to investigate potential interactions between decomposition products. The wide variability in chemical compositions that users may have been exposed to as a result of variations in vaping behavior must also be explored in future works.

2.5 Supplemental Information

2.5.1 Temperature Measurements

The protocol for the measurement of the e-cigarette heating element was adapted from Chen et al. (19) A fresh cartridge was filled with VEA oil so the oil level sat above the atomizer base; the cartridge was then connected to the pen battery. To measure the temperature of the heating element upon battery activation, two 1 mm grounded k-type thermocouple wires (MN Measurement Instruments), one inserted into the air tube of the cartridge and rested on the surface of the ceramic heating element and one kept suspended to measure ambient air temperature as a device control, were connected to a 4-channel data logger (Extech). The battery of the vape pen was activated for 4 s to heat the device, then allowed to rest for the remainder of a 1 min cycle. The data logger recorded temperatures every 1 s over the 1 min cycle. The peak heating temperatures of each cycle were averaged to determine the overall temperature of the heating element used in this study.
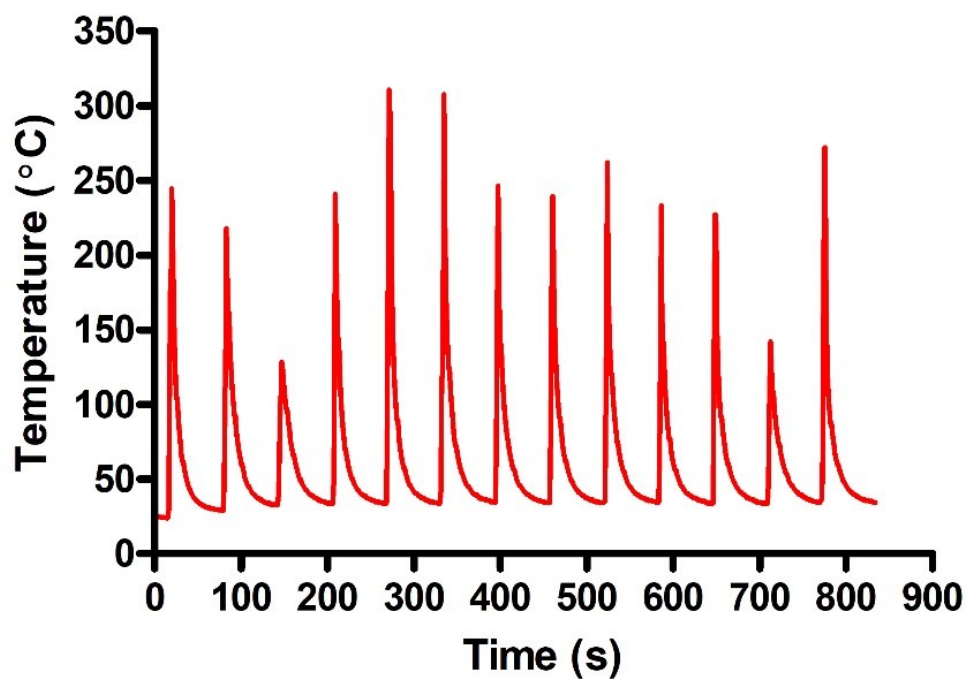
Figure S2.1. Temperature profile of e-cigarette heating element. Temperature measurements were taken every 1 s for each 1-minute cycle. The battery was activated for 4 s to heat the coil, then allowed to rest for the remainder of the minute.
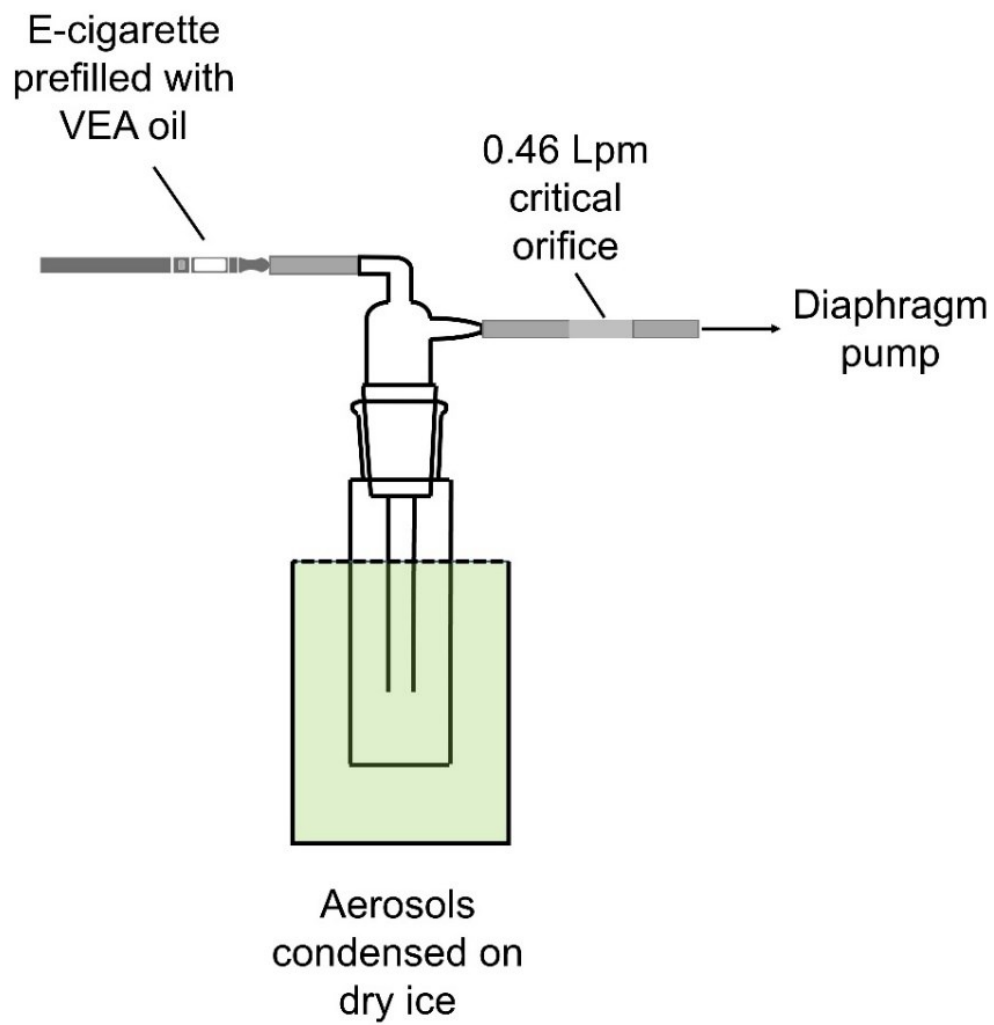
Figure S2.2. Schematic of experimental set up of VEA vaping emission collection. All emissions were generated using a 0.46 L min^{-1} critical orifice to restrict the flow rate. Emissions were vaped into a glass cold trap submerged in dry ice; condensed emissions were dissolved in acetonitrile (ACN) for chemical analysis and cell culture media for cell exposure analysis.
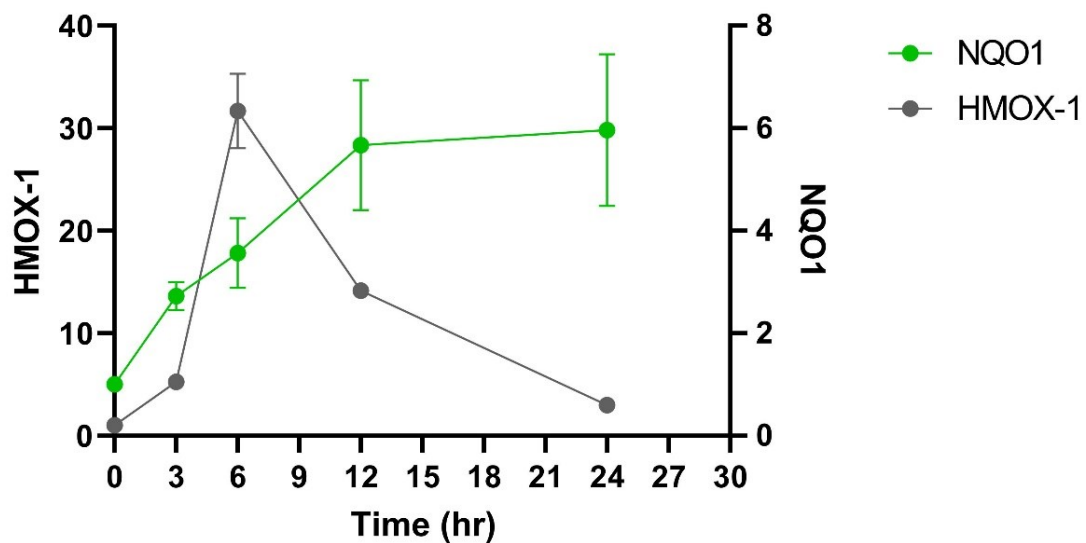
Figure S2.3. Gene expression analysis of *HMOX-1* and *NQO1* genes after 0, 3, 6, 12, and 24 hr exposure to VEA vaping emissions. *HMOX-1* expression was found to peak at 6 hr, while *NQO1* expression peaked at 24 hr. These peak timepoints were used to analyze gene expression of all treatments used. Results are expressed as the mean fold change ($\log_2$) over unexposed controls and normalized to a housekeeping gene (ACTB) ± standard error of the mean (SEM) of 3 samples for each treatment (n=3).
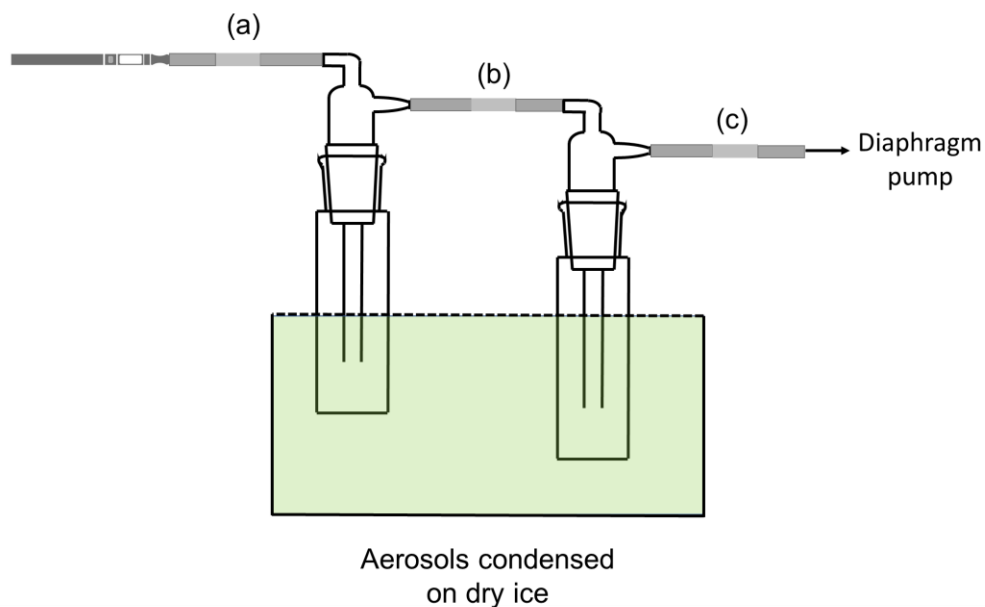
Figure S2.4. Schematic of set up of collection efficiency experiments using a Scanning Electrical Mobility Spectrometer (SEMS). VEA vaping emissions were generated using a diaphragm pump with a flow rate controlled by a 0.46 L min^{-1} critical orifice. The particle volume and number concentrations were measured at three different sites: (a) directly after emission from the e-cigarette, (b) the outflow of one cold trap placed on dry ice to collect condensed emissions, and (c) the outflow of a second cold trap placed on dry ice. The SEMS operated at a flow rate of 0.33 L min^{-1}.
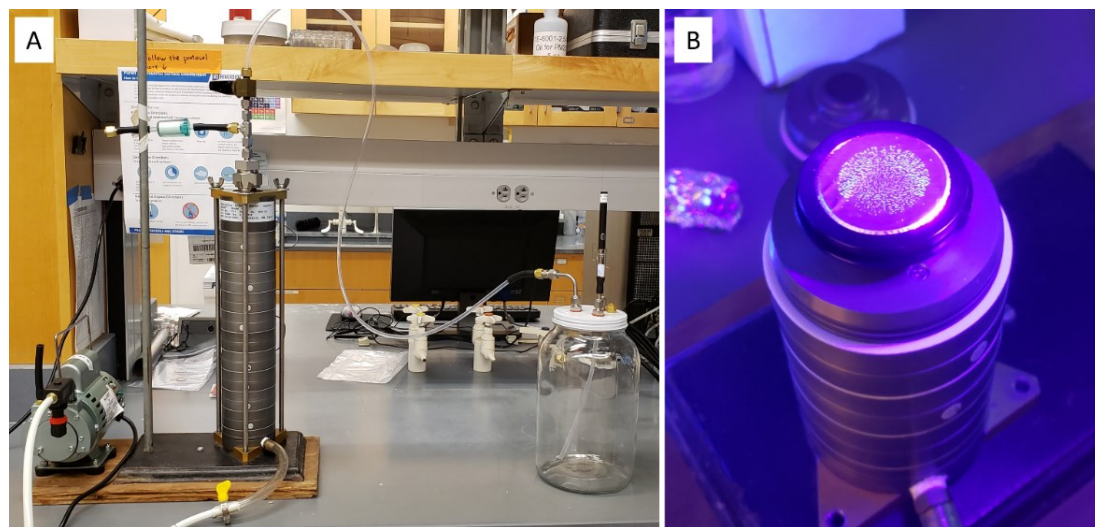
Figure S2.5. (A) Experimental set up of MOUDI size-fractioned VEA vaping aerosols. A 0.46 L min^{-1} critical orifice was used to restrict the flow rate vaping emissions were generated at; filtered room air was used to compensate to reach the 30 L min^{-1} necessary for MOUDI collection. (B) 0.27 µm green fluorescent microspheres deposited at 0.18-0.32 µm MOUDI stage to confirm stage cut sizes. Photos in both panels were taken by authors.
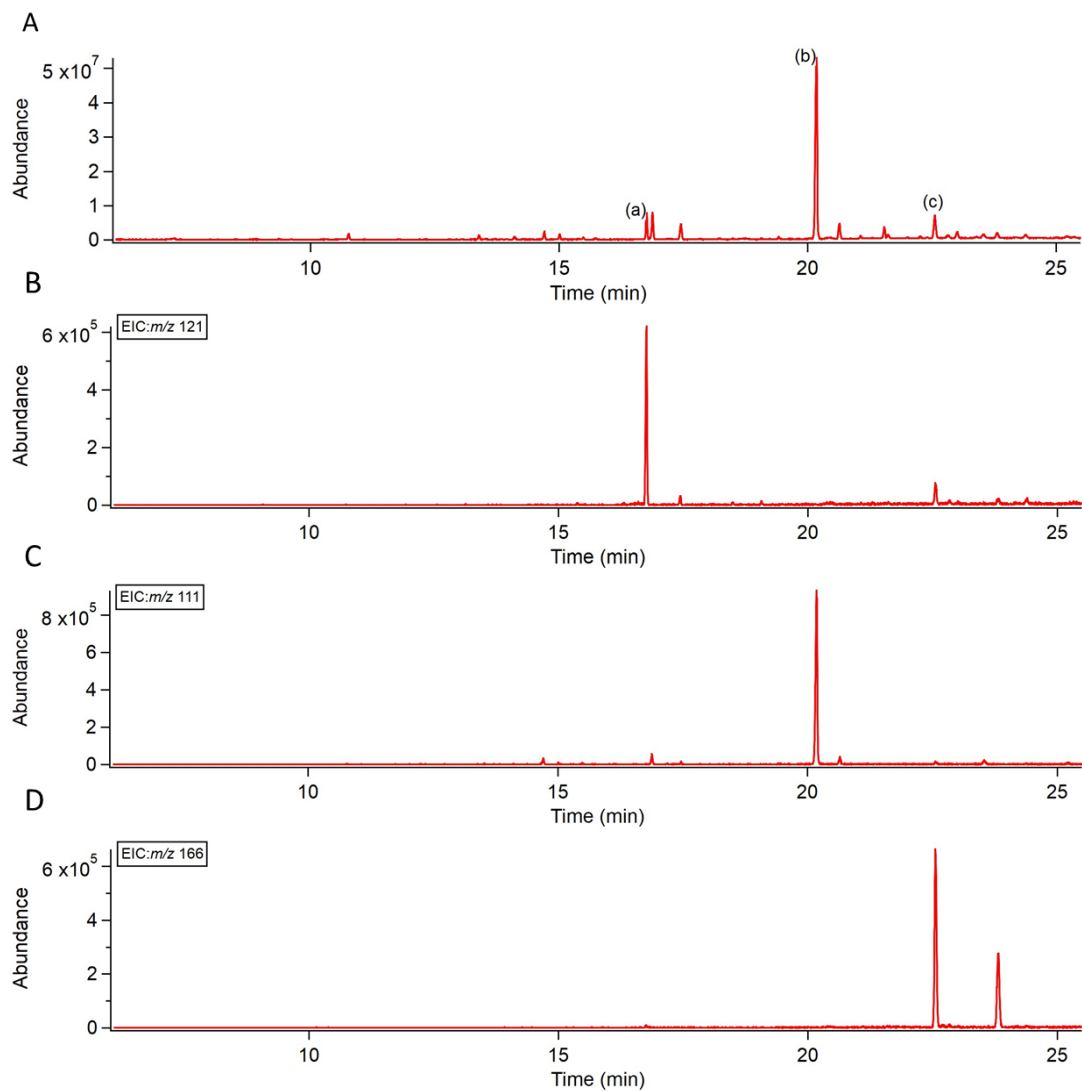
Figure S2.6. Chromatograms obtained from a polar Rtx-VMS fused silica separation column. (A) Total ion chromatograph of vitamin E acetate (VEA) vaping emissions showing (peak a) duroquinone (DQ), (peak b) 3,7,11-trimethyl-1-dodecanol, and (peak c) durohydroquinone (DHQ) at retention times of approximately 16, 20, and 22 minutes, respectively; (B) extracted ion chromatogram (EIC: *m/z* 121) used to identify DQ; (C) extracted ion chromatogram (EIC: *m/z* 111) used to identify 3,7,11-trimethyl-1-dodecanol; (D) extracted ion chromatogram (EIC: *m/z* 166) used to identify DHQ.
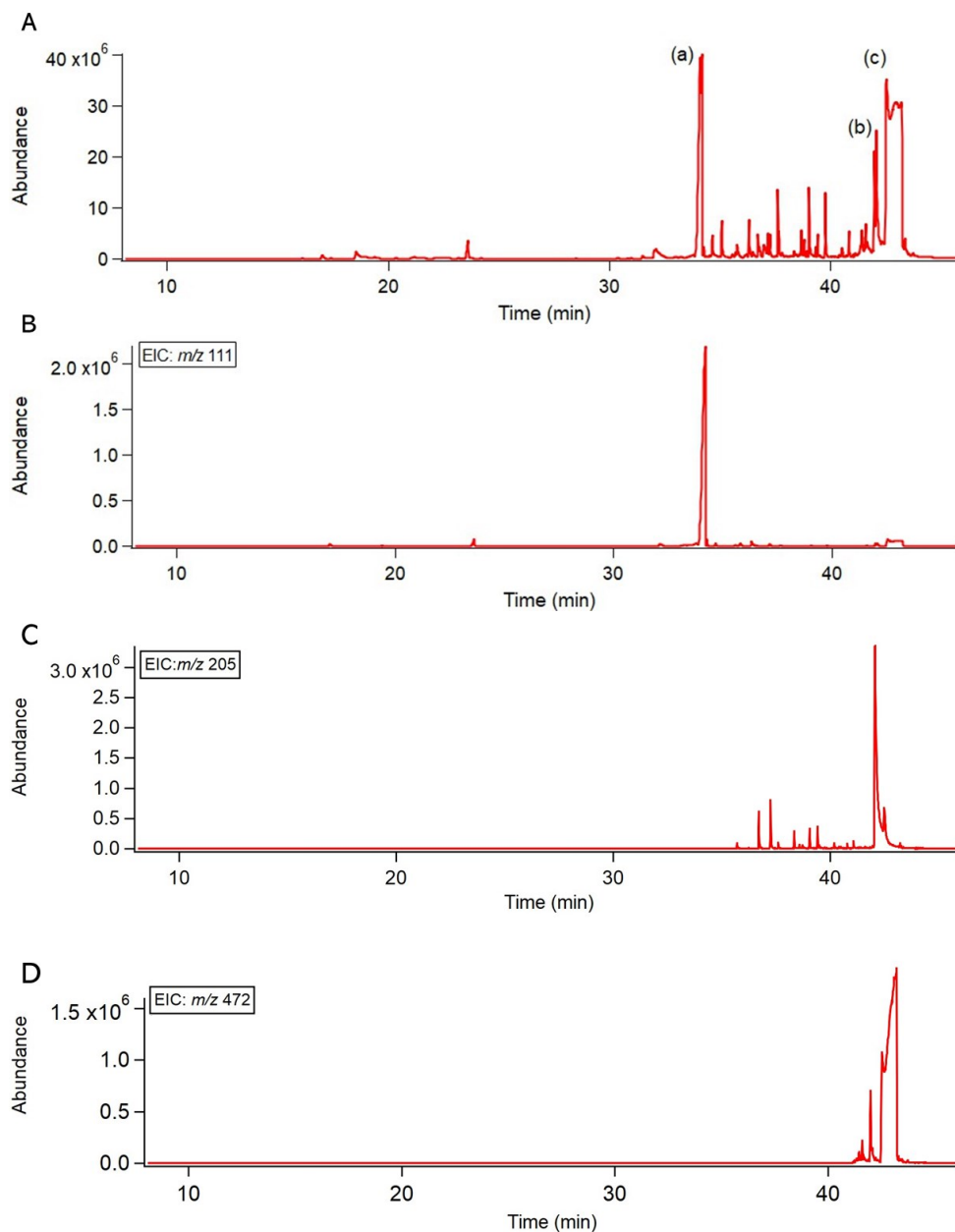
Figure S2.7. Chromatograms obtained from a non-polar J&W Scientific DB-5MS separation column. (A) Total ion chromatograph of VEA vaping emissions showing (peak a) 1-pristene, (peak b) vitamin E, and (peak c) VEA at retention times of approximately 35, 42, and 43 minutes, respectively; (B) extracted ion chromatogram (EIC: *m/z* 111) used to identify 1-pristene, (C) extracted ion chromatogram (EIC: *m/z* 205) used to identify vitamin E, and (D) extracted ion chromatogram (EIC: *m/z* 472) used to identify VEA.

Figure S2.8. DCF reaction scheme; non-fluorescent 2',7'-Dichlorofluorescein diacetate can be hydrolyzed with (a) NaOH for acellular systems or (b) cellular esterases for cellular systems, then oxidized by ROS to form the fluorescent DCF product.
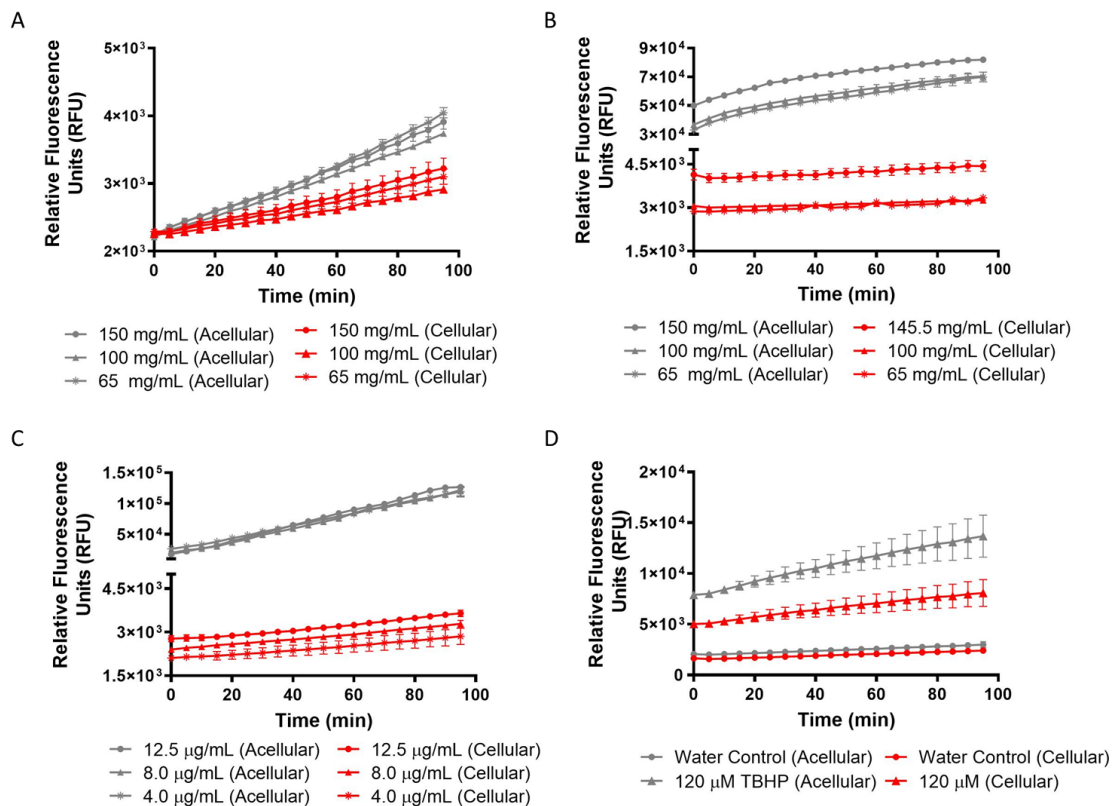
Figure S2.9. Fluorescence intensity of $DCFH_2$ oxidized by (A) unvaped VEA, (B) VEA vaping emissions, (C) DQ standard, and (D) device and positive controls in the acellular versus cellular system. Fluorescence intensity was measured at 5 min intervals for a total of 75 minutes. Results were normalized to their cytotoxicity at 75 minutes. Each experiment was run alongside a solvent blank of DMSO or untreated cells in cell culture media as a negative control. Fluorescence intensity was consistently lower in the cellular system than the acellular.

2.6 References

1.   Miech, R.; Johnston, L.; O'Malley, P. M.; Bachman, J. G.; Patrick, M. E., Adolescent Vaping and Nicotine Use in 2017–2018 — U.S. National Estimates. *N. Engl. J. Med.* **2019,** *380* (2), 192-193.

2.   McKeganey, N.; Barnard, M.; Russell, C., Vapers and vaping: E-cigarettes users views of vaping and smoking. *Drugs (Abingdon Engl)* **2018,** *25* (1), 13-20.

3.   CDC Outbreak of Lung Injury Associated with the Use of E-Cigarette, or Vaping, Products. https://www.cdc.gov/tobacco/basic_information/e-cigarettes/severe-lung-disease.html#map-cases (accessed 7/29/2021).

4.   Lozier, M. J.; Wallace, B.; Anderson, K.; Ellington, S.; Jones, C. M.; Rose, D.; Baldwin, G.; King, B. A.; Briss, P.; Mikosz, C. A., Update: demographic, product, and substance-use characteristics of hospitalized patients in a nationwide outbreak of e-cigarette, or vaping, product use–associated lung injuries—United States, December 2019. *MMWR Morb. Mortal. Wkly* **2019,** *68* (49), 1142.

5.   Layden, J. E.; Ghinai, I.; Pray, I.; Kimball, A.; Layer, M.; Tenforde, M.; Navon, L.; Hoots, B.; Salvatore, P. P.; Elderbrook, M., Pulmonary illness related to e-cigarette use in Illinois and Wisconsin—preliminary report. *N. Engl. J. Med.* **2019**.

6.   Blount, B. C.; Karwowski, M. P.; Shields, P. G.; Morel-Espinosa, M.; Valentin-Blasini, L.; Gardner, M.; Braselton, M.; Brosius, C. R.; Caron, K. T.; Chambers, D.; Corstvet, J.; Cowan, E.; De Jesús, V. R.; Espinosa, P.; Fernandez, C.; Holder, C.; Kuklenyik, Z.; Kusovschi, J. D.; Newman, C.; Reis, G. B.; Rees, J.; Reese, C.; Silva, L.; Seyler, T.; Song, M.-A.; Sosnoff, C.; Spitzer, C. R.; Tevis, D.; Wang, L.; Watson, C.; Wewers, M. D.; Xia, B.; Heitkemper, D. T.; Ghinai, I.; Layden, J.; Briss, P.; King, B. A.; Delaney, L. J.; Jones, C. M.; Baldwin, G. T.; Patel, A.; Meaney-Delman, D.; Rose, D.; Krishnasamy, V.; Barr, J. R.; Thomas, J.; Pirkle, J. L., Vitamin E Acetate in Bronchoalveolar-Lavage Fluid Associated with EVALI. *N. Engl. J. Med.* **2020,** *382* (8), 697-705.

7.   Duffy, B.; Li, L.; Lu, S.; Durocher, L.; Dittmar, M.; Delaney-Baldwin, E.; Panawennage, D.; LeMaster, D.; Navarette, K.; Spink, D., Analysis of Cannabinoid-Containing Fluids in Illicit Vaping Cartridges Recovered from Pulmonary Injury Patients: Identification of Vitamin E Acetate as a Major Diluent. *Toxics* **2020,** *8* (1).

8.   Berton, T. R.; Conti, C. J.; Mitchell, D. L.; Aldaz, C. M.; Lubet, R. A.; Fischer, S. M., The effect of vitamin E acetate on ultraviolet-induced mouse skin carcinogenesis. *Mol. Carcinog.* **1998,** *23* (3), 175-184.

9.   Ogunwale, M. A.; Li, M.; Ramakrishnam Raju, M. V.; Chen, Y.; Nantz, M. H.; Conklin, D. J.; Fu, X.-A., Aldehyde Detection in Electronic Cigarette Aerosols. *ACS Omega* **2017,** *2* (3), 1207-1214.

10.   Wu, D.; O'Shea, D. F., Potential for release of pulmonary toxic ketene from vaping pyrolysis of vitamin E acetate. *PNAS* **2020,** *117* (12), 6349-6355.

11.   Jiang, H.; Ahmed, C. M. S.; Martin, T. J.; Canchola, A.; Oswald, I. W. H.; Garcia, J. A.; Chen, J. Y.; Koby, K. A.; Buchanan, A. J.; Zhao, Z.; Zhang, H.; Chen, K.; Lin, Y.-H., Chemical and Toxicological Characterization of Vaping Emission Products from Commonly Used Vape Juice Diluents. *Chem. Res. Toxicol.* **2020,** *33* (8), 2157-2163.

12.   Ross, D.; Siegel, D., NQO1 in protection against oxidative stress. *Curr. Opin. Toxicol.* **2018,** *7*, 67-72.

13.   Attia, S. M., Deleterious Effects of Reactive Metabolites. *Oxid. Med. Cell. Longev.* **2010,** *3*, 948013.

14.   Bolton, J. L.; Trush, M. A.; Penning, T. M.; Dryhurst, G.; Monks, T. J., Role of quinones in toxicology. *Chem. Res. Toxicol.* **2000,** *13* (3), 135-160.

15.   O'Brien, P. J., Molecular mechanisms of quinone cytotoxicity. *Chem. Biol. Interact.* **1991,** *80* (1), 1-41.

16.   Shang, Y.; Zhang, L.; Jiang, Y.; Li, Y.; Lu, P., Airborne quinones induce cytotoxicity and DNA damage in human lung epithelial A549 cells: The role of reactive oxygen species. *Chemosphere* **2014,** *100*, 42-49.

17.   Li, N.; Venkatesan, M. I.; Miguel, A.; Kaplan, R.; Gujuluva, C.; Alam, J.; Nel, A., Induction of Heme Oxygenase-1 Expression in Macrophages by Diesel Exhaust Particle Chemicals and Quinones via the Antioxidant-Responsive Element. *J. Immunol.* **2000,** *165* (6), 3393-3401.

18.   Williams, M.; Li, J.; Talbot, P., Effects of Model, Method of Collection, and Topography on Chemical Elements and Metals in the Aerosol of Tank-Style Electronic Cigarettes. *Sci. Rep.* **2019,** *9* (1), 13969.

19.   Chen, W.; Wang, P.; Ito, K.; Fowles, J.; Shusterman, D.; Jaques, P. A.; Kumagai, K., Measurement of heating coil temperature for e-cigarettes with a "top-coil" clearomizer. *PLOS ONE* **2018,** *13* (4), e0195925.

20.   Chen, J. Y.; Jiang, H.; Chen, S. J.; Cullen, C.; Ahmed, C. M. S.; Lin, Y.-H., Characterization of electrophilicity and oxidative potential of atmospheric carbonyls. *Environ. Sci.: Processes Impacts* **2019,** *21* (5), 856-866.

21.   Chen, X.; Zhong, Z.; Xu, Z.; Chen, L.; Wang, Y., $2'$,$7'$-Dichlorodihydrofluorescein as a fluorescent probe for reactive oxygen species measurement: Forty years of application and controversy. *Free Radical Res.* **2010,** *44* (6), 587-604.

22. Son, Y.; Mainelis, G.; Delnevo, C.; Wackowski, O. A.; Schwander, S.; Meng, Q., Investigating E-Cigarette Particle Emissions and Human Airway Depositions under Various E-Cigarette-Use Conditions. *Chem. Res. Toxicol.* **2020,** *33* (2), 343-352.

23. Son, Y.; Mishin, V.; Laskin, J. D.; Mainelis, G.; Wackowski, O. A.; Delnevo, C.; Schwander, S.; Khlystov, A.; Samburova, V.; Meng, Q., Hydroxyl Radicals in E-Cigarette Vapor and E-Vapor Oxidative Potentials under Different Vaping Patterns. *Chem. Res. Toxicol.* **2019,** *32* (6), 1087-1095.

24. Mikheev, V. B.; Klupinski, T. P.; Ivanov, A.; Lucas, E. A.; Strozier, E. D.; Fix, C., Particle size distribution and chemical composition of aerosolized vitamin E acetate. *Aerosol Sci. Technol.* **2020,** *54* (9), 993-998.

25. Pence, H. E.; Williams, A., ChemSpider: An Online Chemical Information Resource. *J. Chem. Educ.* **2010,** *87* (11), 1123-1124.

26. Chen, J. Y.; Canchola, A.; Lin, Y.-H., Carbonyl Composition and Electrophilicity in Vaping Emissions of Flavored and Unflavored E-Liquids. *Toxics* **2021,** *9* (12).

27. Lynch, J.; Lorenz, L.; Brueggemeyer, J. L.; Lanzarotta, A.; Falconer, T. M.; Wilson, R. A., Simultaneous Temperature Measurements and Aerosol Collection During Vaping for the Analysis of Δ(9)-Tetrahydrocannabinol and Vitamin E Acetate Mixtures in Ceramic Coil Style Cartridges. *Front. Chem.* **2021,** *9,* 734793-734793.

28. Zhao, T.; Shu, S.; Guo, Q.; Zhu, Y., Effects of design parameters and puff topography on heating coil temperature and mainstream aerosols in electronic cigarettes. *Atmos. Environ.* **2016,** *134*, 61-69.

29. Wagner, J.; Chen, W.; Vrdoljak, G., Vaping cartridge heating element compositions and evidence of high temperatures. *PLOS ONE* **2020,** *15* (10), e0240613.

30. Geiss, O.; Bianchi, I.; Barrero-Moreno, J., Correlation of volatile carbonyl yields emitted by e-cigarettes with the temperature of the heating coil and the perceived sensorial quality of the generated vapours. *Int. J. Hyg. Environ. Health* **2016,** *219* (3), 268-277.

31. Ushikusa, T.; Maruyama, T.; Niiya, I., Pyrolysis Behavior and Thermostability of Tocopherols. *JOCS* **1991,** *40* (12), 1073-1079.

32. Saliba, N. A.; El Hellani, A.; Honein, E.; Salman, R.; Talih, S.; Zeaiter, J.; Shihadeh, A., Surface chemistry of electronic cigarette electrical heating coils: Effects of metal type on propylene glycol thermal decomposition. *J. Anal. Appl. Pyrolysis* **2018,** *134*, 520-525.

33. Iso, Biological evaluation of medical devices—Part 5: Tests for in vitro cytotoxicity. *IOS, Switzerland* **2009**.

34.   LeBel, C. P.; Ischiropoulos, H.; Bondy, S. C., Evaluation of the probe 2', 7'-dichlorofluorescin as an indicator of reactive oxygen species formation and oxidative stress. *Chem. Res. Toxicol.* **1992,** *5* (2), 227-231.

35.   Aranda, A.; Sequedo, L.; Tolosa, L.; Quintas, G.; Burello, E.; Castell, J. V.; Gombau, L., Dichloro-dihydro-fluorescein diacetate (DCFH-DA) assay: A quantitative method for oxidative stress assessment of nanoparticle-treated cells. *Toxicol. in Vitro* **2013,** *27* (2), 954-963.

36.   Wang, H.; Joseph, J. A., Quantifying cellular oxidative stress by dichlorofluorescein assay using microplate reader. *Free Radic. Biol. Med.* **1999,** *27* (5-6), 612-616.

37.   Huang, W.; Zhang, Y.; Zhang, Y.; Fang, D.; Schauer, J. J., Optimization of the Measurement   of   Particle-Bound   Reactive   Oxygen   Species   with $2'$,$7'$ -dichlorofluorescin (DCFH). *Water Air Soil Pollu.t* **2016,** *227* (5), 164.

38.   Reiniers, M. J.; van Golen, R. F.; Bonnet, S.; Broekgaarden, M.; van Gulik, T. M.; Egmond, M. R.; Heger, M., Preparation and Practical Applications of $2'$,$7'$ -Dichlorodihydrofluorescein in Redox Assays. *Anal. Chem.* **2017,** *89* (7), 3853-3857.

39.   Klotz, L.-O.; Steinbrenner, H., Cellular adaptation to xenobiotics: Interplay between xenosensors, reactive oxygen species and FOXO transcription factors. *Redox Biology* **2017,** *13*, 646-654.

40.   Sarniak, A.; Lipińska, J.; Tytman, K.; Lipińska, S. Endogenous mechanisms of reactive oxygen species (ROS) generation *Postepy Hig Med Dosw (Online)*, **2016,** *14 (0)*, 1150-1165.

41.   Banerjee, S.; Ghosh, J.; Sil, P. C., Drug metabolism and oxidative stress: cellular mechanism and new therapeutic insights. *J. Biochem. Anal. Biochem.* **2016,** *5* (225), 2161-1009.

42.   Brubacher, J. L.; Bols, N. C., Chemically de-acetylated $2'$,$7'$ -dichlorodihydrofluorescein diacetate as a probe of respiratory burst activity in mononuclear phagocytes. *J. Immunol Meth* **2001,** *251* (1), 81-91.

43.   Erard, M.; Dupré-Crochet, S.; Nüße, O. A.-O., Biosensors for spatiotemporal detection of reactive oxygen species in cells and tissues. *Am. J. Physiol. Regul. Integr. Comp. Physiol,* **2018,** *314* (5), 1522-1490.

44.   Livak, K. J.; Schmittgen, T. D., Analysis of relative gene expression data using real-time quantitative PCR and the 2(-Delta Delta C(T)) Method. *Methods*, **2001**, *25* (4), 402-408.

45.   Tan, A. S.; Berridge, M. V., Evidence for NAD(P)H:quinone oxidoreductase 1 (NQO1)-mediated quinone-dependent redox cycling via plasma membrane electron

transport: A sensitive cellular assay for NQO1. *Free Radical Biol. Med.* **2010,** *48* (3), 421-429.

46.   Merker, M. P.; Bongard, R. D.; Krenz, G. S.; Zhao, H.; Fernandes, V. S.; Kalyanaraman, B.; Hogg, N.; Audi, S. H., Impact of pulmonary arterial endothelial cells on duroquinone redox status. *Free Radical Biol. Med.* **2004,** *37* (1), 86-103.

47.   Audi, S. H.; Bongard, R. D.; Dawson C. A.; Siegel, D.; Roerig, D. L.; Merker, M. P.; Duroquinone reduction during passage through the pulmonary circulation. *Am. J. Physiol. Lung Cell Mol. Physiol.* **2003,** *285* (5), L1116-31.

48.   Bianchet, M. A.;   Faig, M.; Amzel, L. M., Structure and Mechanism of NAD[P]H:Quinone Acceptor Oxidoreductases (NQO). In *Methods in Enzymology*, Academic Press: 2004; Vol. 382, pp 144-174.

49.   Gozzelino, R.; Jeney, V.; Soares, M. P., Mechanisms of Cell Protection by Heme Oxygenase-1. *Annu. Rev. Pharmacol. Toxicol.* **2010,** *50* (1), 323-354.

50.   Kansanen, E.; Jyrkkänen, H.-K.; Levonen, A.-L., Activation of stress signaling pathways by electrophilic oxidized and nitrated lipids. *Free Radical Biol. Med.* **2012,** *52* (6), 973-982.

51.   Escobar, Y.-N. H.; Nipp, G.; Cui, T.; Petters, S. S.; Surratt, J. D.; Jaspers, I., In Vitro Toxicity and Chemical Characterization of Aerosol Derived from Electronic Cigarette Humectants Using a Newly Developed Exposure System. *Chem. Res. Toxicol.* **2020,** *33* (7), 1677-1688.

52.   Ross, D.; Siegel, D., Functions of NQO1 in Cellular Protection and CoQ10 Metabolism and its Potential Role as a Redox Sensitive Molecular Switch. *Front. Physiol.* **2017,** *8*.

53.   Carvalho, T. C.; Peters, J. I.; Williams, R. O., Influence of particle size on regional lung deposition – What evidence is there? *Int. J. Pharm.* **2011,** *406* (1), 1-10.

54.   Lippmann, M.; Yeates, D. B.; Albert, R. E., Deposition, retention, and clearance of inhaled particles. *Br. J. Ind. Med.* **1980,** *37* (4), 337.

55.   Grosjean, E.; Grosjean, D., The Gas Phase Reaction of Unsaturated Oxygenates with Ozone: Carbonyl Products and Comparison with the Alkene-Ozone Reaction. *J. Atmos. Chem.* **1997,** *27* (3), 271-289.

56.   Weschler, C. J., Ozone in indoor environments: concentration and chemistry. *Indoor air* **2000,** *10* (4), 269-288.

57.   Su, W.-C.; Wong, S.-W.; Buu, A., Deposition of E-cigarette aerosol in human airways through passive vaping. *Indoor Air* **2021,** *31* (2), 348-356.

58.   Ranpara, A.; Stefaniak, A. B.; Williams, K.; Fernandez, E.; LeBouf, R. F., Modeled Respiratory Tract Deposition of Aerosolized Oil Diluents Used in Δ(9)-THC-

Based Electronic Cigarette Liquid Products. *Front. Public Health* **2021,** *9*, 744166-744166.

59. Lanzarotta, A.; Falconer, T. M.; Flurer, R.; Wilson, R. A., Hydrogen Bonding between Tetrahydrocannabinol and Vitamin E Acetate in Unvaped, Aerosolized, and Condensed Aerosol e-Liquids. *Anal. Chem.* **2020,** *92* (3), 2374-2378.

60. Muthumalage, T.; Lucas, J. H.; Wang, Q.; Lamb, T.; McGraw, M. D.; Rahman, I., Pulmonary Toxicity and Inflammatory Response of Vape Cartridges Containing Medium-Chain Triglycerides Oil and Vitamin E Acetate: Implications in the Pathogenesis of EVALI. *Toxics* **2020,** *8* (3).

61. DiPasquale, M.; Gbadamosi, O.; Nguyen, M. H. L.; Castillo, S. R.; Rickeard, B. W.; Kelley, E. G.; Nagao, M.; Marquardt, D., A Mechanical Mechanism for Vitamin E Acetate in E-cigarette/Vaping-Associated Lung Injury. *Chem. Res. Toxicol.* **2020**.

62. Hayeck, N.; Zoghzoghi, C.; Karam, E.; Salman, R.; Karaoghlanian, N.; Shihadeh, A.; Eissenberg, T.; Zein El Dine, S.; Saliba, N. A., Carrier Solvents of Electronic Nicotine Delivery Systems Alter Pulmonary Surfactant. *Chem. Res. Toxicol.* **2021,** *34* (6), 1572-1577.

63. Li, Y.; Burns, A. E.; Tran, L. N.; Abellar, K. A.; Poindexter, M.; Li, X.; Madl, A. K.; Pinkerton, K. E.; Nguyen, T. B., Impact of e-Liquid Composition, Coil Temperature, and Puff Topography on the Aerosol Chemistry of Electronic Cigarettes. *Chem. Res. Toxicol.* **2021,** *34* (6), 1640-1654.

64. Braymiller, J. L.; Barrington-Trimis, J. L.; Leventhal, A. M.; Islam, T.; Kechter, A.; Krueger, E. A.; Cho, J.; Lanza, I.; Unger, J. B.; McConnell, R., Assessment of Nicotine and Cannabis Vaping and Respiratory Symptoms in Young Adults. *JAMA Network Open* **2020,** *3* (12), e2030189-e2030189.

Chapter 3: Temperature dependence of emission product distribution from vaping of vitamin E acetate

3.0 Abstract

Nearly two years after vitamin E acetate (VEA) was identified as the potential cause of the 2019–2020 outbreak of e-cigarette, or vaping product-associated lung injuries (EVALI), the toxicity mechanisms of VEA vaping are still yet to be fully understood. Studies since the outbreak have found that e-liquids such as VEA undergo thermal degradation during the vaping process to produce various degradation products, which may pose a greater risk of toxicity than exposure to unvaped VEA. Additionally, a wide range of customizable parameters–including the model of e-cigarette used, puffing topography, or the applied power/temperature used to generate aerosols–have been found to influence the physical properties and chemical compositions of vaping emissions. However, the impact of heating coil temperature on the chemical composition of VEA vaping emissions has not been fully assessed. In this study, we investigated the emission product distribution of VEA vaping emissions produced at temperatures ranging from 176 to 356°C, corresponding to a variable voltage vape pen set at 3.3 to 4.8V. VEA degradation was found to be greatly enhanced with increasing temperature, resulting in a shift towards the production of lower molecular weight compounds, such as the redox active duroquinone (DQ) and short-chain alkenes. Low temperature vaping of VEA resulted in the production of long-chain molecules, such as phytol, exposure to which has been suggested to induce lung damage in previous studies. Furthermore, differential product distribution was observed in VEA degradation products generated from vaping

and from pyrolysis using a tube furnace in the absence of the heating coil at equivalent temperatures, suggesting the presence of external factors such as metals or oxidation that may enhance VEA degradation during vaping. Overall, our findings indicate that vaping behavior may significantly impact the risk of exposure to toxic vaping products and potential for vaping-related health concerns.

3.1 Introduction

After the 2019–2020 outbreak of e-cigarette or vaping product use-associated lung injury (EVALI) in which the Centers for Disease Control and Prevention (CDC) reported over 2,800 hospitalizations of patients displaying symptoms of acute respiratory distress, (1) serious public health concerns have been raised about the safety of e-cigarettes. In the initial investigations, evidence has supported that vaping of vitamin E acetate (VEA), a synthetic form of vitamin E (VE) that was used to "cut" or dilute black market or homemade tetrahydrocannabinol (THC), was a major cause of the onset of EVALI symptoms. (1–3) Several different mechanisms of toxicity have been proposed since the outbreak, yet the exact causative agents and molecular mechanisms through which VEA vaping emissions resulted in lung toxicity are still not well understood.

VE and VEA alone are considered safe for dermatological application in skin-care products (4) and as well as for consumption in foods and dietary supplements. (5) Several studies since the outbreak, however, have found that e-liquids like VEA undergo major thermal decomposition during the vaping process to form products that are often more toxic than the parent oil. (6–8) VEA in particular has been found to decompose into a wide range of emission products including VE, alkenes such as 1-pristene, (8, 9) alcohol-

containing compounds such as 3,7,11-trimethyl-1-dodecanol, durohydroquinone (DHQ), (6) and durohydroquinone monoacetate (DHQMA), (8, 9) and carbonyl-containing compounds such as ketene, (7, 10) 4-acetoxy-2,3,5-trimethyl-6-methylene-2,4-cyclohexadienone (ATMMC), (9) and duroquinone (DQ). (3, 6, 7) Still, the overall risk of exposure of each identified product to those who vaped VEA is unclear. For example, ketene gas has been hypothesized to form from the cleavage of the acetate group of VEA. However, this reaction has been calculated to only be feasible at temperatures exceeding 500°C–temperatures that are likely to only occur under "dry puff" conditions. (10, 11)

The operating temperature of the vape device is one of many parameters–including the model of e-cigarette used, puff duration, interval between puffs, etc.–that a user may alter to customize their vaping experience. (12, 13) A few studies to date have investigated the impact of increased temperature on the size and volume distribution of emitted vaping aerosols, reporting that greater coil temperatures result in larger puff volumes, but decrease the size of emitted particles. (14–16) A recent study in 2021 found that the emission of volatile degradation products, including various carbonyl-containing species, was significantly enhanced when temperature was increased from 170 to 280°C. (17) In addition, increased coil temperature and characteristics of the vape device have also been found to influence other aspects of vaping emissions, such as the release of metals and the level of carbonyl-containing compounds or radical species. (16, 18, 19) E-cigarette atomizers and heating elements are often comprised of various transition metals including nickel, iron, and chromium (20, 21) which not only pose a risk of metal toxicity to vape users, (22) but may play a role in the catalysis of thermal degradation of the e-

liquid. One study by Saliba et al. (2018) found that e-cigarette filament wires had a significant impact on the production of carbonyl-containing compounds from propylene glycol (PG) vaping, lowering the temperature required to form carbonyl species by nearly 200°C. (23) However, the factors affecting the chemical composition of e-cigarette degradation products have yet to be fully characterized.

The objective of this study was to examine the influence of variable temperature on the product distribution of e-cigarette vaping emissions, using VEA as a model e-liquid. To do so, we performed a non-targeted analysis of the aerosol-phase constituents at relevant, mid-range vaping temperatures using gas chromatography/mass spectrometry (GC/MS). We hypothesized that elevated temperature of the heating coil during vaping could enhance thermal degradation of VEA, causing a shift in emission product distribution and toxicity in vapers. VEA vaping emissions were produced at coil temperatures ranging between 176 to 356°C using a variable voltage vape pen and analyzed using GC/MS with electron ionization (EI) to assess how emission product identity and concentration changes as a function of temperature. In addition, pure pyrolysis of VEA without the influence of the device was also investigated using a tube furnace to investigate potential catalysis by the device itself. The results from this study contribute to our current understanding of the toxicity mechanisms underlying VEA vaping emissions and have significant implications for the potential health risks associated with the use of other e-liquids.

3.2 Materials and Methods

3.2.1 Materials

DL-alpha tocopherol acetate (VEA, > 97%), DL-alpha tocopherol (vitamin E, > 97%), tetramethyl-1,4- benzoquinone (DQ, > 98%), durohydroquinone (DHQ, > 95%), 2-methyl-heptene (> 98%), trimethylhydroquinone (> 98%), and phytol (> 95%) were purchased from Tokyo Chemical Industry (TCI America, Inc.). 1, 3, 5-trichlorobenzene (TCB, 98%) was purchased from Alfa Aesar. Acetonitrile (ACN, 99.95%) was purchased from Fisher Chemical.

3.2.2 Temperature Measurement

A pen-style e-cigarette battery (Vapros Spinner II, 1650 mAh) was used as a model variable voltage e-cigarette for this study. This vape pen has set nominal voltages of 3.3, 3.8, 4.3, and 4.8 V. These voltages were confirmed using a multimeter to measure the actual voltage of the battery upon activation.

The set-up of the temperature measurements can be seen in **Figure S3.1** in the supporting information (SI). The protocol for the thermocouple measurement of the e-cigarette coil and oil temperatures was adapted from Chen et al. (11) To measure the temperature at each voltage setting, the pen was connected to a fresh cartridge (CCell TH2; 0.5 mL, 2.2 Ω) that was filled with VEA standard oil until the oil level sat just above the atomizer base. The oil level in the cartridge was kept consistent between each reading, as the amount of oil in the cartridge has been previously shown to affect the temperatures the coil may reach. (11, 18) Three 1 mm grounded k-type thermocouple

69

wires (MN Measurement Instruments) were connected to a 4-channel data logger (Mo. SDL200; Extech). One thermocouple was kept suspended to measure the temperature of ambient air as a device control. The second thermocouple was inserted into the air flow tube of the cartridge and allowed to rest on the surface of the ceramic coil. This position was chosen to record temperature across all voltage settings as it not only provided the most consistent measurements, but certain positioning of the probe resulted in the battery shutting off, likely to prevent overheating or burning in the event of the air flow tube being blocked during real-use scenarios. The third thermocouple was inserted into the glass casing of the cartridge to submerge the end of the probe in VEA oil in contact with the atomizer. The thermocouples allowed for simultaneous measurement of the coil and the parent oil in the cartridge when the battery was activated. Temperatures were recorded by the data logger every 1 s over a 1 min cycle. The vape pen was activated by holding the power button for 4 s to heat the coil, then allowed to rest for the remainder of the cycle. A total of 13 cycles–including 3 initial preconditioning cycles–were measured.

3.2.3 E-cigarette collection

The procedure for collection of VEA vaping emissions at each temperature setting was adapted from previous studies. (6, 7) Prior to each collection, a fresh cartridge was filled with VEA standard oil, weighed, and preconditioned by taking 3–5 puffs. The vaping emissions were collected using a cold trap apparatus maintained at -40°C (Across International LLC). The particle collection efficiency of the cold trap system at the flow rate used in this study has been reported previously (≥ 99% by volume). (24) To collect aerosol emissions, one 4 s puff was taken at intervals of 1 min to maintain consistency

with the temperature measurement procedure. Puffs were generated at each temperature using a 0.4 L min^{-1} air flow rate, which was controlled by a 0.46 L min^{-1} critical orifice connected a diaphragm pump (Gast Manufacturing Inc.). For each setting, the vape pen was operated until approximately 100 mg of VEA had been consumed; this consumption was typically achieved within 10–20 puffs. In instances where more puffs were required, the vape pen was allowed to rest at 20 puffs for 10–20 minutes to prevent overheating of the battery.

Condensed emission products were dissolved in 1 mL of ACN, with 10 μL of 1, 3, 5-TCB solution (2 μg μL^{-1}) added to each sample as an internal standard for chemical analysis. Emissions were analyzed immediately after collection or stored at -80°C to prevent any aging effects.

3.2.4 Tube Furnace Experiments

To determine the impact of the device on the degradation of e-liquids, pure pyrolysis of VEA oil was simulated using a tube furnace reactor system (OTF-1200X; MTI Corporation). The schematic of the set up for these experiments is shown in **Figure S3.2**. An alumina crucible containing 100 mg of VEA standard oil was weighed, and then placed into a high temperature quartz tube furnace capable of reaching temperatures as high as 1200°C. The tube furnace was initially set to 23°C, then ramped to each temperature setting (176, 237, 322, or 356°C; corresponding to the measured coil temperatures described in section 3.2.3) at a rate of 10°C min^{-1}, and then held at the target temperature for 75 minutes to allow for VEA oil to be evenly heated. Inert argon gas was

flowed through the system at a rate of 0.18 L min^{-1} (controlled by a critical orifice) to carry the VEA pyrolysis products into cold trap apparatus kept at -40°C. After 75 minutes, the tube furnace was programed to return to room temperature before the alumina crucible was removed and re-weighed to determine the amount of VEA that was consumed. Pyrolysis products condensed in the cold trap were dissolved in 1 mL of ACN and concentrated to 100 μL using a gentle N$_2$ gas stream. Then, 10 μL of 1, 3, 5-TCB solution (2 μg μL^{-1}) was added to each sample as an internal standard for chemical analysis.

3.2.5 GC/MS Analysis of Vaping Emissions

VEA decomposition products were identified and quantified using GC/MS (Agilent 6890N GC and 5975C inert MSD equipped with an EI ion source) analysis. Large molecular weight and non-polar degradation products were analyzed by directly injecting 2 μL of sample into an Agilent J&W DB-5MS column (30 m × 0.25 mm i.d., 0.25 μm film) for separation. A solvent delay of 6 min was used; the GC was initially set to 60°C for 1 min, then ramped to 150°C at a rate of 3°C min^{-1}, held at 150°C for 2 min, ramped to 310°C at a rate of 20°C min^{-1}, and then held at 310°C for 5 min. Smaller molecular weight, polar degradation products were analyzed by directly injecting 2 μL of sample into a Rtx-VMS fused silica column (30 m × 0.25 mm i.d., 1.4 μm film). A solvent delay of 6 min was used. The GC was set to 35°C for 1 min, ramped to 240°C at a rate of 10°C min^{-1}, and held 4 min. The detailed procedures for the operation of GC/MS can be found in a previous publication. (25)

3.2.6 Identification of Emission Products

Degradation products were identified using the NIST 2008 mass spectral database. Compounds with probability $\geq$ 50% and match factor scores $\geq$ 800 were considered as good matches. (26, 27) For compounds that were suspected to be present in our spectra but could not be identified using the NIST library due to lack of available standards, Quantum Chemistry Electron Ionization Mass Spectrometry (QCEIMS) was used to simulate theoretical EI mass spectra of molecules. (28) The detailed procedures for QCEIMS calculations can be found in the supporting information. Peak abundances were normalized to the 1,3,5-TCB internal standard for quantification.

3.3 Results

3.3.1 Temperature Measurement

Figure 3.1 shows the temperature profiles of the e-cigarette coil (**Figure 3.1A–D**) and VEA oil in the cartridge (**Figure 3.1E–H**) operated at each voltage setting. Peak coil temperature at each voltage setting was fairly consistent between each measurement with no significant increase after consecutive use, which agrees with previous reports. (11) Though the starting temperature after 1 min of rest increased slightly with subsequent measurements, the starting temperature never exceeded 33°C. In contrast, the temperature of the oil in the cartridge increased with each subsequent measurement until seeming to plateau.
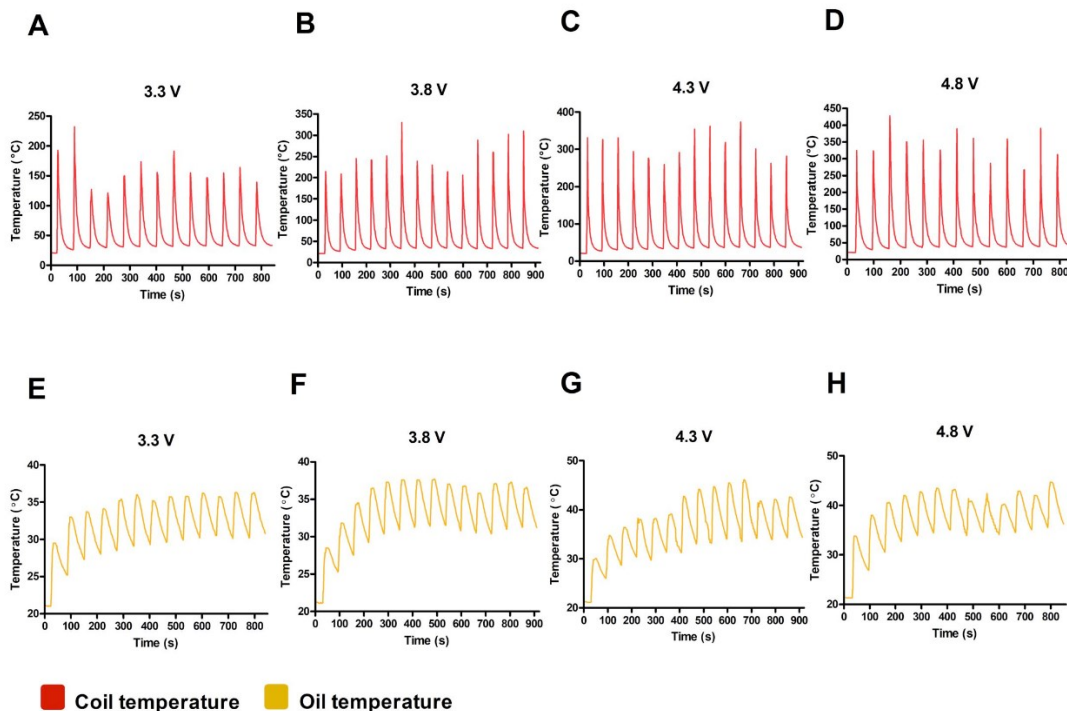
Figure 3.1. E-cigarette temperature profiles Temperature profiles of (A-D) e-cigarette coil at 3.3, 3.8, 4.3, and 4.8 V, and (E-H) VEA oil in contact with the atomizer tube at 3.3, 3.8, 4.3 and 4.8 V. Measurements were taken every 1 s over a 1 min cycle; the battery was activated to heat the coil for 4 s, then the pen was allowed to rest for the remaining time.

The peak temperatures of both the coil and the oil were then taken and plotted as a function of voltage, as shown in **Figure 3.2**. Coil temperature showed a strong positive linear relationship with applied voltage (Fig 3.2A; $R^2 = 0.987$), whereas oil temperature increased linearly with voltage until 41°C (Fig 3.2B), where the peak temperatures at 4.3 and 4.8 V do not significantly differ. This is likely due to the specific heat capacity of VEA; (29) at higher voltages. Visible discoloration to the oil and wick could be seen during temperature measurements, indicating that the specific heat capacity of the oil in

the cartridges may have been exceeded and part of the stored VEA may have been transformed before it is vaped (**Figure S3.3**).
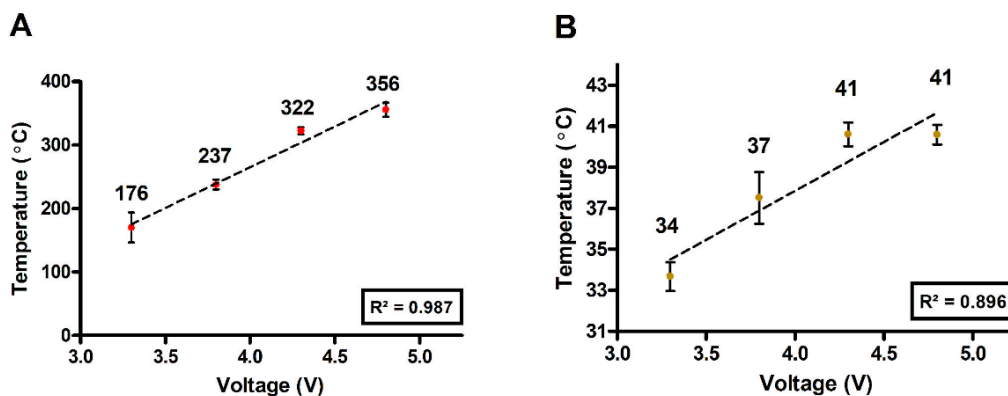
Figure 3.2. Average peak temperatures vs. voltage. Linear graph of (A) coil and (B) oil average peak temperatures versus each voltage setting of the e-cigarette device.

3.3.2 Temperature Dependence of Emission Product Distribution

The total ion chromatographs (TIC) obtained from GC/MS analysis of VEA vaping emissions produced at each temperature setting are shown in **Figure 3.3**. Overall, clear temperature dependent degradation of VEA vaping emissions can be seen as the amount and abundance of degradation products substantially increases with increasing coil temperature.
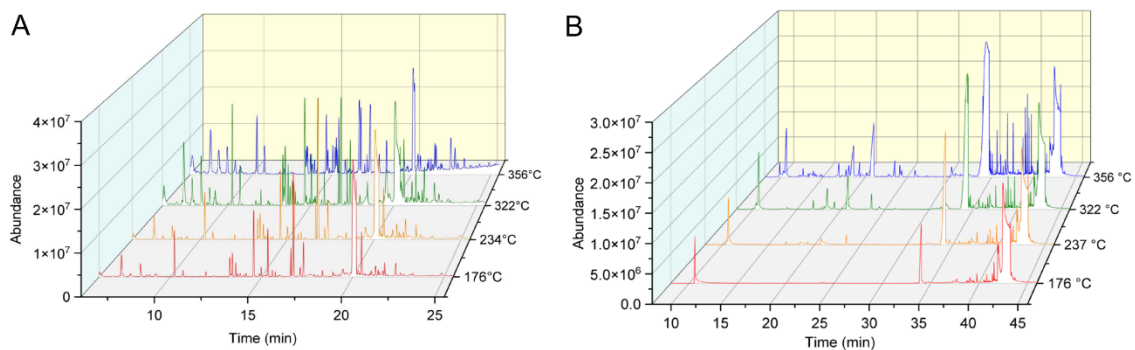
Figure 3.3. Total ion chromatographs (TIC) of VEA vaping emissions collected at 176, 234, 322, and 356 °C. TIC obtained from (A) a polar Rtx-VMS fused silica separation column and (B) a non-polar J&W Scientific DB-5MS separation column.

Analysis of the GC/MS results revealed 19 compounds that were able to be tentatively identified based on consistent NIST MS spectral library match scores of 800 or greater. One other compound, 1-pristene, was not found in the NIST library and thus was identified based on comparison with previously reported mass spectra (8) and a mass spectrum generated with the QCEIMS program that found signature fragments of *m/z* 266, 111, and 126, which are consistent with our results (**Figure S3.4**). A summary of the identified compounds and chemical information identified from PubChem (30) can be found in the supporting information (**Table S3.1**). Many of the products described here, such as phytol, 2,3,5-trimethyl-1,4-benzenediol and 2-hydroxy-4-methoxy-3,6-dimethyl benzaldehyde, have not been previously detected from VEA vaping to our knowledge. An isomer of 2,3,5-trimethyl-1,4-benzenediol has also recently been identified as a substantial VEA degradation product at temperatures ≥ 220°C. (17) Authentic standards were purchased for 2-methyl-1-heptene, phytol, and 2,3,5-trimethyl-1,4-benzenediol to confirm identities of observed products (**Figure S3.5-S3.7**, respectively). Other

compounds, such as vitamin E, DQ, DHQ, 1-pristene, and 3,7,11-trimethyl-1-dodecanol, have been consistently identified as VEA decomposition products (3, 6–9). Several products, such as DHQMA (9) or ketene, (7) that have been previously reported in VEA vaping emissions could not be found in our spectra, likely due to the limitations of the emission collection and analysis method described in section 3.4.

A heatmap of the mass fractions of degradation products generated at each temperature is shown in **Figure 3.4**. Products that contribute to the majority of the observed VEA degradation (mass fractions ≥ 0.05) were separated from the total heatmap to better visualize the change in each concentration as a function of temperature. VEA, 1-pristene, and 3,7,11-trimethyl-1-dodecanol were found to be the most dominant vaping emission products at all of temperature settings, while other compounds, such as duroquinone, durohydroquinone, and 2-methyl-1-heptene steadily increase in concentration as temperature increases. Furthermore, certain compounds including 2,3,5-trimethyl-1,4-benzenediol, 2,6-dimethyl-1,6-heptadiene, 3,7-dimethyl-1-octene, and 3-methyl-1-octene are not produced in concentrations above the detection limit of our instrument until 322°C, which suggests a potential risk that users who operated vaping devices at lower temperatures would not be exposed to. However, while most identified compounds appear to increase in concentration as temperature increases, phytol and 2,6,10-trimethyl-dodecane are produced at detectable levels at 176 and 237°C but cannot be found at higher temperatures. Another recent study has also detected production of phytol when vitamin E were heated in a microchamber/thermal extractor at 250°C. (31) It

is possible that at these compounds are stable at lower temperatures but begin to break

down into degradation products themselves as the temperature increases.
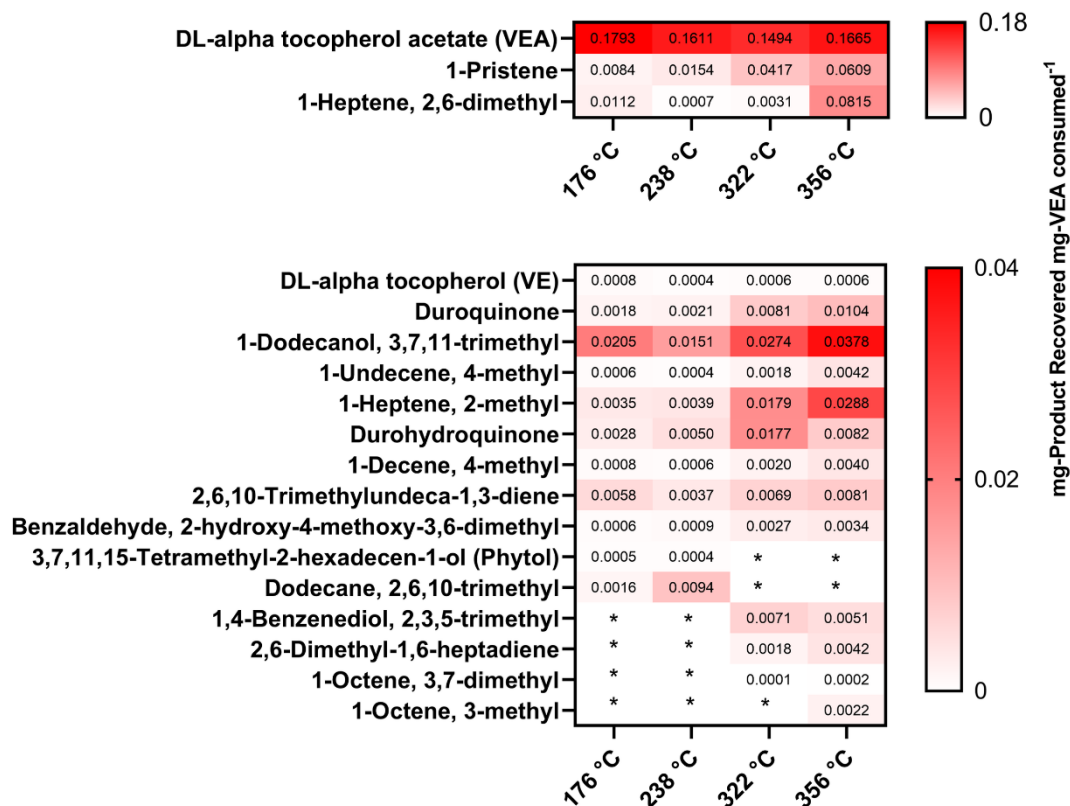
Figure 3.4. Heatmap of VEA vaping emission product distribution at 176, 237, 322, and 356 °C. Compounds were identified via NIST mass spectral library and included based on frequency and consistency of detection throughout all collections. Asterix indicates that the concentration of a product was below the detection limit of the instrument.

Another important pattern to note is the increase in compounds that may pose a

risk of oxidative damage to lungs, such as DQ and 2,3,5-trimethyl-1,4-benzenediol, at

higher concentrations. While not investigated in this study, prior research has shown that

increased temperature may result in the enhanced emission of carbonyl-containing

compounds when vaping e-liquids containing propylene glycol and glycerin (PG and VG). (16, 18) Thus, vaping VEA at greater temperature settings may also carry the risk of exposure to highly electrophilic molecules and subsequent oxidative lung injury.

In order to better understand the interactions between temperature and the generated emission products, a Pearson correlation analysis was performed (**Figure 3.5**). Overall, all but four of the identified compounds were strongly correlated with temperature ($R \geq 0.6$). Compounds such as DQ, 1-pristene, 2-methyl-1-heptene, 2-hydroxy-4-methoxy-3,6-dimethyl benzaldehyde, and 2,6-dimethyl-1,6-heptadiene, were very well correlated with temperature ($R \geq 0.9$), indicating a strong increase in concentration as temperature increases. VEA and phytol, in contrast, were strongly anti-correlated with temperature ($R \leq -0.6$), while VE and 2,6,10-trimethyl-dodecane were moderately anti-correlated with temperature ($R \leq -0.37$). In addition, VEA was found to be weakly to strongly anti-correlated with all degradation products excepting phytol and VE, which demonstrate a strong positive correlation ($R > 0.5$). These results support our analysis of the mass fractions, indicating that as temperature increases, thermal decomposition of VEA is heightened.
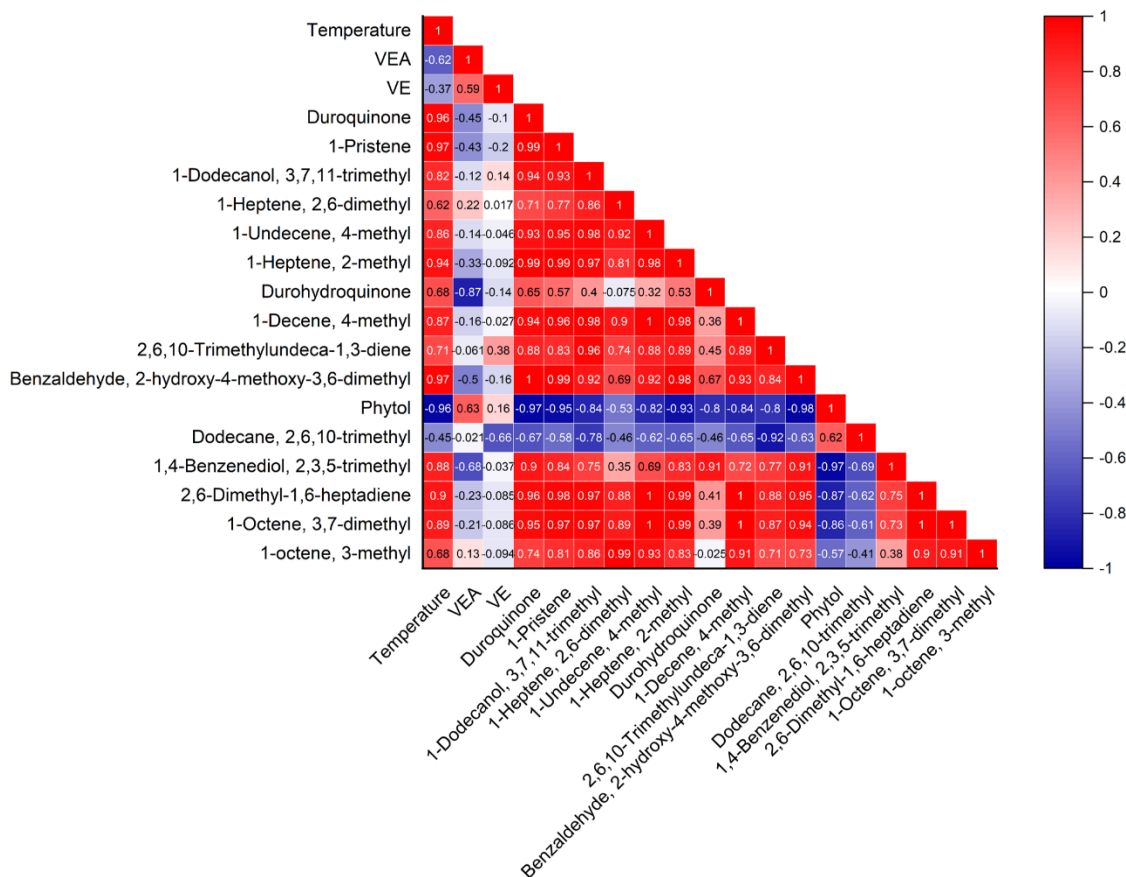
Figure 3.5. Correlation matrix for production of VEA degradation products and temperature. Pearson correlation analysis results depicting interactions between temperature and VEA degradation, and interactions between concentrations of degradation products. Positive correlations (R > 0) are depicted in red, while strong negative correlations (R < 0) are depicted in blue.

Further analysis of the correlations between degradation products shows that phytol is strongly anti-correlated with all VEA degradation products (R < -0.8) with the exception of 2,6,10-trimethyl-dodecane, which was found to have a strong positive correlation with phytol (R = 0.62). Phytol was also found to be strongly correlated with VEA (R = 0.63), likely because as more VEA was evaporated during the vaping process, the greater the chance of degradation into phytol. These relationships further suggest that while some degradation products may be stable at high temperatures, phytol may further

decompose into shorter-chain alcohols, alkanes, and alkenes and enhance the production of VEA vaping emission products. Phytol is known both as a precursor for the synthesis of VE and vitamin K12, (32, 33) as well as a byproduct of chlorophyll degradation. (33, 34) Inhalation of aerosolized phytol has previously been shown to induce lung injury in exposed rats (35, 36). In addition, phytol is a long chain alkyl alcohol compound, meaning that it has the potential to induce damage to the membrane of cells in a biological system. (37, 38) Overall, the toxicity of phytol raises questions about the safety of vaping not only VEA, but cannabis-containing vape products that may result in phytol production.

These results clearly indicate that the product distributions of VEA vaping emissions are highly dependent on the operating temperature of the vape pen. As a result, the exposure for vape users operating the same e-cigarette products at different temperatures may differ significantly.

3.3.3 Potential Catalysis of VEA Vaping Pyrolysis

Previous reports of VEA pyrolysis indicate that VEA begins to degrade starting at ~200–240°C. (39, 40) However, our results clearly demonstrate degradation of VEA and formation of products such as DQ at 176°C, indicating that the device itself may play a larger role in the decomposition of VEA than initially anticipated. Previous study in our lab has also found substantial formation of DQ at 218°C–several hundred degrees lower than what has been predicted. (24) To further understand if the device itself may impact the thermal degradation of VEA, pure pyrolysis of VEA oil was carried out using a tube

furnace reactor. After 75 minutes, the average mass loss of VEA heated at 176, 237, 322, and 356°C was found to be 0.11 ± 0.091, 0.37 ± 0.11, 3.7 ± 0.072 and 7.1 ± 0.0016 mg of VEA consumed. At 176 and 237°C, VEA was fairly stable; substantial consumption of VEA oil was not observed until the two higher temperatures, despite clear consumption at all temperatures during the vaping collection.

Figure 3.6 demonstrates the product distribution of VEA degradation products collected and analyzed using GC/MS. Here, we did not observe substantial thermal decomposition of VEA when heated at 176°C for 75 minutes, which greatly contrasts with the degradation of VEA at 176°C for only 4 s during the vaping collection. At 237°C, the parent VEA molecule was the only detectable emission product, indicating that VEA again did not degrade at this lower temperature, though 237°C was enough to evaporate VEA so that it could be collected in the cold trap. Degradation products were only detectable from samples collected at 322 and 356°C, though the number of products and abundance of observed peaks are drastically reduced when compared to the vaping emissions. It should be noted that the tube furnace is capable of heating VEA at more accurate and consistent temperatures than the vape pen itself, which often saw temperature fluctuations that may influence results.
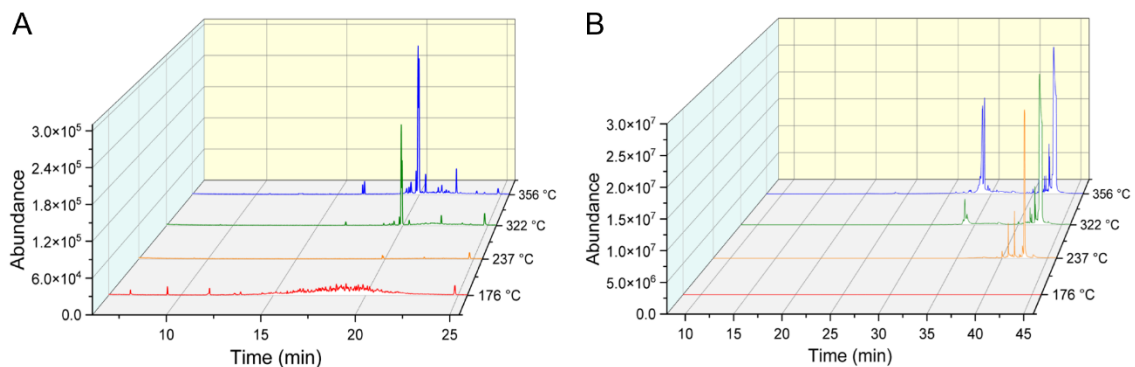
Figure 3.6. TIC of tube furnace pyrolysis emissions collected at 176, 234, 322, and 356 °C. TIC of tube furnace pyrolysis emissions collected at 176, 234, 322, and 356 °C obtained from (A) a polar Rtx-VMS fused silica separation column and (B) a non-polar J&W Scientific DB-5MS separation column.

The stark difference in product distribution provides evidence that VEA vaping emissions may not be the result of pure pyrolysis alone. Instead, external factors such as the device elements themselves or environmental interactions may play a role in the catalysis of VEA degradation. The cartridge used in this study is a newer THC cartridge that contains a ceramic heating element, a nichrome filament wire, a fibrous wick/insulation wrap through which oil was delivered to the heating element, and a stainless steel air flow tube and heating element housing that the oil remained in direct contact with. (20) The emission of metals during the vaping process has been documented in several prior studies, (21, 41–43) but the interaction between VEA and the metal components of the vape device are still being investigated. Saliba et al. (23) recently found that interaction between a metal heating element and PG greatly decreased the temperature required to observe PG thermal decomposition. Certain metals such as stainless steel, which is present in the cartridge used in this study, resulted in a nearly

300°C reduction in required temperature compared to pure pyrolysis, highlighting a clear interaction between the PG decomposition and the device itself.

Furthermore, a study by Jaegers et al. (44) found that pyrolysis alone in an anaerobic environment was not able to induce thermal degradation of PG and VG at low temperatures (< 200°C), despite previous studies observing degradation at temperatures as low as 149°C during vaping. (45) However, when heated in an aerobic environment, thermal decomposition was observed at 133 and 175°C, both without and with the addition of metal oxides Cr_2O_3 and ZrO_2, (44) suggesting that oxidation is a key process during vaping. In combination with the results shown here, evidence highly suggests that pure pyrolysis alone may not be the only pathway for VEA degradation. During the vaping process, not only may VEA come into direct contact with metals that are present in the filament wire or stainless-steel body, but VEA must also come into contact with molecular oxygen in ambient air. These interactions may promote VEA degradation at temperatures lower than predicted under pure pyrolysis conditions. Ultimately, it is then possible that compounds such as DQ or ketene may be able to form at lower temperatures than what is theoretically calculated if these interactions are considered. However, further study is required to fully understand the effects of the e-cigarette device and vaping environment on the degradation of e-liquids.

3.3.4 Limitations

There are several limitations to the study presented here that should be noted. First, this study presents a range of decomposition products that were identified using a -40°C cold trap and GC/MS analysis. Approximately 40% of the mass of VEA consumed by the vape pen could be attributed to the compounds identified here. However, compounds with high vapor pressure, such as ketene, that have been previously reported from VEA pyrolysis may not have been efficiently captured using the cold trap method described in this study. This method is expected to better traps particle-phase compounds that are able to condense at -40°C and are stable enough to transfer from the cold trap to collection vials at room temperature and is unable to capture highly volatile or reactive VEA vaping emission products. For example, ketene, which is expected to form during VEA pyrolysis, has an estimated boiling point of -56°C (30) and, as a result, was not expected to be observed in our collection. Furthermore, highly volatile and/or reactive compounds such as ketene and various low molecular weight carbonyl-containing species, etc., often require additional derivatization methods that were not used in this study to be observed using GC/MS. (7, 45)

This study was also only able to identify compounds with mass spectra that could be found in the NIST mass spectral library. While PubChem currently reports over 111 million unique chemical structures, (30) the NIST library used in this study contains MS fragmentation patterns for only 242,466 compounds. (27) As such, a large portion of the TIC for each collection could not be matched to a known compound (match scores < 600). Furthermore, several peaks were observed that were believed to be co-elution of

two or more products, which prevented clear analysis of the fragmentation patterns. Several identified products, such as VEA, may also have multiple isomeric forms that have only slight differences in their retention times and mass spectra that the NIST library matching program is unable to account for. In the case of VEA, all peaks were assumed to be and quantified as the same α form, but it is possible for VEA to exist in α, β, γ, or δ forms. This may be true for other structures identified in this study. The use of QCEIMS to identify products that cannot be found in the NIST database, such as 1-pristene, is a potential avenue for further identification of vaping product emissions (46), though its use for non-target analysis is limited if the researcher does not have a proposed structure in mind to simulate fragmentation. While this study was able to account for ~40% of the mass consumed by the pen during the vaping process, the remaining mass is likely attributable to these uncaptured volatile or reactive products, as well as degradation products that were captured, but unable to be identified at this time.

Finally, the vaping topography used in this study was adapted from previous literature on nicotine vaping and optimized for capture of particles in the cold trap system. (24) Real-word nicotine vape users have been reported to inhale between 50–80 mL/puff at greater flow rates than used in this study, (47, 48) whereas parameters for THC-vaping have not been well-characterized at this time. (49) The production yields of VEA degradation products reported in this study could consequently differ for those who vaped at higher flow rates. The temperature dependence of product distribution, however, remains true.

3.4 Conclusions

This study assessed the impact of variable temperature and environmental factors on the distribution of particle-phase VEA vaping emission products. Our results support prior research that as the applied temperature of the e-cigarette coil increases, the identities and concentrations of VEA degradation products change considerably. Higher temperatures greatly promote the decomposition of both the parent VEA as well as larger molecular weight degradation products such as VE, phytol, and 2,6,10-trimethyl-dodecane. Moreover, we observed differential product distributions when VEA was vaped versus when VEA was heated in the absence of the device, suggesting that low temperature pyrolysis observed during vaping may require the presence of a catalyst present in the device or surrounding environment. However, further study is required to fully understand this phenomenon and its effect on VEA degradation. Overall, these results provide evidence that temperature and external factors play an important role in VEA decomposition during the vaping process. As each of these compounds may have different chemical properties and toxicity mechanisms, changes in these vaping parameters may impact the exposure to both active and passive vape users who inhale emission products capable of remaining in the air for longer periods of time. (50) In the case of EVALI symptoms, it is possible that there is no one toxicity mechanism through which VEA vaping emission acts; instead, with a wide range of compounds that could form at different temperatures, multiple pathways may interact to cause damage.

While temperature and the vaping device clearly impact the degradation of the e-liquid used, it is important to note the wide range of customizable vaping parameters including the e-liquids used, the flow rate applied, the puff duration and interval between puffs, and more. Many of these parameters have already been found to significantly impact the degradation of e-liquids used and thus the health risks to vape users. (13, 15, 41, 51) It is very likely that the severity of vaping related lung injuries is dependent on the interactive effects of these customizations; two parameters may synergistically promote degradation of an e-liquid, while others may interact antagonistically to suppress degradation. Further studies are required to fully understand how these varying parameters and external factors may together impact exposure.

3.5 Supplemental Information

3.5.1 Materials and Methods
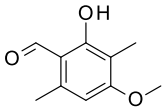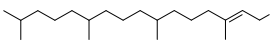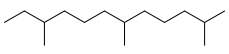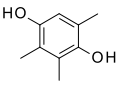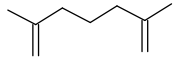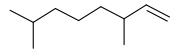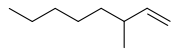
3.5.1.1 QCEIMS

The simulated electron impact (EI) mass spectrum for 1-pristene was generated using the Quantum Chemical Electron Ionization Mass Spectra (QCEIMS) program. (53,54) The molecule of interest was visualized using Gaussview 6. The geometry of the investigated systems was optimized using the DFT/ 6-31G(d) level of theory with a hybrid functional B3LYP. To make the constructed systems interests compatible with QCEIMS, 3-D coordinates were extracted from the optimized (*.log) output files and converted to Turbmole format (*.tmol) format using Openbabel. The cartesian coordinates of the optimized 1-pristene structure can be found in **Table S3.2**.

Within QCEIMs, the standalone method GFN-xTB2 method with D4/SV(P) basis set was used for the molecular dynamic calculations. Each system was run with the following parameters: 70 eV ionization energy, 500 K initial temperature, 0.25 fermotsecond time steps with 1425 parallel cluster runs and an impact excess energy (IEE)/atom of 0.6eV. The theoretical spectra were exported using the QCEIMS plotms program and visualized with a python script.

Table S3.1. Summary of VEA vaping emission products.

Name	Formula	M.W.[a]	CAS #	Structure	EIC	Average NIST Match Score[c]
DL-alpha tocopherol acetate (VEA)	$C_{31}H_{52}O_3$	472.7	58-95-7		472, 430	902
DL-alpha tocopherol (VE)	$C_{29}H_{50}O_2$	430.7	10191-41-0		205	895
Duroquinone	$C_{10}H_{12}O_2$	164.2	527-17-3		121	892
1-Pristene[d]	$C_{19}H_{38}$	266.5	2140-82-1		111, 266	N/A
1-Dodecanol, 3,7,11-trimethyl	$C_{15}H_{32}O$	228.41	6750-34-1		111	856
1-Heptene, 2,6-dimethyl	C_9H_{18}	126.24	3074-78-0		69, 126	848
1-Undecene, 4-methyl	$C_{12}H_{24}$	168.32	74630-39-0		57, 126	800
1-Heptene, 2-methyl	C_8H_{16}	112.21	15870-10-7		56, 112	801
Durohydroquinone	$C_{10}H_{14}O_2$	166.22	527-18-4		164	890
1-Decene, 4-methyl	$C_{11}H_{22}$	154.29	13151-29-6		71, 112	839
2,6,10-trimethylundeca-1,3-diene	$C_{14}H_{26}$	194.36	20056-22-8		109	817

90

Name	Formula	M.W.[a]	CAS	Structure	EIC[b]	Score[c]
Benzaldehyde, 2-hydroxy-4-methoxy-3,6-dimethyl	$C_{10}H_{12}O_3$	180.2	34883-15-3		180	823
3,7,11,15-Tetramethyl-2-hexadecen-1-ol (Phytol)	$C_{20}H_{40}O$	296.5	150-86-7		123	804
Dodecane, 2,6,10-trimethyl	$C_{15}H_{32}$	212.41	3891-98-3		71, 85	832
1,4-Benzenediol, 2,3,5-trimethyl	$C_9H_{12}O_2$	152.19	700-13-0		152	836
2,6-Dimethyl-1,6-heptadiene	C_9H_{16}	124.22	51708-83-9		109	876
1-Octene, 3,7-dimethyl	$C_{10}H_{20}$	140.27	4984-01-04		55, 140	853
1-Octene, 3-methyl	C_9H_{18}	126.24	13151-08-01		55, 70	813

Summary of compounds identified from VEA vaping emission at each temperature. Information for each compound was obtained from PubChem. (30)

[a] M.W.: Molecular Weight (g mol^{-1})
[b] EIC: extracted ion chromatograph; ion selected for quantification
[c] Average match score over all collections
[d] tentative identification based on QCEIMS

Table S3.2. Cartesian Coordinates for optimized 1-pristene structure calculated by DFT/B3LYP/6-31G(d) level of theory using Gaussian 16W.

C	1.4556	2.5588	-0.4419
C	0.1548	2.5618	0.3875
C	-1.0279	1.8209	-0.2468
C	-3.5385	1.3131	-0.0081
C	-2.2859	1.9557	0.6197
C	2.1424	1.1834	-0.5674
C	2.3946	0.5004	0.7801
C	-3.3939	-0.1882	-0.3362
C	3.0745	-0.869	0.6531
C	1.2248	3.1483	-1.8381
C	-3.1609	-1.0999	0.8754
C	-4.7563	1.5737	0.8849
C	4.4851	-0.8724	0.0339
C	-2.9747	-2.5739	0.4878
C	5.0206	-2.3064	-0.0179
C	5.4639	0.0175	0.8
C	-1.8207	-2.8385	-0.4504
C	-0.443	-2.5224	0.0546
C	-2.0145	-3.3627	-1.6705
H	2.158	3.2241	0.0791
H	0.3402	2.1775	1.3962
H	-0.1409	3.6105	0.5312
H	-0.7624	0.7681	-0.3705
H	-1.2459	2.2263	-1.2402

H	-3.727	1.8254	-0.9616
H	-2.0951	1.5249	1.6099
H	-2.4872	3.0225	0.7836
H	1.5337	0.5206	-1.1952
H	3.0942	1.3243	-1.0927
H	1.4397	0.3266	1.2883
H	2.9791	1.1582	1.4324
H	-4.3073	-0.5205	-0.8474
H	-2.5885	-0.3114	-1.0677
H	3.1233	-1.3144	1.6556
H	2.4275	-1.5257	0.0587
H	0.7095	4.1125	-1.7772
H	2.1829	3.3172	-2.342
H	0.6359	2.4797	-2.4738
H	-4.0164	-1.0369	1.5575
H	-2.2852	-0.7625	1.4402
H	-4.943	2.6496	0.9733
H	-4.6115	1.1804	1.8961
H	-5.6566	1.1152	0.4628
H	4.4258	-0.5093	-0.9988
H	-3.9131	-2.9391	0.0505
H	-2.8218	-3.162	1.4017
H	5.1201	-2.7309	0.987
H	6.0048	-2.3371	-0.4974
H	4.3494	-2.9518	-0.5944
H	5.5127	-0.2643	1.8573

H	5.1748	1.0711	0.7395
H	6.473	-0.0651	0.3818
H	0.3325	-2.8176	-0.6603
H	-0.3302	-1.4514	0.2388
H	-0.2497	-3.0576	0.9899
H	-3.0093	-3.6015	-2.0314
H	-1.1832	-3.5626	-2.3382
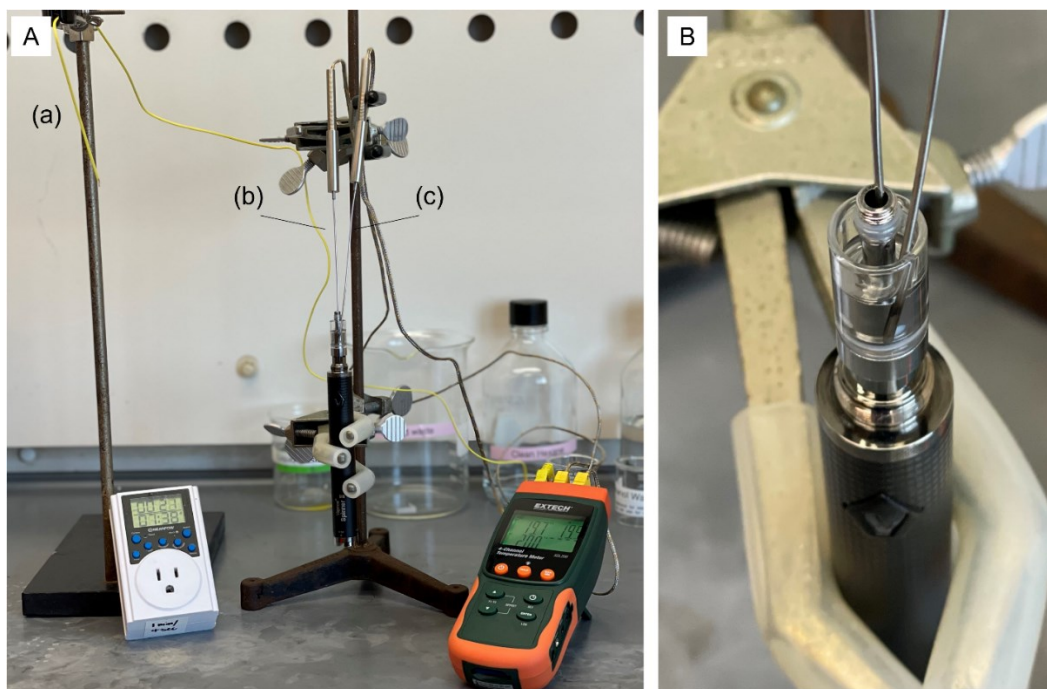
Figure S3.1. Set up of e-cigarette temperature measurements. (A) Set-up of temperature measurements. Set up of e-cigarette temperature measurements. Three k-type thermocouple wires were connected to a data logger, which recorded the temperature of (a) ambient air, (b) the ceramic coil of the e-cigarette cartridge, and (c) VEA oil in contact with the atomizer tube every 1s. (B) Close up of thermocouples inserted into the cartridge.
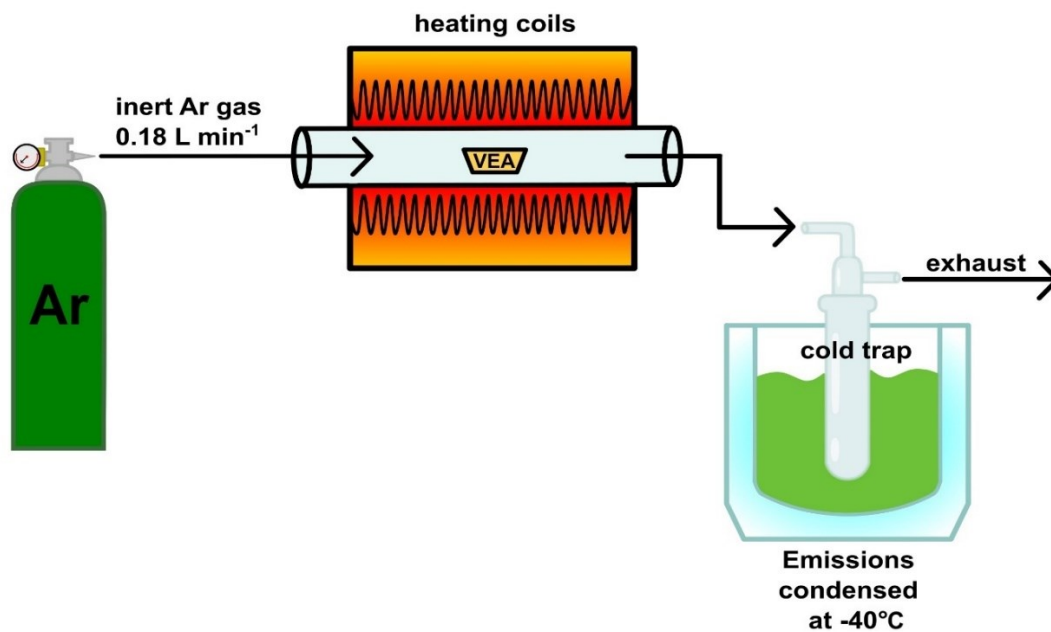
Figure S3.2. Schematic diagram of a high temperature quartz tube-furnace system. Gas flow is regulated by a 0.18 L min^{-1} critical orifice and argon gas is delivered into the quartz tube by a gas tank. Pyrolysis of VEA occurs as the furnace is heated by heating coils and generated aerosol is carried into a cold trap. The exhaust is removed via fume extractor.

Figure S3.3. Cartridges heated at 176 and 356 °C. Visible degradation and discoloration could be seen in the cartridge heated at 356 °C (right) versus the cartridge heated at 176 °C (left) after 13 cycles of 4s battery activation during temperature measurements.
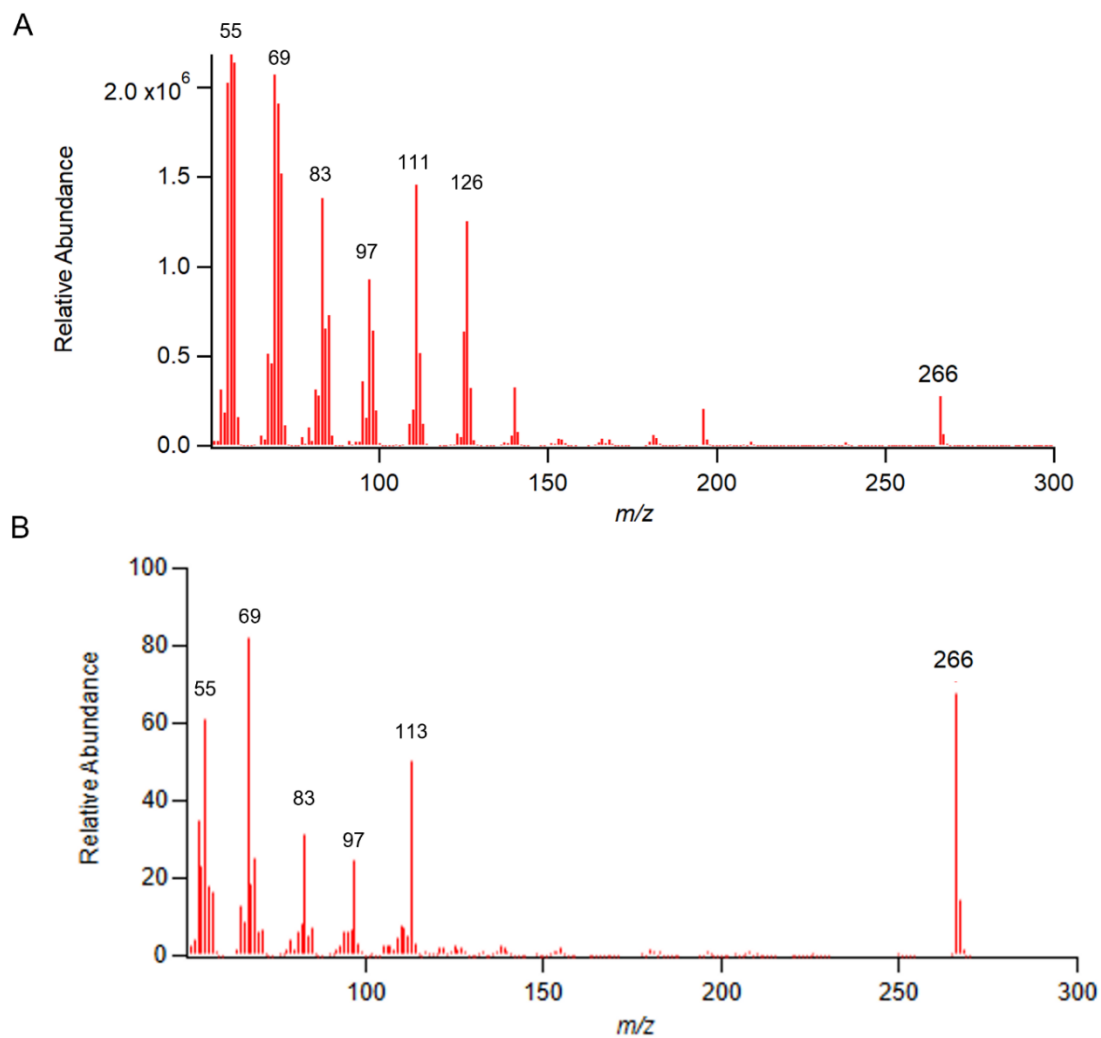
Figure S3.4. Comparison of mass spectra for 1-pristene identification. (A) Experimental mass spectrum obtained from vaping of VEA containing signature fragments with *m/z:* 266 (consistent with the molecular ion of 1-pristene), 111, 126, 97, 83, 69, 55. These identified fragments are consistent with the experimental mass spectrum identified as 1-pristene by Mikheev et al (55). (B) Simulated mass spectrum of 1-pristene obtained using QCEIMS containing signature fragments of *m/z:* 266, 111, 97, 83, 69, and 55.
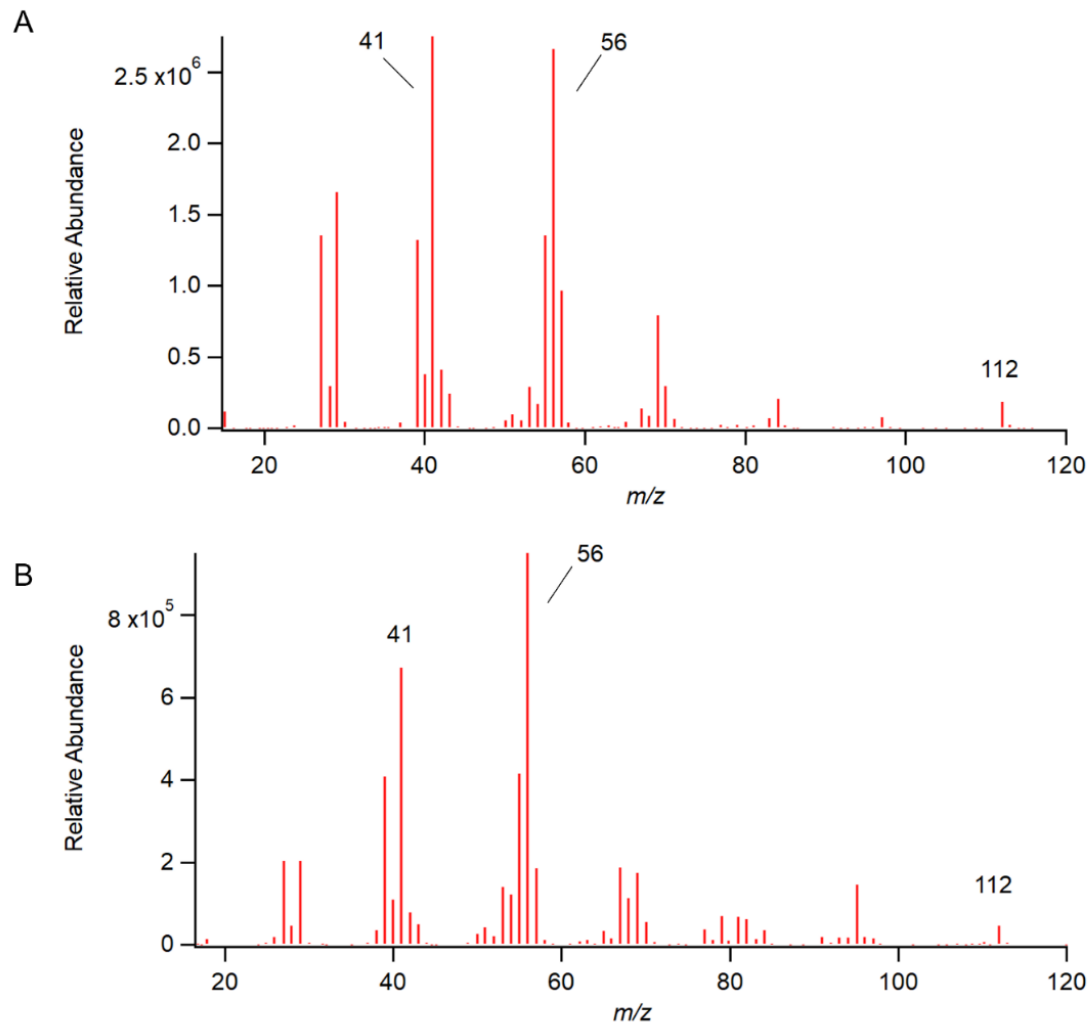
Figure S3.5. Comparison of mass spectra for 2-methyl-1-heptene identification (A) Experimental mass spectrum obtained from vaping of VEA containing signature fragments with *m/z:* 41, 56, and 112, consistent with 2-methyl-1-heptene. (B) Mass spectrum of authentic 2-methyl-1-heptene standard containing *m/z*: 41, 56, 112.
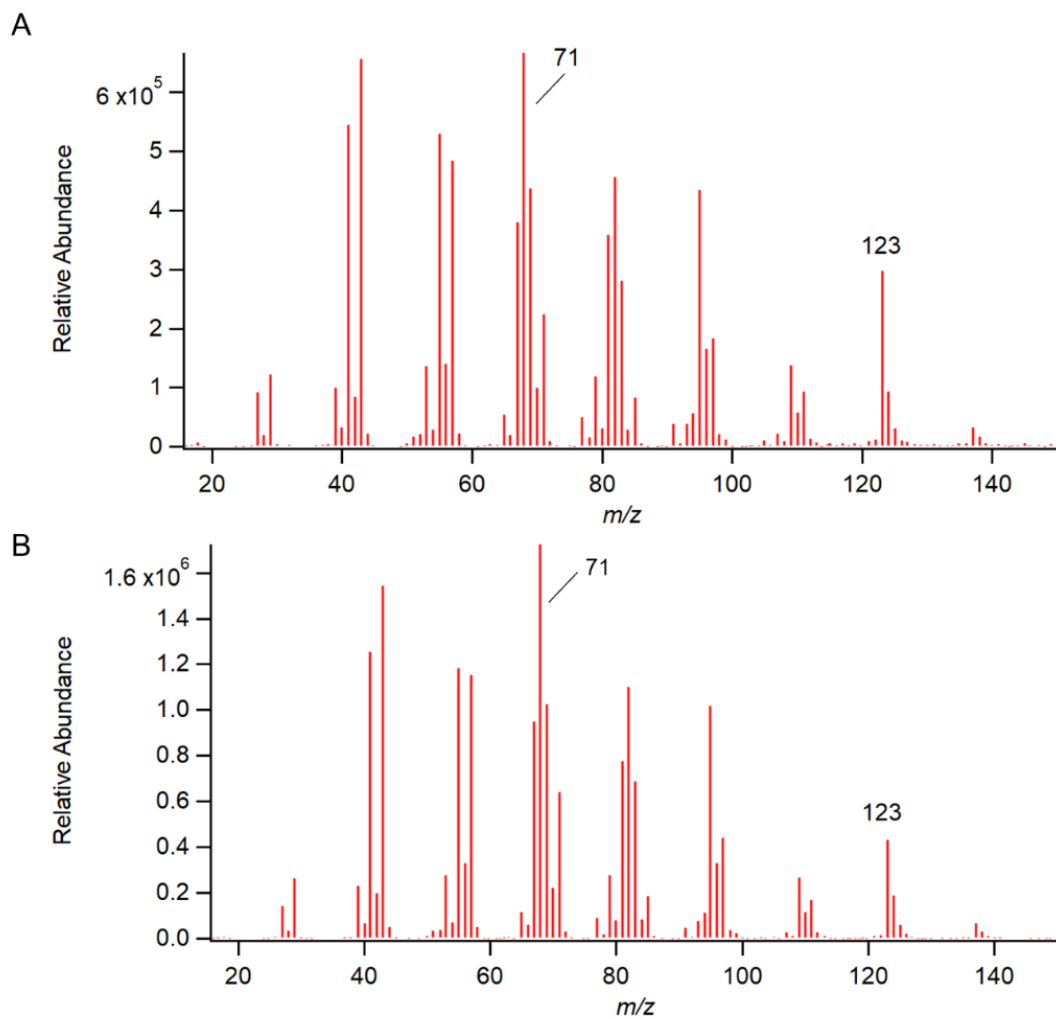
Figure S3.6. Comparison of mass spectra for phytol identification. (A) Experimental mass spectrum obtained from vaping of VEA containing signature fragments with *m/z:* 123 and 71, consistent with the natural isomer of phytol. (B) Mass spectrum of authentic phytol standard (natural isomer) containing *m/z*: 123 and 71.
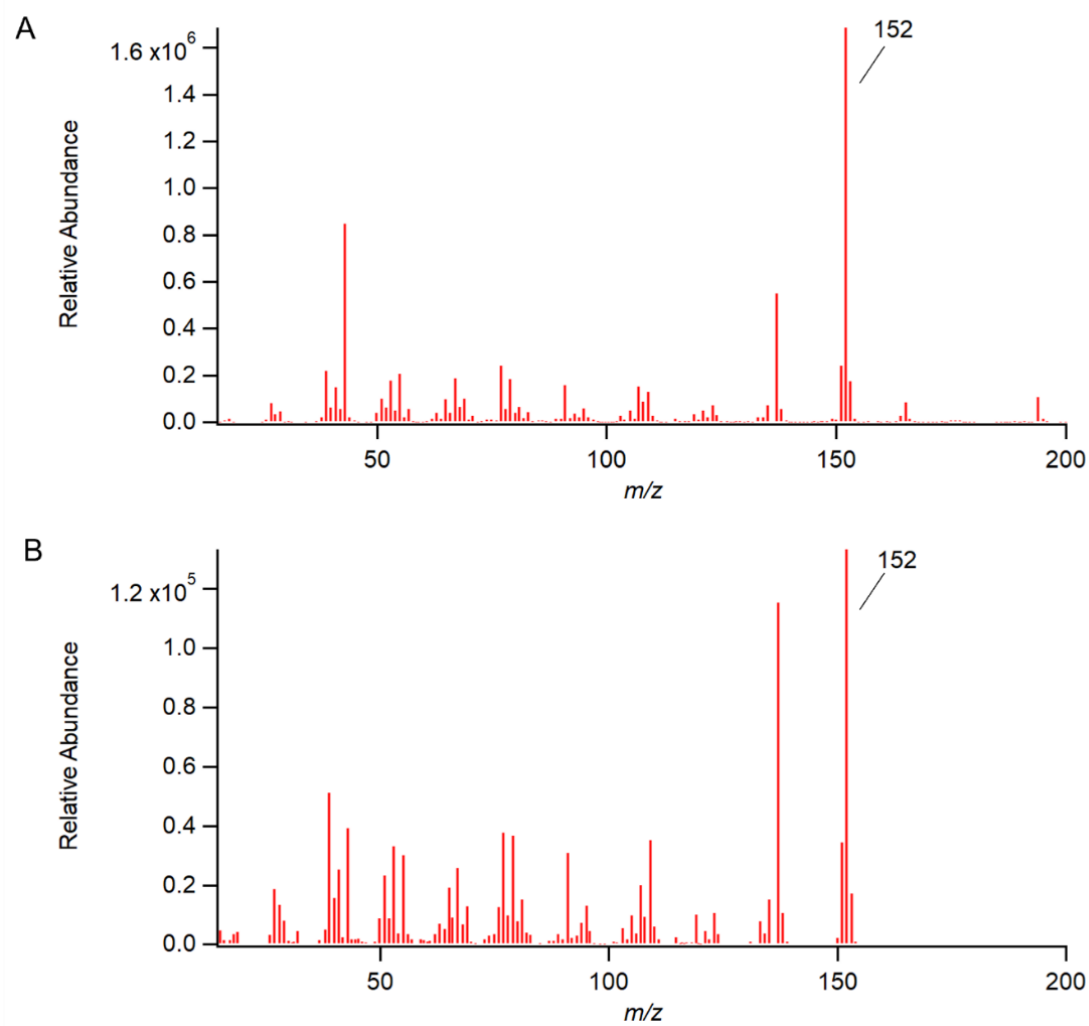
Figure S3.7. Comparison of mass spectra for 2,3,5-trimethyl-1,4-benzenediol identification. (A) Experimental mass spectrum obtained from vaping of VEA containing signature fragments with *m/z:* 152, consistent with 2,3,5-trimethyl-1,4-benzenediol. (B) Mass spectrum of authentic 2,3,5-trimethyl-1,4-benzenediol standard containing *m/z*: 152.

3.6 References

1.	CDC. Outbreak of Lung Injury Associated with the Use of E-Cigarette, or Vaping, Products. https://www.cdc.gov/tobacco/basic_information/e-cigarettes/severe-lung-disease.html.

2.	Blount, B. C.; Karwowski, M. P.; Shields, P. G.; Morel-Espinosa, M.; Valentin-Blasini, L.; Gardner, M.; Braselton, M.; Brosius, C. R.; Caron, K. T.; Chambers, D.; Corstvet, J.; Cowan, E.; De Jesús, V. R.; Espinosa, P.; Fernandez, C.; Holder, C.; Kuklenyik, Z.; Kusovschi, J. D.; Newman, C.; Reis, G. B.; Rees, J.; Reese, C.; Silva, L.; Seyler, T.; Song, M.-A.; Sosnoff, C.; Spitzer, C. R.; Tevis, D.; Wang, L.; Watson, C.; Wewers, M. D.; Xia, B.; Heitkemper, D. T.; Ghinai, I.; Layden, J.; Briss, P.; King, B. A.; Delaney, L. J.; Jones, C. M.; Baldwin, G. T.; Patel, A.; Meaney-Delman, D.; Rose, D.; Krishnasamy, V.; Barr, J. R.; Thomas, J.; Pirkle, J. L., Vitamin E Acetate in Bronchoalveolar-Lavage Fluid Associated with EVALI. *N. Engl. J. Med.* **2019,** *382* (8), 697-705.

3.	Duffy, B.; Li, L.; Lu, S.; Durocher, L.; Dittmar, M.; Delaney-Baldwin, E.; Panawennage, D.; LeMaster, D.; Navarette, K.; Spink, D., Analysis of Cannabinoid-Containing Fluids in Illicit Vaping Cartridges Recovered from Pulmonary Injury Patients: Identification of Vitamin E Acetate as a Major Diluent. *Toxics* **2020,** *8* (1).

4.	Shapiro, S. S.; Saliou, C., Role of vitamins in skin care. *Nutrition* **2001,** *17* (10), 839-844.

5.	Kumar, C. T.; Reddy, V. K.; Prasad, M.; Thyagaraju, K.; Reddanna, P., Dietary supplementation of Vitamin E protects heart tissue from exercise-induced oxidant stress. *Mol. Cell. Biochem.* **1992,** *111* (1), 109-115.

6.	Jiang, H.; Ahmed, C. M. S.; Martin, T. J.; Canchola, A.; Oswald, I. W. H.; Garcia, J. A.; Chen, J. Y.; Koby, K. A.; Buchanan, A. J.; Zhao, Z.; Zhang, H.; Chen, K.; Lin, Y.-H., Chemical and Toxicological Characterization of Vaping Emission Products from Commonly Used Vape Juice Diluents. *Chem. Res. Toxicol.* **2020,** *33* (8), 2157-2163.

7.	Wu, D.; O'Shea, D. F., Potential for release of pulmonary toxic ketene from vaping pyrolysis of vitamin E acetate. *PNAS* **2020,** *117* (12), 6349-6355.

8.	Mikheev, V. B.; Klupinski, T. P.; Ivanov, A.; Lucas, E. A.; Strozier, E. D.; Fix, C., Particle size distribution and chemical composition of aerosolized vitamin E acetate. *Aerosol Sci. Technol.* **2020,** *54* (9), 993-998.

9.	Lynch, J.; Lorenz, L.; Brueggemeyer, J. L.; Lanzarotta, A.; Falconer, T. M.; Wilson, R. A., Simultaneous Temperature Measurements and Aerosol Collection During Vaping for the Analysis of Δ9-Tetrahydrocannabinol and Vitamin E Acetate Mixtures in Ceramic Coil Style Cartridges. *Front. Chem.* **2021,** *9*, 643.

10.   Narimani, M.; da Silva, G., Does 'Dry Hit' vaping of vitamin E acetate contribute to EVALI? Simulating toxic ketene formation during e-cigarette use. *PLOS ONE* **2020,** *15* (9), e0238140.

11.   Chen, W.; Wang, P.; Ito, K.; Fowles, J.; Shusterman, D.; Jaques, P. A.; Kumagai, K., Measurement of heating coil temperature for e-cigarettes with a "top-coil" clearomizer. *PLOS ONE* **2018,** *13* (4), e0195925.

12.   Dibaji, S. A. R.; Guha, S.; Arab, A.; Murray, B. T.; Myers, M. R., Accuracy of commercial electronic nicotine delivery systems (ENDS) temperature control technology. *PLOS ONE* **2018,** *13* (11), e0206937.

13.   Talih, S.; Balhas, Z.; Eissenberg, T.; Salman, R.; Karaoghlanian, N.; El Hellani, A.; Baalbaki, R.; Saliba, N.; Shihadeh, A., Effects of User Puff Topography, Device Voltage, and Liquid Nicotine Concentration on Electronic Cigarette Nicotine Yield: Measurements and Model Predictions. *Nicotine Tob. Res.* **2015,** *17* (2), 150-157.

14.   Lechasseur, A.; Altmejd, S.; Turgeon, N.; Buonanno, G.; Morawska, L.; Brunet, D.; Duchaine, C.; Morissette, M. C., Variations in coil temperature/power and e-liquid constituents change size and lung deposition of particles emitted by an electronic cigarette. *Physiol. Rep.* **2019,** *7* (10), e14093.

15.   Zhao, T.; Shu, S.; Guo, Q.; Zhu, Y., Effects of design parameters and puff topography on heating coil temperature and mainstream aerosols in electronic cigarettes. *Atmos. Environ.* **2016,** *134*, 61-69.

16.   Li, Y.; Burns, A. E.; Tran, L. N.; Abellar, K. A.; Poindexter, M.; Li, X.; Madl, A. K.; Pinkerton, K. E.; Nguyen, T. B., Impact of e-Liquid Composition, Coil Temperature, and Puff Topography on the Aerosol Chemistry of Electronic Cigarettes. *Chem. Res. Toxicol.* **2021,** *34* (6), 1640-1654.

17.   Vas, G., Evaluation of Vitamin E Acetate Volatile Degradation Products; a possible Connection to the EVALI Epidemic. Rev. Sep. Sci. **2021** *3*(1), e21004

18.   Geiss, O.; Bianchi, I.; Barrero-Moreno, J., Correlation of volatile carbonyl yields emitted by e-cigarettes with the temperature of the heating coil and the perceived sensorial quality of the generated vapours. *Int. J. Hyg. Environ. Health* **2016,** *219* (3), 268-277.

19.   Sleiman, M.; Logue, J. M.; Montesinos, V. N.; Russell, M. L.; Litter, M. I.; Gundel, L. A.; Destaillats, H., Emissions from Electronic Cigarettes: Key Parameters Affecting the Release of Harmful Chemicals. *Environ. Sci. Technol.* **2016,** *50* (17), 9644-9651.

20.   Wagner, J.; Chen, W.; Vrdoljak, G., Vaping cartridge heating element compositions and evidence of high temperatures. *PLOS ONE* **2020,** *15* (10), e0240613.

21. Omaiye, E. E.; Williams, M.; Bozhilov, K. N.; Talbot, P., Design features and elemental/metal analysis of the atomizers in pod-style electronic cigarettes. *PLOS ONE* **2021,** *16* (3), e0248127.

22. Bonner, E.; Chang, Y.; Christie, E.; Colvin, V.; Cunningham, B.; Elson, D.; Ghetu, C.; Huizenga, J.; Hutton, S. J.; Kolluri, S. K.; Maggio, S.; Moran, I.; Parker, B.; Rericha, Y.; Rivera, B. N.; Samon, S.; Schwichtenberg, T.; Shankar, P.; Simonich, M. T.; Wilson, L. B.; Tanguay, R. L., The chemistry and toxicology of vaping. *Pharmacol. Ther.* **2021,** *225*, 107837.

23. Saliba, N. A.; El Hellani, A.; Honein, E.; Salman, R.; Talih, S.; Zeaiter, J.; Shihadeh, A., Surface chemistry of electronic cigarette electrical heating coils: Effects of metal type on propylene glycol thermal decomposition. *J. Anal. Appl. Pyrolysis* **2018,** *134*, 520-525.

24. Canchola, A.; Ahmed, C. M. S.; Chen, K.; Chen, J. Y.; Lin, Y.-H., Formation of Redox-Active Duroquinone from Vaping of Vitamin E Acetate Contributes to Oxidative Lung Injury. *Chem. Res. Toxicol.* **2022.**

25. Chen, J. Y.; Jiang, H.; Chen, S. J.; Cullen, C.; Ahmed, C. M. S.; Lin, Y.-H., Characterization of electrophilicity and oxidative potential of atmospheric carbonyls. *Environ. Sci.: Processes & Impacts* **2019,** *21* (5), 856-866.

26. Stein, S. E., Chemical substructure identification by mass spectral library searching. *J. Am. Soc. Mass Spectrom.* **1995,** *6* (8), 644-655.

27. Stein, S., Mass Spectral Reference Libraries: An Ever-Expanding Resource for Chemical Identification. *Anal. Chem.* **2012,** *84* (17), 7274-7282.

28. Grimme, S., Towards First Principles Calculation of Electron Impact Mass Spectra of Molecules. *Angew. Chem. Int. Ed.* **2013,** *52* (24), 6306-6312.

29. Gerasimov, P. A.; Gubareva, A. I.; Blokh, E. L.; Cherkasova, T. G.; Berezovykh, V. V., Physicochemical properties ofα-tocopherol acetate. *Pharma. Chem.* **1985,** *19* (10), 730-732.

30. Kim, S.; Chen, J.; Cheng, T.; Gindulyte, A.; He, J.; He, S.; Li, Q.; Shoemaker, B. A.; Thiessen, P. A.; Yu, B.; Zaslavsky, L.; Zhang, J.; Bolton, E. E., PubChem in 2021: new data content and improved web interfaces. *Nucleic Acids Res.* **2021,** *49* (D1), D1388-D1395.

31. Duffy, B.; Li, L.; Lu, S.; Durocher, L.; Dittmar, M.; Delaney-Baldwin, E.; Panawennage, D.; LeMaster, D.; Navarette, K.; Spink, D., Analysis of Cannabinoid-Containing Fluids in Illicit Vaping Cartridges Recovered from Pulmonary Injury Patients: Identification of Vitamin E Acetate as a Major Diluent. *Toxics* **2020,** *8* (1).

32.   LeBouf, R. F.; Ranpara, A.; Ham, J.; Aldridge, M.; Fernandez, E.; Williams, K.; Burns, D. A.; Stefaniak, A. B., Chemical Emissions From Heated Vitamin E Acetate—Insights to Respiratory Risks From Electronic Cigarette Liquid Oil Diluents Used in the Aerosolization of Δ9-THC-Containing Products. *Front. Public Health* **2022,** *9.*

33.   Byju, K.; Vasundhara, G.; Anuradha, V.; Nair, S. M.; Kumar, N. C., Presence of phytol, a precursor of vitamin E in Chaetomorpha antinnina. *Mapana Journal of Sciences* **2013,** *12* (2), 57-65.

34.   vom Dorp, K.; Hölzl, G.; Plohmann, C.; Eisenhut, M.; Abraham, M.; Weber, A. P. M.; Hanson, A. D.; Dörmann, P., Remobilization of Phytol from Chlorophyll Degradation Is Essential for Tocopherol Synthesis and Growth of Arabidopsis. *Plant Cell* **2015,** *27* (10), 2846-2859.

35.   Russo, E. B., Taming THC: potential cannabis synergy and phytocannabinoid-te6penoid entourage effects. *B. J. Pharmacol.* **2011,** *163* (7), 1344-1364.

36.   Schwotzer, D.; Gigliotti, A.; Irshad, H.; Dye, W.; McDonald, J., Phytol, not propylene glycol, causes severe pulmonary injury after inhalation dosing in Sprague-Dawley rats. *Inhalation Toxicol.* **2021,** *33* (1), 33-40.

37.   Ojo, O. O.; Ajayi, S. B.; Nwaechefu, O. O.; Ejidike, I. P., GC-MS Analysis and Attenuation of Bleomycin-Induced Lung Fibrosis by Fractionated Methanolic Extract of Cissampelos Owariensis in Wistar Rats. *J. Herbs Spices Med. Plants* **2020,** *26* (2), 155-171.

38.   Patocka, J.; Nepovimova, E.; Kuca, K., Toxic Alcohols: Aliphatic Unsaturated Alcohols. *MMSL* **2016,** *85* (4), 171-181.

39.   Baker, R. C.; Kramer, R. E., Cytotoxicity of short-chain alcohols. *Annu. Rev. Pharmacol. Toxicol.* **1999,** *39* (1), 127-150.

40.   Efsa Panel on Food Contact Materials, E. F.; Processing, A., Safety assessment of the substance α-tocopherol acetate for use in food contact materials. *EFSA Journal* **2016,** *14* (3), 4412.

41.   Ushikusa, T.; Maruyama, T.; Niiya, I., Pyrolysis behavior and thermostability of tocopherols. *JOCS* **1991,** *40* (12), 1073-1079.

42.   Williams, M.; Li, J.; Talbot, P., Effects of Model, Method of Collection, and Topography on Chemical Elements and Metals in the Aerosol of Tank-Style Electronic Cigarettes. *Sci. Rep.* **2019,** *9* (1), 13969.

43.   Williams, M.; Villarreal, A.; Bozhilov, K.; Lin, S.; Talbot, P., Metal and Silicate Particles Including Nanoparticles Are Present in Electronic Cigarette Cartomizer Fluid and Aerosol. *PLOS ONE* **2013,** *8* (3), e57987.

44.   Gonzalez-Jimenez, N.; Gray, N.; Pappas, R. S.; Halstead, M.; Lewis, E.; Valentin-Blasini, L.; Watson, C.; Blount, B., Analysis of Toxic Metals in Aerosols from Devices Associated with Electronic Cigarette, or Vaping, Product Use Associated Lung Injury. *Toxics* **2021,** *9* (10).

45.   Jaegers, N. R.; Hu, W.; Weber, T. J.; Hu, J. Z., Low-temperature (<200 °C) degradation of electronic nicotine delivery system liquids generates toxic aldehydes. *Sci. Rep.* **2021,** *11* (1), 7800.

46.   Chen, J. Y.; Canchola, A.; Lin, Y.-H., Carbonyl Composition and Electrophilicity in Vaping Emissions of Flavored and Unflavored E-Liquids. *Toxics* **2021,** *9* (12).

47.   Wang, S.; Kind, T.; Tantillo, D. J.; Fiehn, O., Predicting in silico electron ionization mass spectra using quantum chemistry. *J. Cheminform.* **2020,** *12* (1), 63.

48.   Cunningham, A.; Slayford, S.; Vas, C.; Gee, J.; Costigan, S.; Prasad, K., Development, validation and application of a device to measure e-cigarette users' puffing topography. *Sci. Rep.* **2016,** *6* (1), 35071.

49.   Behar, R. Z.; Hua, M.; Talbot, P., Puffing Topography and Nicotine Intake of Electronic Cigarette Users. *PLOS ONE* **2015,** *10* (2), e0117222.

50.   Braymiller, J. L.; Barrington-Trimis, J. L.; Leventhal, A. M.; Islam, T.; Kechter, A.; Krueger, E. A.; Cho, J.; Lanza, I.; Unger, J. B.; McConnell, R., Assessment of Nicotine and Cannabis Vaping and Respiratory Symptoms in Young Adults. *JAMA Network Open* **2020,** *3* (12), e2030189-e2030189.

51.   Su, W.-C.; Lin, Y.-H.; Wong, S.-W.; Chen, J. Y.; Lee, J.; Buu, A., Estimation of the dose of electronic cigarette chemicals deposited in human airways through passive vaping. *J. Expo. Sci. Environ. Epidemiol.* **2021**.

52.   Son, Y.; Mishin, V.; Laskin, J. D.; Mainelis, G.; Wackowski, O. A.; Delnevo, C.; Schwander, S.; Khlystov, A.; Samburova, V.; Meng, Q., Hydroxyl Radicals in E-Cigarette Vapor and E-Vapor Oxidative Potentials under Different Vaping Patterns. *Chem. Res. Toxicol.* **2019,** *32* (6), 1087-1095.

53. Grimme S. Towards First Principles Calculation of Electron Impact Mass Spectra of Molecules. *Angew. Chem. Int. Ed.* **2013**, *52* (24), 6306 - 6312.

54.   Koopman J, Grimme S. Calculation of Electron Ionization Mass Spectra with Semiempirical GFNn-xTB Methods. *ACS Omega*. **2019**, *4* (12), 15120 - 15133

55.   Mikheev VB, Klupinski TP, Ivanov A, Lucas EA, Strozier ED, Fix C. Particle size distribution and chemical composition of aerosolized vitamin E acetate. *Aerosol Sci. Technol*. 2020, *54* (9), 993 - 998.

Chapter 4: External Factors Modulating Vaping-Induced Thermal Degradation of Vitamin E Acetate

4.0 Abstract

Despite previous studies indicating the thermal stability of vitamin E acetate (VEA) at low temperatures, VEA has been shown to readily decompose into various degradation products such as alkenes, long-chain alcohols, and carbonyls such as duroquinone (DQ) at vaping temperatures of <200 °C. While most models simulate the thermal decomposition of e-liquids under pyrolysis conditions, numerous factors, including vaping behavior, device construction, and the surrounding environment, may impact the thermal degradation process. In this study, we investigated the role of the presence of molecular oxygen (O_2) and transition metals in promoting thermal oxidation of e-liquids, resulting in greater degradation than predicted by pure pyrolysis. Thermal degradation of VEA was performed in inert (N_2) and oxidizing atmospheres (clean air) in the absence and presence of Ni–Cr and Cu–Ni alloy nanopowders, metals commonly found in the heating coil and body of e-cigarettes. VEA degradation was analyzed using thermogravimetric analysis (TGA) and gas chromatography/mass spectrometry (GC/MS). While the presence of O_2 was found to significantly enhance the degradation of VEA at both high (356 °C) and low (176 °C) temperatures, the addition of Cu–Ni to oxidizing atmospheres was found to greatly enhance VEA degradation, resulting in the formation of numerous degradation products previously identified in VEA vaping emissions. O_2 and Cu–Ni nanopowder together were also found to significantly increase the production of OH radicals, which has implications for e-liquid degradation pathways as well as the

potential risk of oxidative damage to biological systems in real-world vaping scenarios. Ultimately, the results presented in this study highlight the importance of oxidation pathways in VEA thermal degradation and may aid in the prediction of thermal degradation products from e-liquids.

4.1 Introduction

Recent research has revealed that the inhalation of aerosols released by e-cigarettes has the potential to negatively impact the lungs of users, despite the prevalent assumption of safety among e-cigarette consumers. (1, 2) Though many commonly used e-liquid ingredients, including propylene glycol (PG), glycerin (VG), and various flavoring agents, are considered safe for consumption or dermal absorption, emitted aerosols are complex mixtures of compounds formed from the thermal degradation of e-liquids that occurs during the vaping process. (3) This process results in the formation of emission products with different physiochemical properties and a risk of toxicity potentially greater than that posed by the parent e-liquids. (3−6) For example, vitamin E acetate (VEA), the proposed cause of the e-cigarette or vaping-associated lung injury (EVALI) outbreak in the United States in 2019, has been found to decompose into thermal degradation products, including vitamin E (VE), various long-chain alcohols, alkenes, carbonyls, and, most notably, the reactive species duroquinone (DQ) and ketene. (3, 4, 7−9) While VEA itself is perceived as safe, the inhalation of electrophilic species like DQ produced during vaping poses a serious risk of oxidative damage to lung tissue. (4, 9−11) As such, to understand the potential health risk to users, the prediction of the

thermal degradation behavior of various e-liquids through computational and experimental methods has been of particular interest in recent e-cigarette research.

In addition to potentially toxic organic products, there is also the potential for the release of metals into the e-liquid and e-cigarette emissions at potentially toxic concentrations. e-Cigarette devices often contain various transition metals, including Ni, Fe, Cu, Cr, etc. (12−15) A recent study by Williams et al. (16) detected particles containing metals such as Sn, Ag, Fe, Ni, Al, and Cr in e-cigarette aerosol emissions. In a similar study, McDaniel et al. (12) found various levels of transition metals, including Cr, Cu, and Ni, in e-cigarette aerosols and leached into the e-liquid. These metals pose a risk of metal toxicity to vape users upon inhalation, (17) and recent studies have suggested a potential catalytic role in the thermal degradation of e-liquids, particularly at low temperatures. (7, 18, 19)

There are several driving factors that have been suggested to influence the physiochemical properties of e-cigarette emissions, including puffing topography (20,21) and temperature. (7, 22) Changes in the temperature used to heat e-liquids during vaping have been demonstrated to affect the size and volume distribution of emitted aerosols, (21, 23) the release of metals (24) or reactive oxygen species (ROS), (25−27) and the chemical composition of e-cigarette emissions. (22, 28) Though use of VEA is not widespread in commercial e-liquids, the extensive efforts to characterize vaping emission products of VEA allow it to be more easily used as a model compound to monitor changes caused by various vaping parameters. In ref (7) our lab found a temperature dependence in the chemical composition of VEA vaping emissions when VEA was vaped

at temperatures ranging from 176 to 356 °C and demonstrated discrepancies in chemical composition when VEA was vaped versus heated without the device. While previous theoretical and experimental studies have demonstrated VEA to be thermally stable up to 250 °C under pure pyrolysis conditions, (29) our studies indicate that VEA degrades into compounds such as DQ when vaped at temperatures of <200 °C. Under pure pyrolysis conditions in an inert argon atmosphere, VEA did not appear to degrade until the temperature exceeded 300 °C. Furthermore, previous studies in our lab have frequently detected DQ in vaping emissions at temperatures significantly lower than those predicted by theoretical calculations. (3, 4, 7)

Discrepancies in the product distribution of VEA vaping emissions and pyrolysis-simulated VEA breakdown at equitable temperatures may indicate the influence of external factors, such as the presence of atmospheric oxygen molecules (O_2) and metal catalysts, on e-liquid degradation. In e-cigarette systems, the presence of metal filament wires has been suggested to have strong catalytic effects on the thermal degradation of PG and VG, reducing the temperature needed to observe carbonyl-containing compounds in vaping emissions. (18, 19) Furthermore, metal catalysis has been found to be an important factor in thermal degradation pathways in analyses of systems such as biochar. (30) The presence of O_2 has also been found to greatly decrease the temperature required to observe the thermal degradation of PG and VG and may play an important role in the low-temperature degradation of e-liquids. (7, 31, 32)

For this reason, we hypothesized that the presence of O_2 and transition metals in the e-cigarette body promotes the thermal oxidation of e-liquids, resulting in greater degradation at low temperatures than what is predicted by pure pyrolysis. To address this hypothesis, we used VEA as a model compound to compare how thermal degradation of organics may be altered when they are heated under inert (N_2) and oxidizing (clean air) atmospheres, with and without the addition of metal alloys. To monitor these changes, we used a combination of gas chromatography/mass spectrometry (GC/MS) and thermogravimetric analysis (TGA). Direct measurement of hydroxyl (OH) radicals was also carried out using the fluorometric terephthalate (TPT) assay. The results of this study further our understanding of the influence of O_2 and metals on the thermal degradation of organic compounds and the resulting health risks upon inhalation.

4.2 Materials and Methods

4.2.1 Materials

Vitamin E acetate (dl-α-tocopherol acetate, VEA, >97%) and disodium terephthalate (TPT, >99%) were purchased from Tokyo Chemical Industry (TCI America, Inc.). Nickel–chromium (Ni–Cr, 99.9%, 8:2 Ni:Cr) and copper–nickel (Cu–Ni, 99.9%, 5:5 Cu:Ni) alloy nanopowders were purchased from US Research Nanomaterials Inc. 1,2,3-Trichlorobenzene (1,2,3-TCB, 98%) and 2-hydroxyterephthalic acid (2-OHTA, >98%) were purchased from Alfa Aesar. Acetonitrile (ACN, 99.95%) was purchased from Fisher Chemical. Phosphate-buffered saline (PBS, 1×) was purchased from Corning.

4.2.2 Thermogravimetric Analysis (TGA)

TGA was performed on a Netzsch TG 209 F1 Libra instrument to characterize the mass changes (loss or gain) of VEA as a function of temperature in the inert and oxidizing atmospheres due to volatilization, decomposition, or oxidation. VEA was added to a 6.8 nm diameter alumina crucible using a rubber syringe with enough sample to coat the bottom of the crucible in a thin layer, which gave a sample mass of approximately 10 mg. The exact mass of the crucible and sample was measured by the instrument at the start of each experiment. VEA was heated using a temperature ramp of 10 K min^{-1} using either N_2 or clean air as a carrier gas. The instrument was operated using a flow rate of 40 mL min^{-1} and an instrument protective flow rate of 10 mL min^{-1}.

4.2.3 Pyrolysis GC/MS

Pyrolysis gas chromatography/mass spectrometry (Pyr-GC/MS) was used to analyze the pyrolysis products of VEA. A CDS 5150 Pyroprobe (CDC Analytical, Inc.) was used to heat 250 mg of VEA at 356 °C in either N_2 or clean air environments. The pyrolysis products were directly injected onto an Agilent HP5-MS fused silica column and analyzed using GC/MS [Agilent 7890 GC and 5975 inert MSD equipped with an electron ionization (EI) ion source] following the ASTM D3452-06 standard method. (33)

4.2.4 Tube Furnace Experiments

Thermal degradation of VEA was simulated using a tube furnace reactor system (OTF-1200X, MTI Corp.) as described in our previous work. (7) One hundred milligrams of VEA was weighed into an alumina crucible, and the crucible placed in a high-temperature quartz tube furnace. Either ultra-high-purity N_2 (Airgas Inc.) or Ultra Zero grade clean air (Airgas Inc.) was used as a carrier gas at a flow rate of 0.18 L min^{-1} to deliver off-gassing products from VEA volatilization or thermal degradation to a cold trap apparatus. The cold trap was kept on dry ice to allow the collection of condensed emission products. The temperature was initially set to 30 °C, ramped to either 356 or 176 °C at a rate of 10 °C min^{-1}, and held for 1 min. The crucible was reweighed after each experiment to determine the mass loss, and 1 mL of ACN was added to the cold trap to dissolve captured emission products for chemical analysis. Cold trap samples were concentrated to 150 μL under a gentle N_2 gas stream. A 50 μL aliquot of each sample was taken for chemical analysis; 5 μL a 1,2,5-TCB (2 μg μL^{-1}) solution was added to each sample as an internal standard.

VEA was heated in N_2 and clean air environments in the absence and presence of 10 mg of Ni–Cr or Cu–Ni alloy nanopowders, which were chosen as representative components of e-cigarette heating coils. (12) A total of six experiments were performed, each with three replicates for statistical analysis.

4.2.5 GC/MS Analysis of Tube Furnace Samples

The samples collected from the tube furnace experiments were analyzed using GC/MS (Agilent 6890N GC and 5975C inert MSD equipped with an EI ion source). Helium was used as the carrier gas. To quantify more polar oxygenated products such as DQ in the collected emissions, 2 μL of each sample was directly injected onto a Restek Rtx-VMS fused silica column [30 m × 0.25 mm i.d. (inside diameter), 1.4 μm film]. The temperature of the GC started at 35 °C, was held for 1 min, was ramped to 240 °C at a rate of 10 °C min^{-1}, and was held for 4 min. To quantify nonpolar compounds such as VEA and 1-pristene, 1 μL of each sample was injected onto an Agilent J&W DB-5MS column (30 m × 0.25 mm i.d., 0.25 μm film). The temperature started at 60 °C, was held for 1 min, was ramped to 310 °C at a rate of 10 °C min^{-1}, and was held for 5 min.

4.2.6 Generation of OH Radicals

Generation of OH radicals was measured using the fluorescent probe disodium terephthalate (TPT), which readily reacts with OH radicals to form the stable fluorescent product 2-OHTA. (34−36) As the formation rate of 2-OHTA is directly proportional to the generation of OH radicals (1:1), the fluorescence of 2-OHTA can be measured using a microplate reader and used to directly quantify OH radical formation during VEA thermal degradation. The outflow of the tube furnace was bubbled through a 30 mL mini-impinger filled with 15 mL of a 5 mM TPT solution in 1× PBS. Once heating was finished, 100 μL of the solution was immediately transferred to a black, clear-bottom 96-well plate (Corning). Fluorescence was measured using a TECAN Spectrafluor plus

microplate reader (excitation at 310 nm, emission at 422 nm). The concentration of 2-OHTA produced was determined on the basis of a calibration curve of 2-OHTA standard fluorescence in 1× PBS (**Figure S4.1**).

4.3 Results

4.3.1 TGA

Dynamic TGA was used to continuously measure the change in the mass of VEA as the temperature was increased to determine the loss of gaseous byproducts formed during pure VEA pyrolysis under N_2 and clean air atmospheres. The results of TGA of VEA heated under N_2 and clean air carrier gases are shown in **Figure 4.1**. A summary of the major differences in the percent mass loss of VEA at various temperatures can be found in Table S1. Ultimately, the percent mass of VEA remaining is consistently greater in the oxidizing atmosphere than in the inert atmosphere. Volatilization of VEA appeared to begin around 250 °C in the inert atmosphere, which agrees with previous literature regarding the boiling point and pyrolysis of VEA. (29,37) Clean air, in comparison, did not show signs of volatilization until temperatures of ≥300 °C had been reached, demonstrating a substantially slower rate of degradation than when heated in N_2 (**Figure 4.1A**). By 400 °C, 1.61% of VEA remained in the crucible in the inert atmosphere, compared to 6.94% that remained in the clean air atmosphere. Furthermore, crucibles heated in N_2 contained either no residue or small amounts of VEA oil remaining inside after heating; in contrast, crucibles heated in clean air contained visible black residue, likely from the mineralization of VEA in the presence of clean air (**Figure 4.1B**). It is likely that, in clean air, VEA may be oxidized by O_2 to form various oxidation products

that require greater temperatures to undergo the transition to the gas phase or decompose into further volatile degradation products. Residue permanently remaining from VEA mineralization may also explain why complete consumption of VEA by 400 °C cannot be seen in clean air compared to the N_2 atmosphere. Notably, the presence of O_2 alone did not appear to promote VEA phase transfer at low temperatures but did result in the production of degradation products with chemical properties different from those of VEA alone.
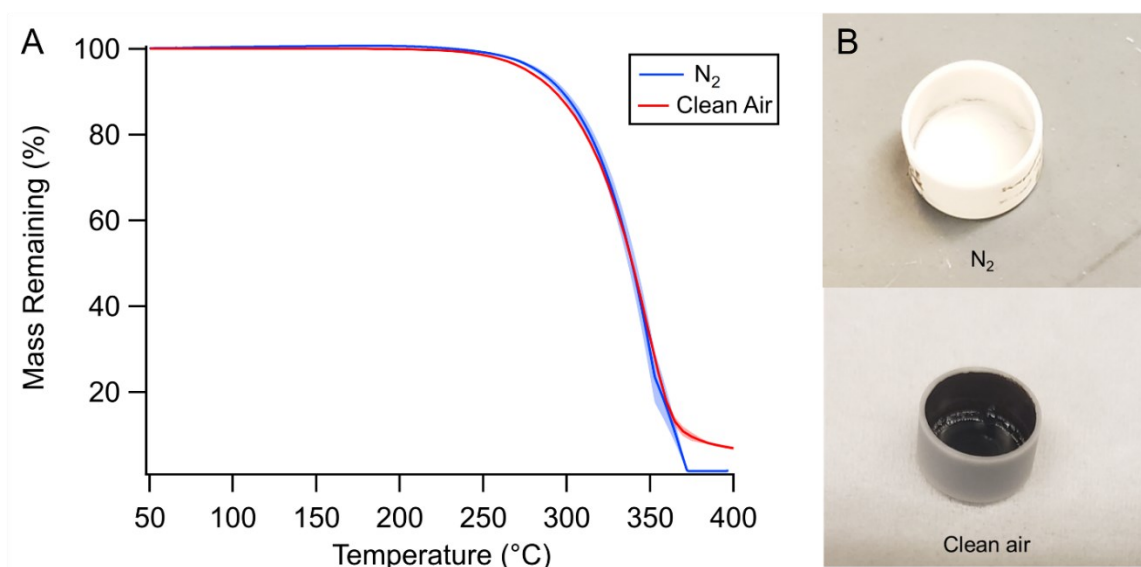
Figure 4.1. (A) TGA curve of VEA heated in N_2 and clean air atmospheres. Results are expressed as the mean of 3 replicates (n=3), ± standard error of the mean (SEM; represented by the shaded area surrounding each line). (B) Images of crucibles after heating to 400 °C; 1.61% of initial mass remained in crucible heated in N_2 (top), 6.94% remained in crucibles heated in clean air (bottom).

4.3.2 Pyr-GC/MS

To further investigate the influence of O_2 on the chemical composition of VEA thermal degradation products, Pyr-GC/MS was used to monitor the breakdown of VEA at 356 °C in N_2 and clean air. This temperature was chosen because 356 °C was the highest average coil temperature to which VEA was exposed while vaping with a CCell TH2 cartridge in our previous work. (7) At this temperature, substantial degradation could be observed in the analysis of vaping emissions, but simulation of pure pyrolysis with inert argon as a carrier gas showed a significantly decreased number and concentration of degradation products.

The total ion chromatograms (TICs) obtained from Pyr-GC/MS in each atmosphere are shown in **Figure 4.2**. A targeted search was performed for previously reported VEA vaping emission products using the NIST 2008 spectral database. A match score of ≥850 and a probability of ≥50% were considered a good match; authentic standards were used to confirm identified peaks when commercially available. Though VEA shows substantial degradation into various compounds in vaping scenarios at 356 °C, (7) no substantial degradation could be observed after heating in the inert N_2 atmosphere (**Figure 4.2A**). Major peaks for VE and VEA were visible at retention times of 38 min (peak 2) and 40.3 min (peak 3), respectively, indicating volatilization of VEA and potential loss of the acetate group at 356 °C. The dominant peaks of VE and VEA are assumed to correspond to the α-isomers based on the initial standard used; smaller peaks corresponding to other common isomers (β, γ, and δ) can also be seen but cannot be differentiated due to the resolution of the mass spectrometer used. Finally, a peak

corresponding to the N₂ carrier gas can be seen at 3.7 min (peak 1). Four peaks in this spectrum could not be identified due to a lack of NIST matches.
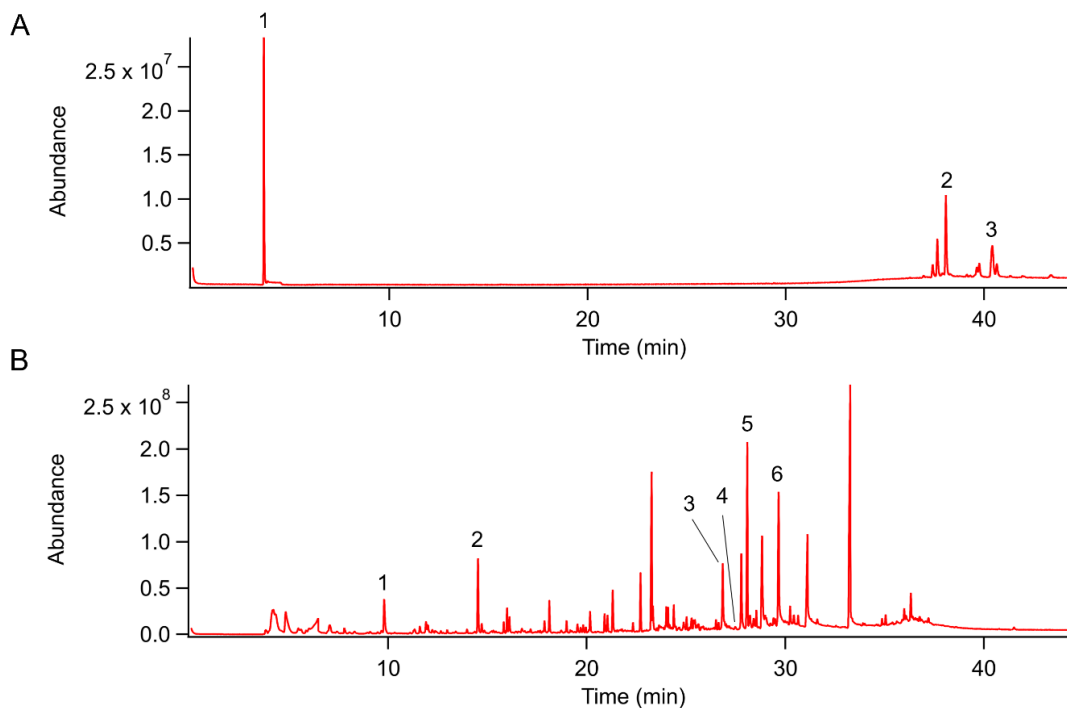
Figure 4.2. Total ion chromatographs (TIC) obtained from Pyr-GC/MS of VEA in (A) N₂ and (B) clean air atmospheres.

When VEA and VE were heated to the same temperature in clean air, their concentrations decreased below the detection limit of the instrument and could not be observed. Instead, a wide range of degradation products commonly observed in vaping emissions could be seen in the resulting TIC (**Figure 4.2B**). Ultimately, analysis of these results found the presence of 4-methyl-1-pentanal (peak 1; tR = 9.805 min), 4-methyl-1-decene (peak 2; tR = 15.830 min), 3,7,11-trimethyl-1-dodecanol (peak 3; tR = 26.84 min), durohydroquinone (DHQ) (peak 4; tR = 27.103 min), 1-pristene (peak 5; tR =

28.073 min), and 2-hydroxy-4-methoxy-3,6-dimethyl benzaldehyde (peak 6; tR = 28.834 min), all of which have been previously detected in VEA vaping emissions. (4, 7−10, 38, 39) DQ was not observed at levels above the detection limit of the instrument, though DQ formation can be assumed due to the detection of 1-pristene and DHQ. (9, 39) Ultimately, it is clear that the presence of O_2 when VEA is heated results in the production of compounds often found in VEA vaping emissions, indicating the importance of oxidation pathways during vaping thermal degradation.

4.3.3 GC/MS Analysis of VEA Thermal Degradation

VEA was then heated in a tube furnace reactor under six different environmental conditions to investigate the effect of the presence of O_2 and metal alloys on the chemical composition of VEA thermal degradation products at high (356 °C) and low (176 °C) temperatures. The amount of mass consumed (i.e., lost as gas-phase compounds through volatilization, decomposition, or oxidation) during the tube furnace reaction at 356 °C remained mostly constant between the environmental conditions, though VEA heated with Cu–Ni alloy nanopowder showed a slight increase in mass consumption compared to the others. The greatest average mass consumption was seen in VEA heated in clean air with Cu–Ni nanopowder (**Figure S4.2A**).

4.3.4 High-Temperature Experiments at 356 °C

Off-gassing products were collected using a cold trap apparatus and analyzed using GC/MS. The TICs obtained from heating VEA under each condition at 356 °C are shown in **Figure 4.3**. Similar to the results obtained in our prior study, (7) substantial

VEA degradation was not observed under inert N_2 atmospheres, nor did the addition of metal nanopowders significantly alter the resulting product distribution. In contrast, the number and abundance of VEA degradation products substantially increased when VEA was heated in oxidizing atmospheres. Furthermore, VEA heated in an oxidizing atmosphere in the presence of Cu–Ni demonstrated the greatest number of peaks compared to other environments, indicating greater degradation of VEA. In addition, after heating in N_2 environments (regardless of the addition of metal nanopowders), VEA oil remained clear with no visible discoloration, whereas after heating in O_2, VEA oil became a dark orange-brown color, indicating the formation of various thermal degradation products in oxidizing atmospheres (**Figure S4.3**).

Six representative degradation products were then chosen for quantification to further investigate how O_2 and metal alloys influence the identity and concentration of compounds formed from VEA degradation. These compounds include VEA [tR = 27.32 min (**Figure 4.3A, C**)], 1-pristene [tR = 19.89 min (**Figure 4.3B, D**)], DQ [tR = 16.69 min (**Figure 4.3B, D**)], 2-hydroxy-4-methoxy-3,6-dimethyl benzaldehyde [tR = 22.67 min (**Figure 4.3B, D**)], 3,7,11-trimethyl-1-dodecanol [tR = 19.21 min (**Figure 4.3B, D**)], and 6,10-dimethyl-2-undecanone [tR = 17.24 min (**Figure 4.3B, D**)]. To quantify the production of each compound, the peak areas were normalized to that of the 1,2,3-TCB internal standard. The concentration of each compound was then expressed as the mass of product normalized to the initial mass of VEA (i.e., milligrams of product recovered per milligram of initial VEA). A two-way analysis of variance (ANOVA) with either a Tukey HSD or Šidák posthoc analysis was used to determine the statistical significance of

treatments. The masses of the representative thermal degradation products formed at 356

°C are shown in **Figure 4.3E**.

Figure 4.3. VEA product distribution under six different environmental conditions at 356 °C. Total ion chromatographs (TIC) were obtained from VEA pyrolysis in (A) N_2 environments in a non-polar separation column, (B) N_2 in a polar separation column, (C) clean air in a non-polar separation column, and (D) clean air in a polar separation column. (E) Masses of thermal degradation products, including VEA, 1-pristene, duroquinone, 2-hydroxy-4-methoxy-3,6-dimethyl benzaldehyde, 3,7,11-trimethyl-1-dodecanol, and 6,10-dimethyl-2-undecanone, formed under N_2 and clean air atmospheres at 356 °C. Results are expressed as the mean ± SEM (n=3). * Indicates $p < 0.05$; ** indicates $p < 0.01$, *** indicates $p < 0.001$.

Regardless of metal alloys, a significantly greater mass of VEA was found in VEA emissions generated under N_2 than under clean air, indicating greater decomposition of VEA in the presence of O_2 than in inert atmospheres. For 1-pristene, the addition of Ni–Cr or Cu–Ni alloy nanopowder in the inert environment resulted in significantly greater mass compared to the absence of metals, with Cu–Ni resulting in the greatest mass across all environments. There was no statistical difference between clean air environments. 3,7,11-Trimethyl-1-dodecanol consistently showed slightly greater (though not statistically significant) masses in the inert atmosphere than in the oxidizing atmosphere. Interestingly, for DQ, 2-hydroxy-4-methoxy-3,6-dimethyl benzaldehyde, and 6,10-dimethyl-2-undecanone, we observed significant differences in recovered masses between the inert and oxidizing atmospheres in the oxidizing atmosphere and in the presence of Cu–Ni nanopowder. Significantly greater DQ masses could be seen in the inert environments in the presence of Cu–Ni nanopowder, while 2-hydroxy-4-methoxy-3,6-dimethyl benzaldehyde and 6,10-dimethyl-2-undecanone demonstrated greater masses in the presence of O_2 and Cu–Ni.

4.3.5 Low Temperature Experiments at 176 °C

Mass consumption at 176 °C showed a trend similar to that seen at 356 °C, with the addition of Cu–Ni nanopowder in either atmosphere resulting in a slight increase in mass consumed compared to the other environments (**Figure S4.2B**). The TIC obtained from heating VEA under each condition at 176 °C also shows a similar pattern, as while the addition of metal nanopowders did not appear to substantially shift the product distribution in an inert atmosphere (**Figure 4.4A, B**), the presence of Cu–Ni nanopowder

resulted in the greatest number and abundance of peaks in an oxidizing atmosphere (**Figure 4.4C, D**), indicating substantial degradation of VEA similar to that seen in low-temperature vaping of VEA. (7) The appearance of the remaining VEA oil after heating to 176 °C, on the contrary, did not visibly differ between any of the environmental conditions (**Figure S4.4**).
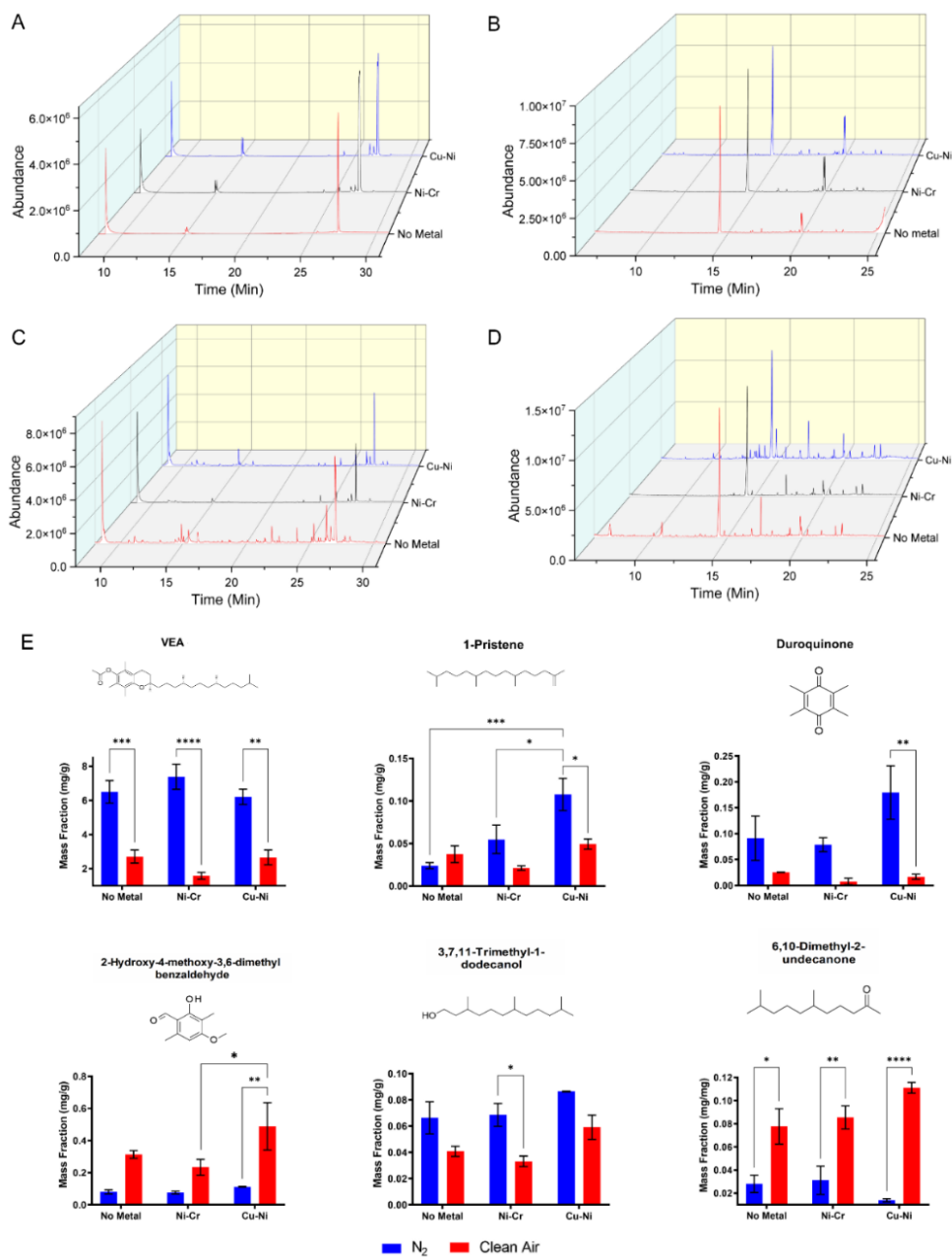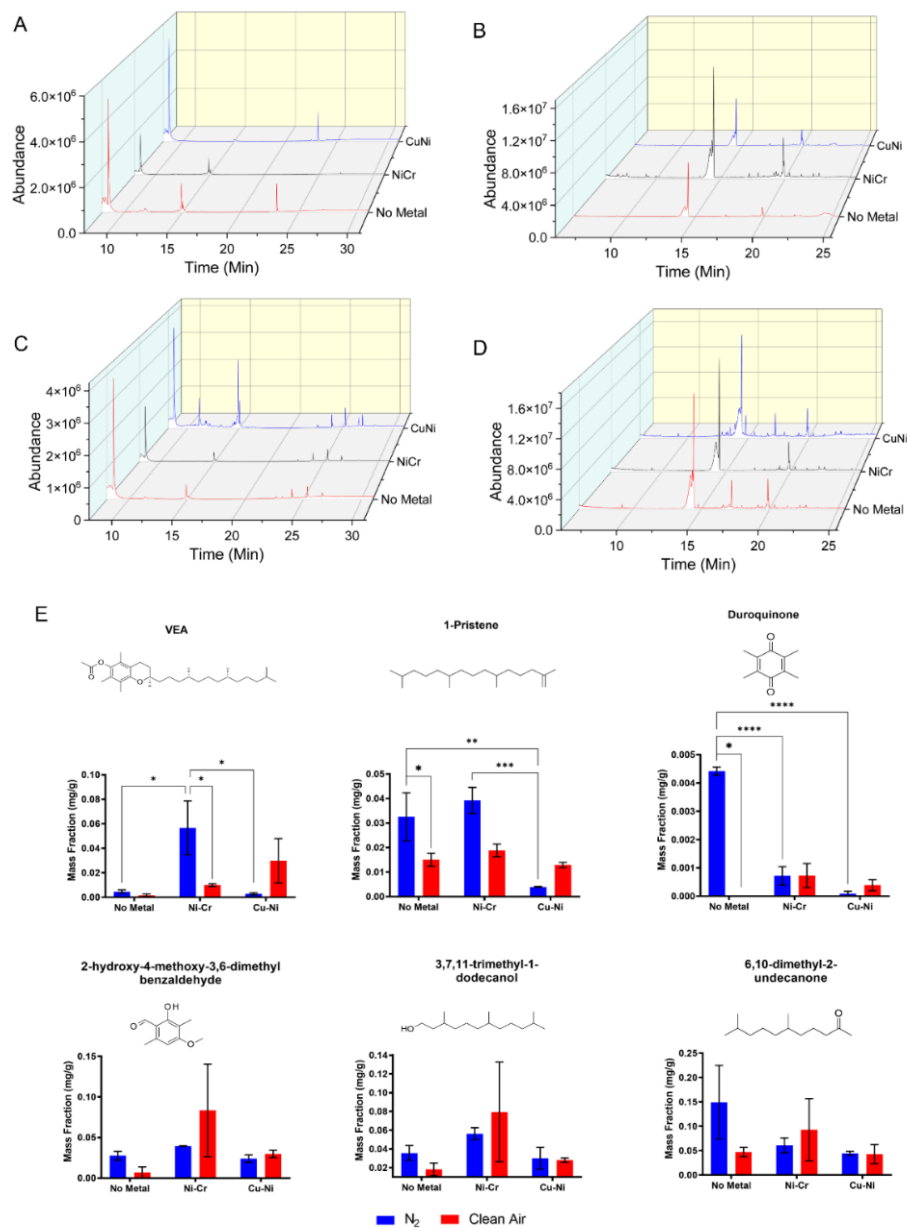
Figure 4.4. VEA product distribution under six different environmental conditions at 176 °C. Total ion chromatographs (TIC) were obtained from VEA pyrolysis in (A) N_2 environments in a non-polar separation column, (B) N_2 in a polar separation column, (C) clean air in a non-polar separation column, and (D) clean air in a polar separation column. (E) Masses of thermal degradation products, including VEA, 1-pristene, DQ, 2-hydroxy-4-methoxy-3,6-dimethyl benzaldehyde, 3,7,11-trimethyl-1-dodecanol, and 6,10-dimethyl-2-undecanone, formed under N_2 and clean air atmospheres at 176 °C. Results are expressed as the mean ± SEM (n=3). * Indicates $p < 0.05$; ** indicates $p < 0.01$.

However, there were notable differences in the normalized masses of each compound, VEA [tR = 27.02 min (**Figure 4.4A, C**)], 1-pristene [tR = 19.90 min (**Figure 4.4B, D**)], DQ [tR = 16.52 min (**Figure 4.4B, D**)], 2-hydroxy-4-methoxy-3,6-dimethyl benzaldehyde [tR = 22.67 min (**Figure 4.4B, D**)], 3,7,11-trimethyl-1-dodecanol [tR = 19.20 min (**Figure 4.4B, D**)], and 6,10-dimethyl-2-undecanone [tR = 17.23 min (**Figure 4.4B, D**)], at 176 °C compared to 356 °C shown in **Figure 4.4E**. Addition of Ni–Cr in the inert atmosphere resulted in significantly greater volatilization of VEA compared to that in the absence of metals; addition of Cu–Ni, however, resulted in greater mass of VEA in the oxidizing atmosphere than in the inert atmosphere, likely indicating greater volatilization of VEA in the presence of O_2 and Cu–Ni, and Ni–Cr in the absence of O_2. Likewise, there was no significant difference in the masses of 2-hydroxy-4-methoxy-3,6-dimethyl benzaldehyde, 3,7,11-trimethyl-1-dodecanol, and 6,10-dimethyl-2-undecanone.

The absence of metals and the presence of Ni–Cr alloy nanopowder in the inert atmosphere resulted in a significant increase in the mass of 1-pristene recovered compared to that in the presence of Cu–Ni; the presence of Cu–Ni in the inert atmosphere resulted in the smallest recovered mass of 1-pristene. There was no statistically significant difference in the oxidizing atmosphere between any treatments. An increase in the mass of 1-pristene in the presence of O_2 and Cu–Ni, compared to N_2 and Cu–Ni, was observed, though the increase was not significant. The masses of DQ recovered showed a trend similar to that of 1-pristene; here, the greatest mass was observed in the inert atmosphere in the absence of metals, with the addition of Ni–Cr and Cu–Ni greatly reducing the mass recovered. In the oxidizing atmosphere, the addition of Ni–Cr or Cu–

Ni to the oxidizing atmosphere resulted in a nonsignificant increase in the mass of DQ when compared to the absence of metals, and a slightly greater mass when O_2 and Cu–Ni were present compared to that with N_2 and Cu–Ni.

4.3.6 Enhanced VEA Thermal Degradation in the Presence of Oxygen and Metals

Overall, the environment in which VEA was heated was observed to have a significant effect on the mass of the chosen compounds. The presence of Cu–Ni, especially in the oxidizing atmosphere, resulted in greater mass consumption and a greater number and abundance of thermal degradation products. Though VEA has been demonstrated to be thermally stable through pyrolysis pathways until higher temperatures are reached, (37) heating in the presence of Cu–Ni and O_2 resulted in substantial degradation of VEA into highly oxygenated products often observed in VEA vaping emissions. In contrast, the addition of Ni–Cr in the oxidizing atmosphere appeared to decrease the number and abundance of VEA degradation products, which concurs with observations made by Saliba et al., (18) who found fresh nichrome wire to be the least reactive of e-cigarette coil types. These results may indicate the enhancement of oxidation pathways by O_2 in the atmosphere and transition metals in the body of the e-cigarette device and provide evidence for the importance of oxidation pathways and metal catalysis in low-temperature vaping.

Enhanced thermal degradation of organic compounds in the presence of metal catalysts has been documented in the literature. Catalysts may improve degradation by reducing the activation energy required for various thermal degradation pathways,

including oxidation pathways. The activation energy required for pyrolysis of biosolids in wastewater treatment has been found to be significantly reduced in the presence of minerals or metal oxides acting as catalysts, reducing the temperature required to observe mass loss and degradation. (40, 41) Moreover, upon investigation of the pyrolysis of biomass for the formation of biofuels, studies have found that the presence of transition metal catalysts allows for thermal degradation of organic compounds at lower pyrolysis temperatures, accelerates pyrolysis, and influences the pyrolysis product distribution. (30, 42, 43) More specifically, Hubble et al. (30) also demonstrated that Cu and Ni are more catalytically efficient than other investigated metal oxides in the pyrolysis of biomass for the formation of biofuels. The presence of Cu in particular demonstrated the ability to catalyze devolatilization of biomass at lower pyrolysis temperatures than commonly reported. It is highly likely that these phenomena can occur in various organic systems other than biosolids or biochar, including the pyrolysis of e-liquids. In essence, these results clearly indicate the potential role of oxidation by O_2 and metal catalysis as important factors to consider when attempting to understand the pathways and required temperatures for e-liquid thermal degradation.

4.3.7 Generation of OH Radicals

In addition to organic oxidants and metal particles, several studies have indicated the potential for vaping to generate various reactive oxygen species (ROS), including superoxide ($O_2^{\bullet-}$) and OH radicals. (4, 21, 26, 44) Recent studies by Son et al. (45) and Zhao et al. (25) have directly measured the formation of OH radicals in vaping emissions; these radicals may not only interact with biological systems to induce oxidative damage

but also induce further oxidation of e-liquids and thermal degradation products, resulting in the formation of highly oxygenated compounds with great oxidative potential. (46)

A few potential sources of OH radicals in e-cigarette systems have been suggested, including through the oxidation of organic e-liquids by O_2 and transition metal redox reactions (such as the Fenton and Fenton-like reactions). (38,45,47,48) To investigate whether enhancement of VEA degradation in the presence of O_2 and Cu–Ni could be attributed to the increased OH production, VEA was heated at 176 °C in N_2 and clean air atmospheres in the presence and absence of Cu–Ni alloy nanopowder, and OH radical formation was directly measured using the TPT assay. In the absence of Cu–Ni alloy nanopowder, the production of OH was significantly increased when VEA was heated in an oxidizing atmosphere compared to an inert atmosphere (**Figure 4.5**). When Cu–Ni was added, the production of OH was significantly enhanced in an oxidizing atmosphere, but the addition of Cu–Ni in the inert atmosphere resulted in no significant difference. These results indicate that atmospheric O_2 is a source of OH formation and that at low temperatures, Cu–Ni may enhance OH formation in the presence of O_2 via catalytic reactions. These findings are consistent with our GC/MS analysis, highlighting the importance of O_2 and oxidation reactions in VEA degradation, as well as the role of metals in catalyzing the reactions.
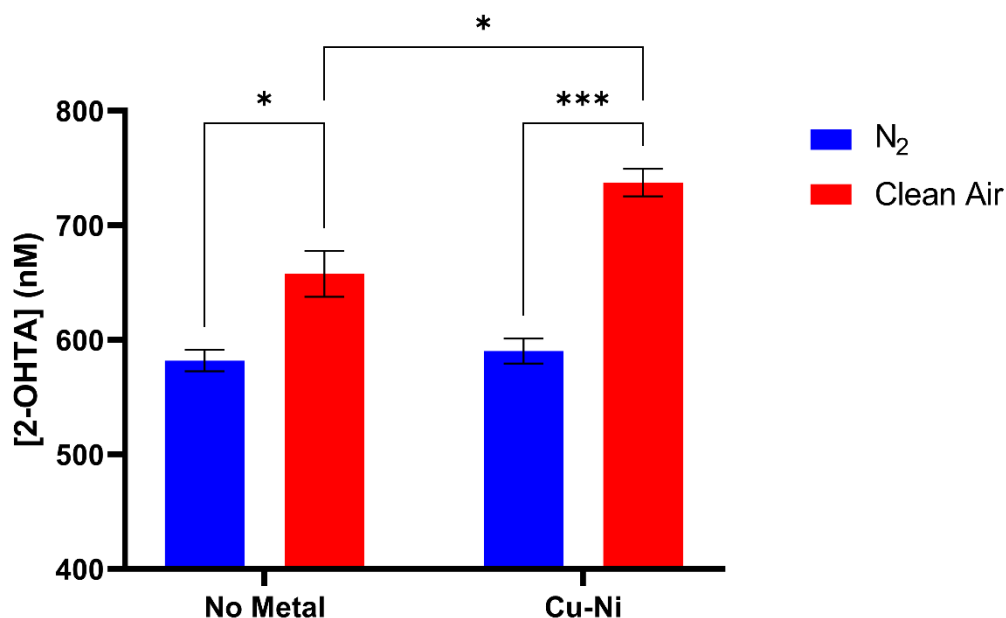
Figure 4.5. 2-OHTA generated by VEA heated in inert (N_2) and oxidizing (clean air) atmospheres in the absence and presence of Cu-Ni alloy nanopowder. Results are expressed the mean ± SEM (n=3). * Indicates $p < 0.05$; *** indicates $p < 0.001$.

Prior research has shown that transition metals, particularly metals such as Fe and Cu, may catalyze the activation of O_2 to form OH radicals. (49) This O_2-dependent OH radical formation pathway may explain why OH radicals are enhanced only in the oxidizing atmosphere, not in the presence of Cu–Ni in the inert atmosphere. However, the presence of OH radicals in the inert atmosphere does suggest a secondary source of OH radicals, potentially from heating of VEA alone, reaction of degradation products in the aqueous media used to trap radicals, or intrusion into the instrument from the lab atmosphere.

Regardless, the presence and enhanced formation of OH radicals are noteworthy as a recent study by Li et al. (38) suggested that many degradation products of VEA may result from OH radical- and O_2-mediated reactions. Radicals such as OH may initiate bond homolysis, dehydration, or H-abstraction on the side chain of VEA, followed by RO_2 radical-mediated chemistry to form highly oxygenated products observed in vaping emissions. (38,50) Such degradation pathways may occur simultaneously through pyrolysis-induced degradation, producing unique compounds that cannot be explained through pyrolysis alone. In our results, the enhanced formation of OH radicals in an oxidizing environment and the increased number of degradation products observed in the presence of O_2 and Cu–Ni provide further evidence of oxidative pathways as a dominant factor in VEA degradation, particularly at low temperatures. Furthermore, the catalytic effect of metals from heating coils in the presence of O_2 at low temperatures may explain the abundance of low-temperature thermal degradation products in vaping scenarios that are not explained through pyrolysis alone. (7)

4.3.8 Potential Limitations

While this study improves our understanding of the catalytic effect of metals when vaping, some limitations must be noted when these results are applied to real-world vaping scenarios. First, this study investigates the influence of three metals commonly found in high abundance in the body of e-cigarette coils and cartridges. (12) It should be noted that real-life devices may contain a mixture of various metal alloys and several metals not investigated here, such as Mn, Zn, Sn, etc. (12,13) Large amounts of other redox-active transition metals, such as Fe, may further alter the chemical composition of

resulting e-cigarette emissions through alternative metal–organic interactions or enhanced production of OH radicals. While this study chose to investigate metals that were representative of common e-cigarette devices, more studies are needed to fully characterize the influence of various metals on the chemical composition of e-cigarette emissions. Additionally, the limitations of the cold trap method have been previously described. (4,7) This method was optimized for the detection of compounds with boiling points at or above the temperature of dry ice without the use of additional derivatization techniques. As a result, while this method is effective for capturing compounds such as VEA and DQ, highly volatile and reactive compounds like ketene and various carbonyls may be produced from VEA degradation but are not detectable. Nonetheless, we do not expect that the inability to detect certain reactive or highly volatile compounds will have a significant impact on the interpretation of our findings.

4.4 Conclusions and Implications

This study examines the effects of O_2 and two metal alloy nanopowders on the chemical composition of e-cigarette emissions. Our results show significant degradation of VEA at high and low temperatures in the presence of O_2 and Cu–Ni alloy nanopowder. Moreover, VEA heated in clean air resulted in significantly greater OH production than in inert atmospheres, with Cu–Ni metal alloy enhancing OH production only in the presence of O_2. Ultimately, these results highlight the importance of oxidation pathways in the low-temperature degradation of e-liquids catalyzed by metals. The production of many oxygenated VEA and other e-liquid vaping products likely cannot be explained by the pyrolysis of VEA alone; rather, it is likely that multiple, simultaneous pathways

degrade the parent oils. As such, the role of O_2 and oxidation pathways must be considered when predicting e-liquid thermal degradation.

Furthermore, the observed presence of OH radicals in VEA emissions not only provides evidence of the role of oxidation in the low-temperature degradation of VEA but also has important implications for the health of vape users. First, as evidenced here, the promotion of OH radical formation likely promotes oxidation and the formation of oxygenated degradation products. Exposure to such products through vaping may result in oxidative damage to biomolecules; (51−54) consideration of OH radical-mediated pathways may assist in predictive models attempting to characterize potential degradation products that may cause harm to users. Second, inhalation of OH radicals alone may pose a serious risk of oxidative damage. OH radicals are considered one of the most strongly oxidizing ROS species. (55,56) These radicals have immense potential to interact with biomolecules such as proteins and lipids in lung lining fluid (56−58) and have been found to induce DNA strand breaks and the formation of oxidative DNA adducts. (59,60) To fully understand the risk of oxidative damage associated with vaping, it is clearly critical to consider the formation of OH radical species and OH-mediated reactions.

Overall, the findings of this study provide insight into the potential role of O_2 and metals in not only e-liquid degradation but also various other systems investigating the inhalation risk of organic compounds heated in the presence of O_2 or metals. These results emphasize that the consideration of many factors is crucial for future exposure and risk assessment. Future studies should focus on the impact of these oxidation pathways and how they interact with other varying parameters (such as puffing topography,

temperature, and design of e-cigarette devices) to influence the chemical composition of vaping emissions.

4.5 Supplemental Information
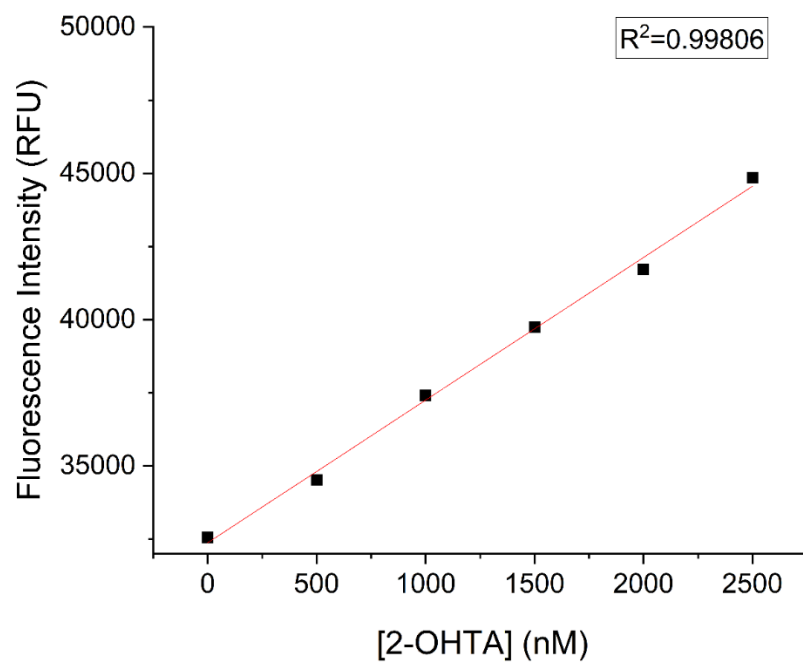
Figure S4.1. Calibration curve for 2-OHTA used for quantification.

Table S4.1. Summary of %-Mass of VEA remaining in crucible at set temperatures.

Temperature (°C)	%-Mass Remaining	
	N_2	Clean Air
100	100.51%	100.12%
200	100.35%	99.94%
250	97.45%	98.58%
300	75.41%	86.99%
350	5.07%	32.89%
400	1.61%	6.94%
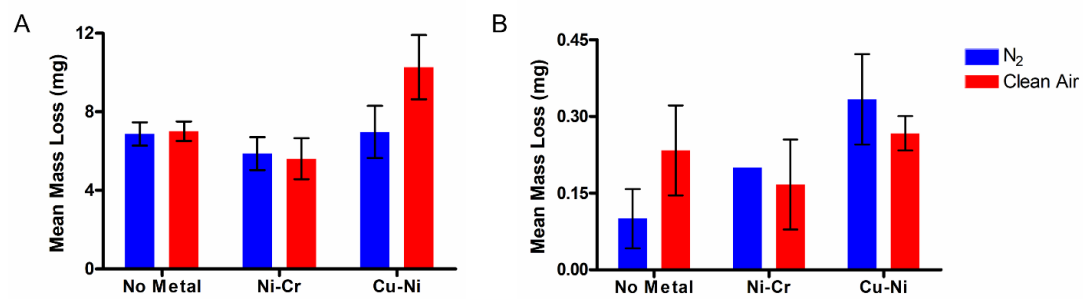
Figure S4.2. Mass of VEA consumed during tube furnace reactions at (A) 356 °C and (B) 176 °C.
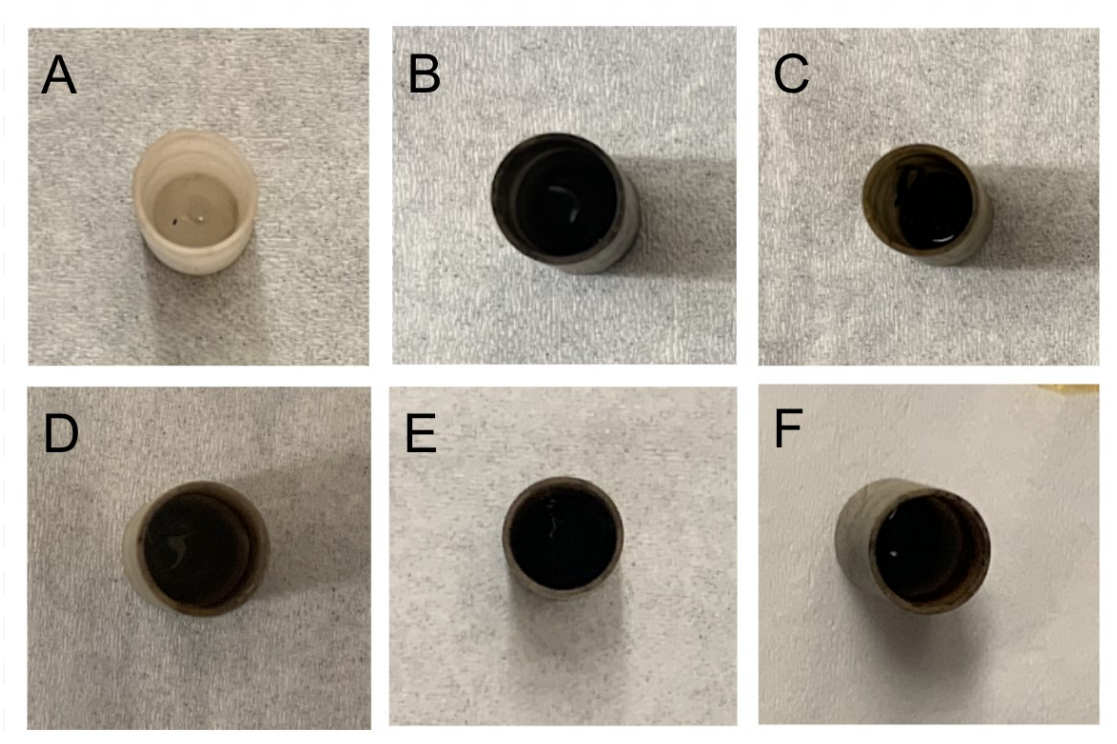
Figure S4.3. Images taken of alumina crucibles after heating at 356 °C under N_2 (A) without metal, (B) with Cu-Ni alloy nanopowder, and (C) with Ni-Cr alloy nanopowder, and under clean air (D) without metal, (E) with Cu-Ni alloy nanopowder, and (F) with Ni-Cr alloy nanopowder. All images were taken by authors.
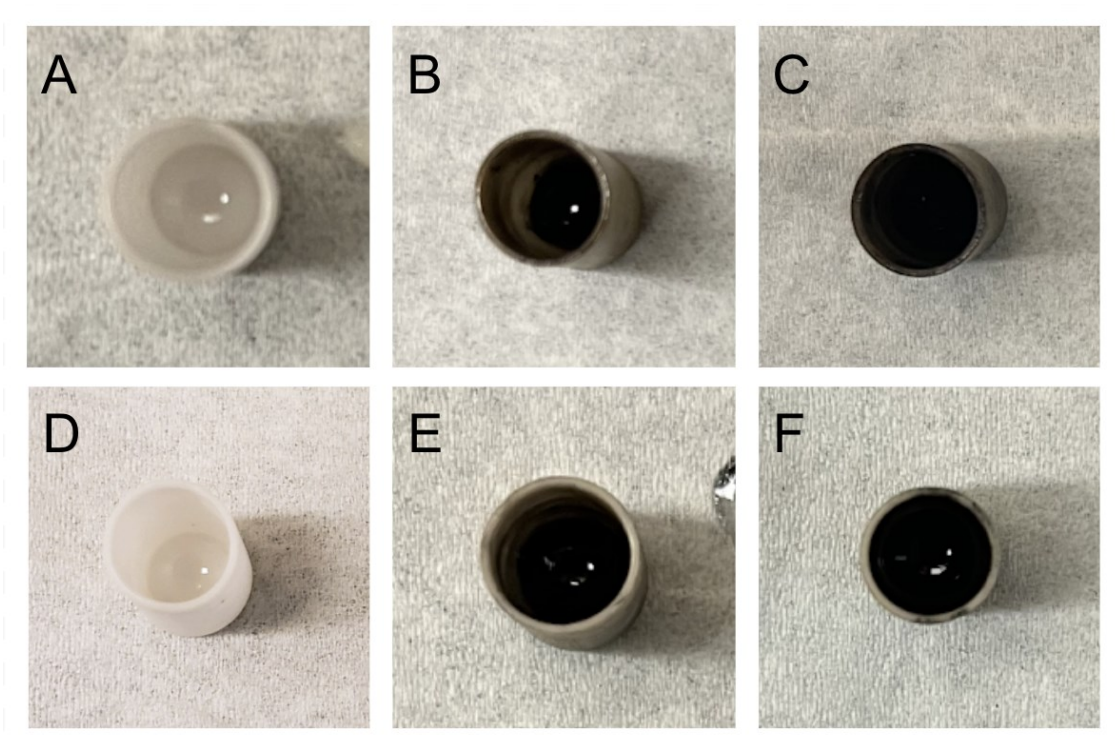
Figure S4.4. Images taken of alumina crucibles after heating at 176 °C under N_2 (A) without metal, (B) with Cu-Ni alloy nanopowder, and (C) with Ni-Cr alloy nanopowder, and under clean air (D) without metal, (E) with Cu-Ni alloy nanopowder, and (F) with Ni-Cr alloy nanopowder. All images were taken by authors.

4.6 References

1.   C.D.C. Outbreak of Lung Injury Associated with the Use of E-Cigarette, or Vaping, Products. https://www.cdc.gov/tobacco/basic_information/e-cigarettes/severe-lung-disease.html

2.   Braymiller, J. L.; Barrington-Trimis, J. L.; Leventhal, A. M.; Islam, T.; Kechter, A.; Krueger, E. A.; Cho, J.; Lanza, I.; Unger, J. B.; McConnell, R., Assessment of Nicotine and Cannabis Vaping and Respiratory Symptoms in Young Adults. *JAMA Network Open* **2020**, *3* (12), e2030189.

3.   Jiang, H.; Ahmed, C. M. S.; Martin, T. J.; Canchola, A.; Oswald, I. W. H.; Garcia, J. A.; Chen, J. Y.; Koby, K. A.; Buchanan, A. J.; Zhao, Z.; Zhang, H.; Chen, K.; Lin, Y.-H., Chemical and Toxicological Characterization of Vaping Emission Products from Commonly Used Vape Juice Diluents. *Chem. Res. Toxicol*. **2020**, *33*(8), 2157-2163.

4.   Canchola, A.; Ahmed, C. M. S.; Chen, K.; Chen, J. Y.; Lin, Y.-H., Formation of Redox-Active Duroquinone from Vaping of Vitamin E Acetate Contributes to Oxidative Lung Injury. *Chem. Res. Toxicol.* **2022**, *35*(2), 254-264.

5.   Chen, J. Y.; Canchola, A.; Lin, Y.-H., Carbonyl Composition and Electrophilicity in Vaping Emissions of Flavored and Unflavored E-Liquids. *Toxics* **2021**, *9*(12), 345.

6.   Bekki, K.; Uchiyama, S.; Ohta, K.; Inaba, Y.; Nakagome, H.; Kunugita, N., Carbonyl Compounds Generated from Electronic Cigarettes. International Journal of Int. *J. Environ. Res. Public Health* **2014**, *11*(11), 11192-11200.

7.   Canchola, A.; Meletz, R.; Khandakar, R. A.; Woods, M.; Lin, Y.-H., Temperature dependence of emission product distribution from vaping of vitamin E acetate. *PLOS ONE* **2022**, *17*(3), e0265365.

8.   Lynch, J.; Lorenz, L.; Brueggemeyer, J. L.; Lanzarotta, A.; Falconer, T. M.; Wilson, R. A., Simultaneous Temperature Measurements and Aerosol Collection During Vaping for the Analysis of Δ9-Tetrahydrocannabinol and Vitamin E Acetate Mixtures in Ceramic Coil Style Cartridges. *Front. Chem.* **2021**, *9*, 643.

9.   Wu, D.; O'Shea, D. F., Potential for release of pulmonary toxic ketene from vaping pyrolysis of vitamin E acetate. *PNAS* **2020**, *117*(12), 6349-6355.

10.   Kovach, A. L.; Carter, R. R.; Thornburg, J. W.; Wiethe, R.; Fennell, T. R.; Wiley, J. L., Thermal Degradants Identified from the Vaping of Vitamin E Acetate. *J. Anal. Toxicol.* **2022**, *46*(7), 750-756.

11.   Matsumoto, S.; Traber, M. G.; Leonard, S. W.; Choi, J.; Fang, X.; Maishan, M.; Wick, K. D.; Jones, K. D.; Calfee, C. S.; Gotts, J. E., Aerosolized vitamin E acetate

causes oxidative injury in mice and in alveolar macrophages. *Am. J. Physiol. Lung Cell Mol. Physiol.* **2022**, *322*(6), L771-L783.

12. McDaniel, C.; Mallampati, S. R.; Wise, A., Metals in Cannabis Vaporizer Aerosols: Sources, Possible Mechanisms, and Exposure Profiles. *Chem. Res. Toxicol.* **2021**, *34*(11), 2331-2342.

13. Omaiye, E. E.; Williams, M.; Bozhilov, K. N.; Talbot, P., Design features and elemental/metal analysis of the atomizers in pod-style electronic cigarettes. *PLOS ONE* **2021**, *16*(3), e0248127.

14. Gonzalez-Jimenez, N.; Gray, N.; Pappas, R. S.; Halstead, M.; Lewis, E.; Valentin-Blasini, L.; Watson, C.; Blount, B., Analysis of Toxic Metals in Aerosols from Devices Associated with Electronic Cigarette, or Vaping, Product Use Associated Lung Injury. *Toxics* **2021**, *9*(10), 240.

15. Gray, N.; Halstead, M.; Gonzalez-Jimenez, N.; Valentin-Blasini, L.; Watson, C.; Pappas, R. S., Analysis of Toxic Metals in Liquid from Electronic Cigarettes. *Int. J. Environ. Res. Public Health* **2019**, *16*(22), 4450.

16. Williams, M.; Villarreal, A.; Bozhilov, K.; Lin, S.; Talbot, P., Metal and Silicate Particles Including Nanoparticles Are Present in Electronic Cigarette Cartomizer Fluid and Aerosol. *PLOS ONE* **2013**, *8*(3), e57987.

17. Chun, L. F.; Moazed, F.; Calfee, C. S.; Matthay, M. A.; Gotts, J. E., Pulmonary toxicity of e-cigarettes. *Am. J. Physiol. Lung Cell Mol. Physiol.* **2017**, 313, (2), L193-L206.

18. Saliba, N. A.; El Hellani, A.; Honein, E.; Salman, R.; Talih, S.; Zeaiter, J.; Shihadeh, A., Surface chemistry of electronic cigarette electrical heating coils: Effects of metal type on propylene glycol thermal decomposition. *J. Anal. Appl. Pyrolysis* 2018, 134, 520-525.

19. Jensen, R. P.; Strongin, R. M.; Peyton, D. H., Solvent chemistry in the electronic cigarette reaction vessel. *Sci. Rep.* **2017**, *7* (1), 1-11.

20. Behar, R. Z.; Hua, M.; Talbot, P., Puffing Topography and Nicotine Intake of Electronic Cigarette Users. *PLOS ONE* **2015**, *10* (2), e0117222.

21. Zhao, T.; Shu, S.; Guo, Q.; Zhu, Y., Effects of design parameters and puff topography on heating coil temperature and mainstream aerosols in electronic cigarettes. *Atmos. Environ.* **2016**, *134*, 61-69.

22. Li, Y.; Burns, A. E.; Tran, L. N.; Abellar, K. A.; Poindexter, M.; Li, X.; Madl, A. K.; Pinkerton, K. E.; Nguyen, T. B., Impact of e-Liquid Composition, Coil Temperature,

and Puff Topography on the Aerosol Chemistry of Electronic Cigarettes. *Chem. Res. Toxicol.* **2021**, *34* (6), 1640-1654.

23.   Lechasseur, A.; Altmejd, S.; Turgeon, N.; Buonanno, G.; Morawska, L.; Brunet, D.; Duchaine, C.; Morissette, M. C., Variations in coil temperature/power and e-liquid constituents change size and lung deposition of particles emitted by an electronic cigarette. *Physiol. Rep.* **2019**, *7* (10), e14093.

24.   Zhao, D.; Navas-Acien, A.; Ilievski, V.; Slavkovich, V.; Olmedo, P.; Adria-Mora, B.; Domingo-Relloso, A.; Aherrera, A.; Kleiman, N. J.; Rule, A. M.; Hilpert, M., Metal concentrations in electronic cigarette aerosol: Effect of open-system and closed-system devices and power settings. *Environ. Res.* **2019**, *174*, 125-134.

25.   Zhao, J.; Zhang, Y.; Sisler, J. D.; Shaffer, J.; Leonard, S. S.; Morris, A. M.; Qian, Y.; Bello, D.; Demokritou, P., Assessment of reactive oxygen species generated by electronic cigarettes using acellular and cellular approaches. *J. Hazard. Mater.* **2018**, *344*, 549-557.

26.   Cirillo, S.; Urena, J. F.; Lambert, J. D.; Vivarelli, F.; Canistro, D.; Paolini, M.; Cardenia, V.; Rodriguez-Estrada, M. T.; Richie, J. P.; Elias, R. J., Impact of electronic cigarette heating coil resistance on the production of reactive carbonyls, reactive oxygen species and induction of cytotoxicity in human lung cancer cells in vitro. *Regul. Toxicol. Pharmacol.* **2019**, *109*, 104500.

27.   Bitzer, Z. T.; Goel, R.; Reilly, S. M.; Foulds, J.; Muscat, J.; Elias, R. J.; Richie, J. P., Effects of Solvent and Temperature on Free Radical Formation in Electronic Cigarette Aerosols. *Chem. Res. Toxicol.* **2018**, *31* (1), 4-12.

28.   Geiss, O.; Bianchi, I.; Barrero-Moreno, J., Correlation of volatile carbonyl yields emitted by e-cigarettes with the temperature of the heating coil and the perceived sensorial quality of the generated vapours. *Int. J. Hyg. Environ. Health* **2016**, *219* (3), 268-277.

29.   Ushikusa, T.; Maruyama, T.; Niiya, I., Pyrolysis behavior and thermostability of tocopherols. *JOCS* **1991**, *40* (12), 1073-1079.

30.   Hubble, A. H.; Ryan, E. M.; Goldfarb, J. L., Enhancing pyrolysis gas and bio-oil formation through transition metals as in situ catalysts. *Fuel* **2022**, *308*, 121900.

31.   Jaegers, N. R.; Hu, W.; Weber, T. J.; Hu, J. Z., Low-temperature (< 200 °C) degradation of electronic nicotine delivery system liquids generates toxic aldehydes. *Sci. Rep.* **2021**, *11* (1), 7800.

32. Zhu, J.; Niu, J.; Das, D.; Cabecinha, A.; Abramovici, H., In-situ TD-GCMS measurements of oxidative products of monoterpenes at typical vaping temperatures: implications for inhalation exposure to vaping products. *Sci. Rep.* **2022**, *12* (1), 1-7.

33. D3452-06, A., Standard Practice for Rubber Identification by Pyrolysis–Gas Chromatography. **2012**.

34. Barreto, J. C.; Smith, G. S.; Strobel, N. H. P.; McQuillin, P. A.; Miller, T. A., Terephthalic acid: A dosimeter for the detection of hydroxyl radicals in vitro. *Life Sciences* **1994**, *56* (4), PL89-PL96.

35. Linxiang, L.; Abe, Y.; Nagasawa, Y.; Kudo, R.; Usui, N.; Imai, K.; Mashino, T.; Mochizuki, M.; Miyata, N., An HPLC assay of hydroxyl radicals by the hydroxylation reaction of terephthalic acid. *Biomed. Chroma.* **2004**, *18* (7), 470-474.

36. Saran, M.; Summer, K. H., Assaying for hydroxyl radicals: Hydroxylated terephthalate is a superior fluorescence marker than hydroxylated benzoate. *Free Radical Res.* **1999**, *31* (5), 429-436.

37. Efsa Panel on Food Contact Materials, E. F.; Processing, A., Safety assessment of the substance α-tocopherol acetate for use in food contact materials. *EFSA Journal* **2016**, *14* (3), 4412.

38. Li, Y.; Dai, J.; Tran, L. N.; Pinkerton, K. E.; Spindel, E. R.; Nguyen, T. B., Vaping Aerosols from Vitamin E Acetate and Tetrahydrocannabinol Oil: Chemistry and Composition. *Chem. Res. Toxicol.* **2022**, *35* (6), 1095-1109.

39. Mikheev, V. B.; Klupinski, T. P.; Ivanov, A.; Lucas, E. A.; Strozier, E. D.; Fix, C., Particle size distribution and chemical composition of aerosolized vitamin E acetate. *Aerosol Sci. Technol.* **2020**, *54* (9), 993-998.

40. Patel, S.; Kundu, S.; Halder, P.; Rickards, L.; Paz-Ferreiro, J.; Surapaneni, A.; Madapusi, S.; Shah, K., Thermogravimetric Analysis of biosolids pyrolysis in the presence of mineral oxides. *Renew. Ener.* **2019**, *141*, 707-716.

41. Shao, J.; Yan, R.; Chen, H.; Yang, H.; Lee, D. H., Catalytic effect of metal oxides on pyrolysis of sewage sludge. *Fuel Process. Technol.* **2010**, *91* (9), 1113-1118.

42. Su, G.; Ong, H. C.; Mofijur, M.; Mahlia, T. M. I.; Ok, Y. S., Pyrolysis of waste oils for the production of biofuels: A critical review. *J. Hazard. Mater.* **2022**, *424*, 127396.

43. Hakeem, I. G.; Halder, P.; Dike, C. C.; Chiang, K.; Sharma, A.; Paz-Ferreiro, J.; Shah, K., Advances in biosolids pyrolysis: Roles of pre-treatments, catalysts, and co-feeding on products distribution and high-value chemical production. *J. Anal. Appl. Pyrolysis* **2022**, *166,* 105608.

44.   Goel, R.; Durand, E.; Trushin, N.; Prokopczyk, B.; Foulds, J.; Elias, R. J.; Richie, J. P., Highly Reactive Free Radicals in Electronic Cigarette Aerosols. *Chem. Res. Toxicol*. **2015**, *28* (9), 1675-1677.

45.   Son, Y.; Mishin, V.; Laskin, J. D.; Mainelis, G.; Wackowski, O. A.; Delnevo, C.; Schwander, S.; Khlystov, A.; Samburova, V.; Meng, Q., Hydroxyl Radicals in E-Cigarette Vapor and E-Vapor Oxidative Potentials under Different Vaping Patterns. *Chem. Res. Toxicol.* **2019**, *32* (6), 1087-1095.

46.   Halliwell, B.; Gutteridge, J. M. C., Free radicals in biology and medicine. Oxford university press, USA: 2015.

47.   Valavanidis, A.; Fiotakis, K.; Bakeas, E.; Vlahogianni, T., Electron paramagnetic resonance study of the generation of reactive oxygen species catalysed by transition metals and quinoid redox cycling by inhalable ambient particulate matter. *Redox Report* **2005**, *10* (1), 37-51.

48.   Laino, T.; Tuma, C.; Moor, P.; Martin, E.; Stolz, S.; Curioni, A., Mechanisms of Propylene Glycol and Triacetin Pyrolysis. *J. Phys. Chem. A*. **2012**, *116* (18), 4602-4609.

49.   Cai, J.; Li, H.; Feng, K.; Cheng, Y.; He, S.; Takaoka, M., Low-temperature degradation of humic acid via titanium zirconium oxide@copper single-atom activating oxygen: Mechanism and pathways. *Chem. Engin. J.* **2022**, *450*, 138239.

50.   Houle, F. A.; Hinsberg, W. D.; Wilson, K. R., Oxidation of a model alkane aerosol by OH radical: the emergent nature of reactive uptake. *Phys. Chem. Chem. Phys.* **2015**, *17* (6), 4412-4423.

51.   Bonner, E.; Chang, Y.; Christie, E.; Colvin, V.; Cunningham, B.; Elson, D.; Ghetu, C.; Huizenga, J.; Hutton, S. J.; Kolluri, S. K.; Maggio, S.; Moran, I.; Parker, B.; Rericha, Y.; Rivera, B. N.; Samon, S.; Schwichtenberg, T.; Shankar, P.; Simonich, M. T.; Wilson, L. B.; Tanguay, R. L., The chemistry and toxicology of vaping. *Pharmacol. Ther.* **2021**, *225*, 107837.

52.   Sundar, I. K.; Javed, F.; Romanos, G. E.; Rahman, I., E-cigarettes and flavorings induce inflammatory and pro-senescence responses in oral epithelial cells and periodontal fibroblasts. *Oncotarget* **2016**, *7* (47), 77196.

53.   Cheng, G.; Guo, J.; Carmella, S. G.; Lindgren, B.; Ikuemonisan, J.; Niesen, B.; Jensen, J.; Hatsukami, D. K.; Balbo, S.; Hecht, S. S., Increased acrolein–DNA adducts in buccal brushings of e-cigarette users. *Carcinogenesis* **2022**, *43* (5), 437-444.

54.   Paiano, V.; Maertens, L.; Guidolin, V.; Yang, J.; Balbo, S.; Hecht, S. S., Quantitative Liquid Chromatography–Nanoelectrospray Ionization–High-Resolution Tandem Mass Spectrometry Analysis of Acrolein-DNA Adducts and Etheno-DNA

Adducts in Oral Cells from Cigarette Smokers and Nonsmokers. *Chem. Res. Toxicol.* **2020**, *33* (8), 2197-2207.

55.   Valavanidis, A.; Salika, A.; Theodoropoulou, A., Generation of hydroxyl radicals by urban suspended particulate air matter. The role of iron ions. *Atmos. Environ.* **2000**, *34* (15), 2379-2386.

56.   Marusawa, H.; Ichikawa, K.; Narita, N.; Murakami, H.; Ito, K.; Tezuka, T., Hydroxyl radical as a strong electrophilic species. *Bioorg. Med. Chem.* **2002**, *10* (7), 2283-2290.

57.   Riley, P. A., Free radicals in biology: oxidative stress and the effects of ionizing radiation. *Int. J. Radiat. Biol.* **1994**, *65* (1), 27-33.

58.   Therond, P. In Oxidative stress and damages to biomolecules (lipids, proteins, DNA), **2006**, 383-389.

59.   Leanderson, P.; Tagesson, C., Cigarette smoke-induced DNA damage in cultured human lung cells: role of hydroxyl radicals and endonuclease activation. *Chem. Biol. Interact.* **1992**, *81* (1-2), 197-208.

60.   Chatgilialoglu, C.; Ferreri, C.; Krokidis, M. G.; Masi, A.; Terzidis, M. A., On the relevance of hydroxyl radical to purine DNA damage. *Free Radical Res.* **2021**, *55* (4), 384-404.

Chapter 5: Conclusions and Implications

This dissertation overall investigates the thermal degradation behavior of VEA as a model e-liquid, and the impact of user- and device-driven parameters on the chemical composition of e-cigarette emissions. At the time of this dissertation, the inhalation toxicity of e-cigarettes is still largely unknown. This gap is partly a result of the difficulty in characterizing the specific chemicals present in e-cigarette emissions, which is made challenging by the wide range of variability in e-cigarette operation. In Chapter 2, the potential role of the thermal degradation products of VEA in EVALI pathology was assessed. Particle-phase VEA vaping products were quantified in the total aerosol and at various size fractions using gas chromatography/mass spectrometry (GC/MS) analysis. Using this approach, large molecular-weight compounds including VEA, vitamin E, 3,7,11-trimethyl-1-docecanol, and 1-pristene as well as quinone and quinone-like compounds duroquinone (DQ) and durohydroquinone (DHQ) were detected. VEA, 3,7,11-Trimethyl-1-docecanol and DQ were all found to exist in particles ≤ 100 nm, indicating the potential risk for e-cigarette aerosol constituents to penetrate deep into the lower respiratory tract of users. In addition, after exposure of DQ and VEA vaping emissions to human airway epithelial cells (BEAS-2B), differential cytotoxicity, ROS generation, and oxidative stress-related gene expression were observed. Exposure to the total aerosol mixture overall resulted in greater oxidative damage compared to DQ alone, which implies the importance of considering potential mixture effects within e-cigarette emissions in order to understand the underlying toxicity mechanisms. The results of Chapter 2 demonstrate that e-cigarette emissions are complex mixtures of compounds

that may have unique toxicological properties that encourage additive, synergistic, or even antagonistic effects on toxicity, and to understand the potential health effects of vaping, researchers must first have a strong grasp on what chemicals and chemical classes users are exposed to. In the future, more work is needed to identify the physiochemical properties of vaping aerosols and potential mixture effects within the emissions.

In Chapter 3, non-target GC/MS analysis was used to identify and quantify compounds found in VEA vaping emissions generated at 4 different voltage settings/heating coil temperatures in order to understand the influence of variable temperature settings on the emission product distribution of e-cigarettes. At lower temperatures, the formation of larger molecular alkenes and long-chain alcohols was preferred. As coil temperature increased, thermal degradation of both VEA and the larger molecular weight VEA degradation products was greatly enhanced, promoting the formation of lower molecular weight alkanes, alkenes, and carbonyl-containing compounds. Furthermore, simulation of VEA pyrolysis in a tube furnace reactor system found VEA to be thermally stable up to temperatures >237 °C; at higher temperatures, the emission product distribution did not correlate with what has been found previously in this Chapter or existing literature. This discrepancy suggested that, despite pyrolysis being considered the primary pathway of vaping thermal degradation at the time of this Chapter's publication, external factors and/or alternate reaction pathways other than pyrolysis may promote low-temperature degradation of e-liquids. The results found in Chapter 3 show that the temperature at which a vaping device is operated can greatly

impact the product emission distribution of vaping aerosols, resulting in the formation of unique compounds with a wide range of chemical properties and potential toxicity mechanisms. These results further support the hypotheses proposed in Chapter 1. There may be no one toxicity mechanism through which VEA vaping emission acts; instead, with a wide range of compounds that could form at different temperatures, multiple pathways may interact to cause damage.

Finally, in Chapter 4, the influence of atmospheric O_2 and transition metals on the thermal degradation behavior and emission product distribution of VEA was further investigated. VEA was heated using a tube furnace reactor system in inert (N_2) and oxidizing atmospheres (clean air) in the absence and presence of Ni–Cr and Cu–Ni alloy nanopowders. Heating in inert atmospheres was found to be insufficient to encourage VEA decomposition at temperatures found to result in significant vaping-induced thermal degradation in Chapter 3. Heating in the presence of molecular oxygen (O_2) and Cu–Ni nanopower greatly promoted significant VEA degradation, resulting in the formation of oxygenated compounds previously found in vaping emissions. The combination of O_2 and Cu–Ni nanopowder was also found to greatly enhance the production of OH radicals. Ni–Cr appeared to have a suppressive effect on VEA decomposition, but further study is required to validate these results and understand the mechanisms involved. The results from Chapter 4 overall provide further evidence of the influence of external factors on e-liquid degradation, as well as support the hypothesis that e-liquid thermal degradation may be a result of multiple reaction pathways, including pyrolysis and OH- or O_2-mediated chemistry. These results have significant implications for not only further study

into the chemistry of e-cigarette emissions, but also the potential risk of oxidative damage to users.

Taken together, the chapters of this dissertation highlight the need for hazard identification of vaping emission components and provide evidence of the importance of understanding external factors when estimating the public health risk of e-cigarettes. While many primary e-cigarette ingredients (excluding active ingredients) like PG and VG are designated as Generally Recognized As Safe (GRAS) for oral, dermal, and inhalation exposure, (1,2) their emissions are complex mixtures that include products such as formaldehyde, acrolein, benzaldehyde, methyl glyoxal and more oxygenated compounds (3,4) that are associated with increased risks of respiratory diseases and cancers (5-8). Furthermore, as described in Chapter 1 of this dissertation, there exists a wide range of customizable options for e-cigarettes. While temperature, metal composition, and the influence of oxygen are discussed here, they only represent a fraction of the potential combinations of settings and device construction that a user could choose for their personal experience. For this reason, further chemical and toxicological characterization of e-cigarette emissions are needed. In order to fully assess the exposure risk of e-cigarettes, future studies should investigate how the parameters investigated in this dissertation and others not fully discussed may interact to influence the chemical composition of vaping emissions.

5.1 References

1. ASTDR Toxicological Profile for Propylene Glycol https://wwwn.cdc.gov/TSP/ToxProfiles/ToxProfiles.aspx?id=1122&tid=240 (accessed 1/20/2024).

2. CDC NIOSH Pocket Guide to Chemical Hazards: Glycerin (Mist) https://www.cdc.gov/niosh/npg/npgd0302.html (accessed 1/20/2024).

3. Chen, J. Y.; Canchola, A.; Lin, Y.-H., Carbonyl Composition and Electrophilicity in Vaping Emissions of Flavored and Unflavored E-Liquids. *Toxics* **2021,** *9* (12).

4. Li, Y.; Burns, A. E.; Tran, L. N.; Abellar, K. A.; Poindexter, M.; Li, X.; Madl, A. K.; Pinkerton, K. E.; Nguyen, T. B., Impact of e-Liquid Composition, Coil Temperature, and Puff Topography on the Aerosol Chemistry of Electronic Cigarettes. *Chem. Res. Toxicol.* **2021,** *34* (6), 1640-1654.

5. IARC Working Group on the Evaluation of Carcinogenic Risks to Humans, Acrolein, Crotonaldehyde, and Arecoline. *IARC Monographs.* **2021,** *128*, 45-158

6. IARC Working Group on the Evaluation of Carcinogenic Risks to Humans, Formaldehyde, 2-Butoxyethanol and 1-tert-Butoxypropan-2-ol. *IARC Monographs.* **2006,** *88*, 37-326

7. Kwak, S.; Choi, Y.S.; Na, G.H.; Bae, C.H.; Song, S.-Y.; Kim, Y.-G. Glyoxal and Methylglyoxal as E-cigarette Vapor Ingredients-Induced Pro-Inflammatory Cytokine and Mucins Expression in Human Nasal Epithelial Cells. *Am. J. Rhinol. Allergy.* **2020,** *35* (2), 213-220

8. Vaca, C. E., Nilsson, J. A., Fang, J. L., & Grafström, R. C. Formation of DNA adducts in human buccal epithelial cells exposed to acetaldehyde and methylglyoxal in vitro. *Chem. Biol. Interact.*, **1998**, *108* (3), 197-208.